LUND UNIVERSITY

3D Verification of Dynamic and Breathing Adapted Radiotherapy using Polymer Gel Dosimetry

Ceberg, Sofie

2010

3D Verification of Dynamic and Breathing Adapted Radiotherapy using Polymer Gel Dosimetry

Sofie Ceberg

Medical Radiation Physics
Department of Clinical Sciences, Malmö
Lund University
Skåne University Hospital, Malmö
2010

LUND UNIVERSITY

Cover: An overlay of the 90% isodose surfaces projected into a 3D view for a measurement (polymer gel in red), a calculation (treatment planning system in purple) and a simulation (Monte Carlo in green) of a prostate VMAT delivery.

Thesis for the Degree of Doctor of Philosophy
Faculty of Science at Lund University
Medical Radiation Physics
Department of Clinical Sciences, Malmö
Skåne University Hospital
SE-205 02 Malmö, Sweden

ISBN 978-91-7473-041-8
Printed in Sweden by Media-Tryck, Lund, 2010

”Ignora motu ignora nature”
Aristoteles (384-322 f.K.)

Abstract

Polymer gel dosimetry has been used since the 1990s, and several studies have shown that this detector system can be used for verification of static absorbed dose distributions in three dimensions (3D). Its unique properties, such as high resolution, normal tissue equivalence and independency of energy, field size and direction of the incident radiation, should also be advantageous for dosimetric verification of radiotherapy using today's and tomorrow's dynamic delivery techniques. However, unfavourable properties have also been reported, such as dose rate-, temperature-, oxygen contamination-, and cooling rate dependencies. It has been shown in this thesis that these shortcomings can be overcome by using a good practice strategy, and that results can be obtained with an uncertainty comparable to other detector systems.

Modern dynamic treatment techniques such as for example breathing adapted radiotherapy have created a need for dosimetry during motion, which poses new challenges. The purpose of this thesis was to investigate the performance of polymer gel dosimetry in such situations. For comparison, measurements using 1D, 2D and quasi-3D detector systems, as well as Monte Carlo simulations, were used to validate the results obtained using gel dosimetry.

The absorbed dose integrating property during fractionated irradiation delivery was investigated for two different polymer gel systems. A fractionation dependency was observed, especially pronounced for one of the systems. This effect was further investigated using compartment modelling. The results indicated that the dose response was approximately independent of the fractionation scheme, provided that the total absorbed dose was delivered during the same total delivery time. Under respiratory-like motion no influence of the dose rate variation related to motion in and out of the beam was observed. Full 3D absorbed dose verifications were also carried out for advanced delivery techniques involving simultaneous beam intensity modulation and gantry rotation around the patient, so called volumetric modulated arc therapy (VMAT). Using both gel measurements and Monte Carlo simulations it was successfully demonstrated that the VMAT plan was both accurately calculated and delivered as planned. Additionally, the performance of a tumour-tracking system during VMAT delivery was investigated. The dosimetric measurements, obtained using both gel and a bi-planar diode array, verified the improved dose conformity when enabling the target tracking system.

In this thesis the unique 3D properties of gel dosimetry were fully utilized, and the known uncertainties were minimized in every step of the procedure. It was shown that polymer gel is a useful tool for relative 3D dosimetry in dynamic and breathing adaptive radiotherapy.

This thesis is based on the following papers, hereafter referred to by their roman numerals:

I **Dose integration characteristics in normoxic polymer gel dosimetry investigated using sequential beam irradiation**
Anna Karlsson, Helen Gustavsson*, Sofie Månsson**, Kim B McCauley and Sven Å.J. Bäck
Phys. Med. Biol. 52: 4697-4706, 2007

II **Verification of dynamic radiotherapy: the potential for 3D dosimetry under respiratory-like motion using polymer gel**
Sofie Ceberg, Anna Karlsson, Helen Gustavsson, Lena Wittgren and Sven Å.J. Bäck
Phys. Med. Biol. 53: N387–N396, 2008

III **Modelling the dose response of polymer gel dosimeters**
Sofie Ceberg, Martin Lepage, Crister Ceberg, Helen Gustafsson and Sven Å.J. Bäck
Manuscript

IV **RapidArc™ treatment verification in 3D using polymer gel dosimetry and Monte Carlo simulation**
Sofie Ceberg, Isabelle Gagne, Helen Gustafsson, Jonas Bengtsson Scherman, Stine S. Korreman, Flemming Kjær-Kristoffersen, Michelle Hilts and Sven Å.J. Bäck
Phys. Med. Biol. 55: 4885–4898, 2010

V **Real-time dynamic MLC tracking of moving target during modulated arc radiotherapy; dosimetric verification using 3D polymer gel and a bi-planar diode array**
Sofie Ceberg, Marianne Falk, Per Munck af Rosenschöld, Helen Gustafsson, Stine S. Korreman and Sven Å.J. Bäck
Submitted to Phys. Med. Biol.

**Sofie Månsson changed her name to Sofie Ceberg in October 2007
*Helen Gustavsson changed her name to Helen Gustafsson in August 2009.

A selection of peer reviewed proceedings and oral presentations at international conferences are listed below:

i **Dosimetric verification of breathing adapted radiotherapy using polymer gel** Sofie Månsson, Anna Karlsson, Helen Gustavsson, Johan Christensson and Sven Å .J. Bäck
Journal of Physics: Conference Series 56 300–303 (2006)

ii **Tumour-tracking radiotherapy: a dosimetric and geometric verification using polymer gel** Sofie Ceberg, Paul Keall, Helen Gustavsson, Fredrik Nordstrom, Jens Zimmerman, Gitte Persson, Joakim Medin, Amit Sawant, Michelle Svatos, Herbert Cattell, Sven Å. J. Bäck and Stine Korreman
Radiother Oncol 88:S24 (2008)

iii **RapidArc™ treatment verification using polymer gel dosimetry** Sofie Ceberg, Helen Gustavsson, Stine Korreman, Joakim Medin, Flemming Kjær-Kristoffersen and Sven Å. J. Bäck
Journal of Physics: Conference Series 164 012052 (2009)

iv **Radiotherapy delivery during motion** Sofie Ceberg and Sven Å. J. Bäck *Journal of Physics: Conference Series (2010), in press*

iv **Tumor-tracking radiotherapy of moving targets; verification using 3D polymer gel, 2D ion-chamber array and biplanar diode array** Sofie Ceberg, Marianne Falk, Per Munck af Rosenschöld, Herbert Cattell, Helen Gustafsson, Paul Keall, Stine Korreman, Joakim Medin, Fredrik Nordström, Gitte Persson, Amit Sawant, Michelle Svatos, Jens Zimmerman and Sven Å. J. Bäck
Journal of Physics: Conference Series (2010), in press

v **3D geometric verification of intraprostatic fiducial guided hypofractionated radiotherapy of prostate cancer using gel dosimetry** Fredrik Nordström, Sofie Ceberg, Sacha af Wetterstedt, Per Nilsson, Crister Ceberg, Sven Å. J. Bäck
Journal of Physics: Conference Series (2010), in press

vi **Tumor-tracking radiotherapy of a moving target during arc delivery: verification using polymer gel and a diode array** Sofie Ceberg, Marianne Falk, Per Munck af Rosenschöld, Helen Gustafsson, Stine Korreman and Sven Å. J. Bäck
Radiother Oncol 96:S74 (2010)

Abbreviations

DOSGEL	The international society for radiotherapy gel dosimetry
AA	Acrylamide
MAA	Methacrylic acid
nMAG	MAA and gelatin based normoxic polymer gel systems
nPAG	AA/BIS and gelatine based normoxic polymer gel systems
BIS	N,N'-methylene-bis-acrylamide
THP	Tetrakis(hydroxymethyl)phosphonium
NMR	Nuclear magnetic resonance
RF	Radio frequent
MSE	Multi-spin echo
TE	Echo time
TR	Repetition time
T2	Transversal relaxation time
R2	Relaxation rate
MRI	Magnetic resonance imaging
PTV	Planning target volume
OAR	Organ at risk
TPS	Treatment planning system
AAA	Anisotropic analytical algorithm
MU	Monitor unit
DVH	Dose volume histogram
CT	Computed tomography
MLC	Multileaf collimator
DMLC	Dynamic multi-leaf collimator
IMRT	Intensity modulated radiotherapy
VMAT	Volumetric modulated arc therapy
BART	Breathing adapted radiotherapy
MC	Monte Carlo
SD	Standard deviation
IR	Infrared
QA	Quality assurance

Table of Contents

1 Introduction

It is estimated that every third person now living in Sweden will be diagnosed with cancer at some point during their life time (The Swedish Cancer Foundation, 2009). Owing to the development of new efficient treatment techniques, today more than 60% of the cancer patients survive their disease.

Approximately half of all cancer patients will receive radiotherapy, either as the only treatment, or as an important part of their total treatment. Many of those who cannot be cured today, as well as those experiencing unnecessary side effects, may potentially benefit greatly from further improvements and developments of new radiation treatment techniques. However, novel treatment techniques are getting increasingly complex, and successful radiotherapy relies on the proper conduct of every step of the planning and delivery of the treatment. Even minor incidents may put the therapeutic effectiveness at a risk. Improved routines for verifying the absorbed dose to the patient are, therefore, highly desirable.

1.1 Why 3D Dosimetry?

There has been a fast development of new radiotherapy delivery techniques in recent years, aiming at decreasing the absorbed dose to healthy tissues without compromising the prescribed target coverage while at the same time decreasing the delivery time. However, techniques for dosimetric verification of these novel and highly advanced radiotherapy methods have not been developed at the same rate. The new advanced delivery techniques are often associated with moving beams, small fields and steep dose gradients. Sometimes also tumour motion needs to be accounted for. For the above reasons, a thorough dosimetric verification should ideally be done in 3D.

An ideal detector system would offer true 3D time resolved (4D) dose measurements that successfully isolate the parameter under investigation. The system should be patient-like, provide high-resolution, be fast, and offer total insight into and control of the potential detector corrections. Awaiting this development, we need to be careful to apply the right detector system at the right place for the right reason.

The dose distribution of a volumetric modulated arc-therapy (VMAT) is created by modulating the output of the linear accelerator and simultaneously rotating the gantry around the target. The multi-leaf collimator (MLC) positions, dose rate and gantry rotation speed are varied during the delivery and the plans often appear with complex

apertures such as single leaf openings and disconnected small segments. Combining this advanced treatment delivery with breathing adapted treatment techniques represent a new level of complexity and a thorough dosimetric verification is therefore necessary.

Polymer gel dosimetry could provide an independent 3D detector system with the desired characteristics. As such, it can be used, for instance, for benchmarking when introducing new treatment techniques in the clinic. This adds an extra dimension to our continuous strive for improved patient safety.

1.2 3D Polymer Gel Dosimetry

The polymer gel dosimeter contains approximately 90% water, 5% radiation sensitive chemicals (monomer) and 5% gel matrix substance (Figure 1). When the dosimeter is exposed to irradiation polymerisation occurs. The matrix holding the new polymer structures in place preserves the spatial information of the exposure. Thus, the induced changes may be read-out to obtain a 3D absorbed dose distribution.

Unlike other detector systems commonly employed in the field of radiotherapy the response of the gel is independent of energy, field size, and the direction of the incident radiation (Olsson et al., 1998, Novotny et al., 2001, De Deene et al., 2006a). Furthermore, the polymer gel is soft tissue equivalent (Keall and Baldock, 1999) and the system functions both as a phantom and a detector. An extensive review on polymer gel dosimetry was recently published (Baldock et al., 2010), describing the history of gel dosimetry and the fundamental principles.

Generally, the use of polymer gel dosimetry involves three steps; fabrication, irradiation, and read-out. When preparing the polymer gel, gelatine, which is used as the matrix substance, and ultra pure deionized water are mixed before adding the monomers.

Oxygen hinders the radiation-induced polymerization through the formation of peroxides (Fuxman et al., 2003, Appleby, 1999). Therefore an oxygen scavenger which binds to the oxygen is added to the gel mixture. The fabrication of the polymer gel has become less complicated after the use of an oxygen scavenger was introduced in the early 2000´s, allowing the preparation to take place under normal levels of oxygen (Fong et al., 2001). These gels are called normoxic gels.

Apart from the glassware, a scale, a hotplate, a thermometer and a stirrer is all the laboratory equipment needed to produce a polymer dosimeter.

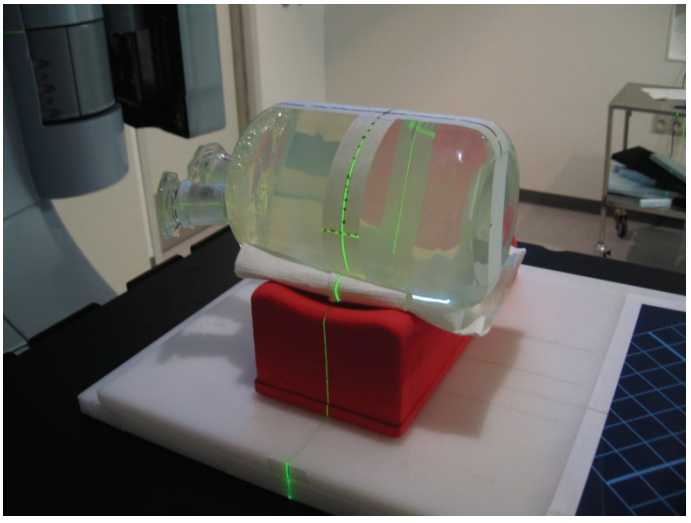

Figure 1. A 1.3 litre gel dosimeter in a glass container.

When the gel dosimeter is irradiated the radiolysis process starts immediately, i.e. water molecules are separated into several highly reactive radicals and ions. It is these entities that affect the monomers in the solution rather than the radiation directly (Fuxman et al., 2003). The number of created reactive free radicals is directly proportional to absorbed dose. The polymerisation process is induced by the free radicals, and the polymer molecule continues to grow through chain propagation reactions. Termination of the polymerisation reaction usually occurs when two polymer chains react and form a stable unit (Fuxman et al., 2003).

Magnetic Resonance Imaging (MRI) is the most commonly used read-out technique for polymer gel dosimetry (Maryanski et al., 1993). The nuclear magnetic resonance (NMR) relaxation rates of the protons in the water pool of the polymer gel are affected with the change in structure that follows upon polymerisation. The transversal relaxation time (T2) decreases exponentially with increasing absorbed dose (Figure 2a), and an approximately linear relation between the absorbed dose and the relaxation rate, R2=1/T2, is achieved within a limited absorbed dose interval (Figure 2b).

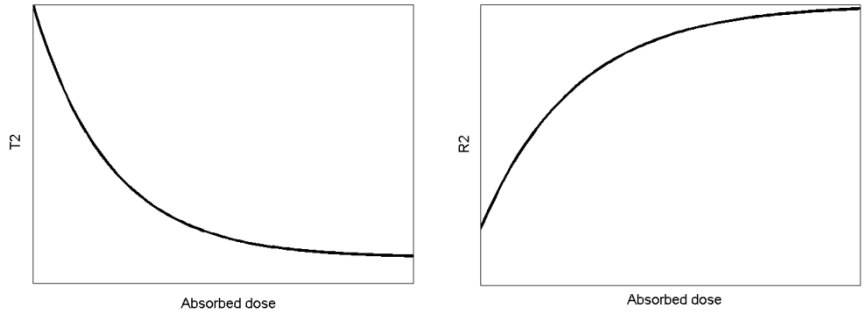

a) **b)**

Figure 2. Schematically drawings of the MRI parameters a) T2 and b) R2 versus absorbed dose for polymer gels.

Other (3D) read-out techniques with specific parameters sensitive to the result of the irradiation can be used to obtain the dose information. For instance, the polymerized gel becomes visibly opaque and the mass density changes. Thus, optical-computed tomography (CT) or X-ray CT (Hilts et al., 2000, Jirasek et al., 2010, Brady et al. 2010) are alternative methods to MRI.

Uncertainty analysis have been carried out for the MRI polymer gel dosimetry procedure (Karlsson, 2007, De Deene et al., 2006). Using a good practice strategy, reliable results can be obtained with an uncertainty comparable to other detector systems (Baldock et al., 2010). By "good practice" it is implied that the whole fabrication-to-evaluation chain is optimized in order to minimize the known uncertainties.

Owing to the advantages mentioned above (Section 1.2), gel dosimetry has been suggested to play an important role in benchmarking the performance of new treatment techniques and in the regular Quality Control (QC) of IMRT (DOSGEL 2006).

1.3 The Objectives of This Thesis

The overall aim of this thesis was to dosimetrically verify advanced dynamic and breathing adapted radiotherapy delivery techniques. Existing techniques as well as systems under development were investigated. Within this overall aim, the following goals were established:

- ✓ To investigate the dose integrating properties of different polymer gel system, in particular the fractionation dependency.

- ✓ To design a compartment model in order to simulate the dose response of the polymer gel dosimeter to various fractionation schemes.

- ✓ To investigate whether polymer gel is a feasible dosimeter for absorbed dose measurements under respiratory-like motion; during respiratory gating and tumour-tracking delivery.

- ✓ To perform and evaluate 3D dosimetric verifications of advanced dynamic and breathing adapted radiotherapy deliveries.

- ✓ To further investigate treatment plans and delivery techniques by using additional detector systems and Monte Carlo simulations.

2 Background

2.1 Dynamic Delivery Techniques

The advantage presented by novel radiotherapy techniques introduced in recent years is the increased possibility to deliver high absorbed dose to the target volume while minimizing the dose to normal tissues. By using these dynamic delivery techniques, involving modulated moving small fields and rotating the linear accelerator gantry, the conformity increases but also the difficulty to dosimetrically verify the actual delivery.

2.1.1 Breathing Adaptive Radiotherapy

Intra-fractional tumour motion, mostly due to respiration, can be a major challenge to the delivery of the desired dose distribution. For instance, tumour movements of 10–20 mm peak-to-peak due to respiratory motion are common, and cases of lung tumour movements of up to 30 mm have been reported in the literature (Seppenwoolde et al., 2002). A primary concern treating these patients is unwanted pulmonary and cardiac irradiation, which implies an increased risk of injury from late toxicity (Korreman et al., 2006).

Several different strategies have been developed to account for and to reduce motion related uncertainties. Today the most widely used approach to account for organ motion is to collect a large data set of measured positions in the respiratory cycle. This data can then be used to calculate the statistical spatial distribution and incorporated into the treatment planning procedure as an additional margin to the Planning Target Volume (PTV) (Langen and Jones, 2001). Another method is to directly introduce respiratory related uncertainties into the dose calculation, by convolving the static dose distribution with a motion function (McCarter and Beckham, 2000). However, although the motion related uncertainties decreases using the above methods, the increased margins, implies an elevated risk of secondary injury. Breathing adapted radiotherapy techniques have been developed, and are under development, to react on this problem.

<u>*Respiratory Gating and Breath-hold*</u>

The most obvious approach to reduce the effects of respiratory motion is to ask the patient not to breathe during beam-on. This period can typically have a duration of 15–30 s. Breath-hold techniques can either be voluntary (Pedersen et al., 2004) or “active” (Wong et al., 1999) (Figure 3).

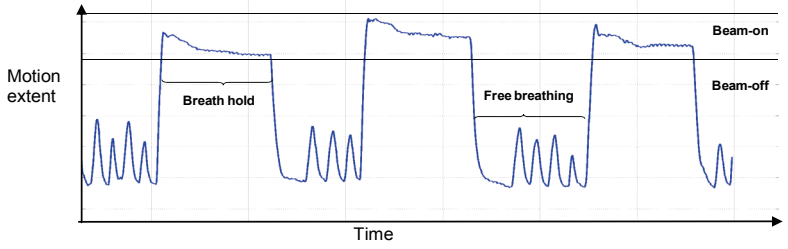

Figure 3. An illustration of the breathing curve during a breath hold delivery. The patient hold a deep inspiration within the gating window, which allows beam on. Between the deep inspirations the patient breathe normally.

Another approach is to turn the beam on only when the target is in a favourable position during the patient's normal respiratory cycle, i.e. the so called respiratory gating technique (Ohara et al., 1989) (Figure 4). The advantages of this approach, when treating lung- and breast cancer patients, are i) a reproducible known position of the target volume and organs at risk (OAR) throughout the treatment, ii) the irradiated lung volume will be reduced, and iii) the cardiac toxicity will be reduced (Korreman et al., 2006).

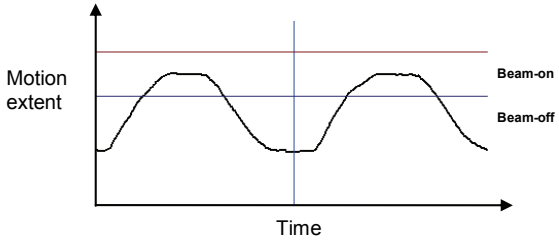

Figure 4. An illustration of a breathing curve during respiratory gating delivery. When the breathing amplitude is in the end of the inspiration phase the beam is turned on.

During deep inspiration, as with breath-hold and respiratory gating methods, the irradiated lung density are reduced due to the 40–50% increase in lung volume compared to the resting value (Giraud et al., 2006). This reduction in lung density can affect the dose to peripheral parts of the target volume due to loss of electronic equilibrium. Monte Carlo simulations have verified this impact on the TPS calculations and demonstrated the risk of target underdosage (Yorke et al., 2002). No 3D dosimetric measurements have verified this underdosage. However, low-density (approximately lung tissue equivalent) polymer gels may enable such measurements (De Deene et al., 2006b, Haraldsson et al., 2006).

Furthermore, depending on the size of the gating window during breath-hold or respiratory gating a certain dose smearing of the field edges due to movement during the beam-on time will remain (Li et al., 2006). This dose smearing effect is not accounted for using conventional treatment planning systems and dosimetric verifications are required. Experimental data have mostly been obtained using ionisation chambers and film (Duan et al., 2006, Li et al., 2006). Published data obtained using 3D polymer gel dosimetry (Ceberg et al., 2008a, Månsson et al., 2006) or another novel 3D dosimetry system (radiochromic plastic, described in Section 2.3.2; Brady et al., 2010) show good agreement between static and gated measurements.

Tumour Tracking

Another method to compensate for respiratory motion during treatment is tumour tracking. This is a novel promising pre-clinical research tool that uses the dynamic multileaf collimator (DMLC) to continuously align and reshape the treatment machine aperture to follow the target motion in real time (Sawant et al., 2008). The DMLC real-time tumour-tracking system developed at Stanford University (Keall et al., 2001) uses two infrared (IR) cameras and passive IR reflecting spheres that are placed on the surface of the patient or detector system. The IR cameras emit a low IR signal that is reflected and analysed for positioning information. Since the IR system samples the marker positions at a frequency of 20 Hz it can not only be used for a precise set-up verification of a patient or detector but also to monitor patient respiratory motion (Jin et al., 2008).

The advantage of this technique is the ability to allow for a tighter margin around the target by continuously following, and adapting, the dose delivery to its motion. Thus the possibility to deliver a high absorbed dose to the target volume while minimizing the dose to normal tissues is increased. Compared to the breath-hold and respiratory gating methods, the tumour tracking technique potentially offers additional benefits such as higher delivery efficiency and less residual target motion.

To enable DMLC tracking, the jaws are withdrawn to allow any leaf pairs to be opened if the target starts to move. On both sides of the MLC shaped opening there are always a constant number of adjacent central leaf pairs, ready to participate if the target begins to move in that direction (Falk et al., 2010). To minimize the transmission between the closed leaf tips of remaining leaf pairs outside the adjacent central leaf pairs, the tracking system moves the non-participating leaves to the side underneath one of the x-jaws. The MLC will be positioned to optimally fit the instantaneous target location and minimize the leakage through the

MLC leaves by moving non-tracking pairs under the nearest jaw. The DMLC-tracking controller methodology also includes beam-off when anomalous situations occur, such as sudden changes in the respiratory pattern or coughing (Sawant et al., 2008).

The real-time beam adaptation is not feasible without precise real-time localization of the tumour position in 3D. This includes parallel and perpendicular motion to the MLC leaf travel direction, in- and out-of-plane rotation as well as translation along the beam direction. Recently, a 4D treatment planning method that accounts for 3D tumour motion was proposed (Suh et al., 2009). The method uses 4D CT and is integrated with the DMLC tumour-tracking delivery. This method opens up for a clinical implementation of the DMLC tumour-tracking system.

However, few dosimetric measurements have been carried out (Zimmerman et al., 2009, Tacke et al., 2010). Dosimetric uncertainties associated with a DMLC tracking system arise from the estimation of the actual target position, possible delay between target motion detection and beam repositioning and output variations due to dissimilar collimator settings in tracking mode compared to static mode.

This pre-clinical DMLC-tumour tracking technique was investigated in Paper V.

2.1.2 Volumetric Arc Therapy

Volumetric Arc Therapy (VMAT) is a novel radiation therapy technique where the treatment is delivered during one or a few rotations of the linear accelerator gantry. The dose distribution in VMAT is created by simultaneously modulating the beam intensity and varying the MLC positions, the rotation speed of the gantry and the dose rate during the treatment (Otto, 2008). The VMAT technique RapidArc from Varian Medical Systems was first introduced clinically in 2008, and, according to a number of planning comparison studies, the target volume coverage and sparing of the normal tissue was better than or as good as conventional intensity modulated radiotherapy (IMRT) (Kjaer-Kristoffersen et al., 2009, Palma et al., 2008, Popescu et al., 2010, Shaffer et al., 2009). Additionally, the number of monitor units (MU) delivered and the treatment time were both decreased compared to IMRT with sliding window technique (Alexander et al., 2008, Palma et al., 2008).

In general, VMAT treatment plans commonly exhibit complex apertures, such as single isolated leaves and disconnected small segments. Furthermore, RapidArc plans are delivered dynamically with leaf and gantry motion up to approximately 1 cm and 2º per second, respectively.

RapidArc treatment planning calculations have previously been verified using Monte Carlo (MC) simulations (Bush et al., 2008, Gagne et al., 2008, Teke et al., 2010), and a recently published paper reported on the dosimetric verification of a VMAT treatment delivery using a bi-planar diode array detector system (described in Section 2.3.1) (Korreman et al., 2009). Very good agreement between the treatment planning system (TPS) and dose measurements was obtained, as well as reproducibility of consecutive deliveries.

This VMAT technique was investigated in Paper IV and V.

2.1.3 Breathing Adapted Volumetric Arc Therapy

The combination of VMAT with a breathing adapted treatment delivery represents a major advanced dynamic delivery procedure, and dosimetric measurements can be technically challenging. Dosimetric uncertainties associated with target motion, gantry motion, small fields and steep dose gradients have to be evaluated in detail, and this requires adequate 3D dose verification tools.

Recently, it was reported that it is feasible to perform DMLC-tracking during a VMAT delivery (Zimmerman et al., 2009). A pre-clinical 3D DMLC-tracking application was dosimetrically evaluated using a 2D ion chamber array (described in Section 2.2.2) and a bi-planar diode array detector system (described in Section 2.3.1). An additional study, also using the bi-planar diode array detector, verified that the dosimetric accuracy was independent of the magnitude of the peak-to-peak displacement (5-25 mm) of the target and not significantly affected by the angle between the leaf trajectory and the target movements (Falk et al. 2010). However, further studies using an independent high resolution 3D detector would be of great interest.

This breathing adapted VMAT technique was investigated in Paper V.

2.2 Conventional Detector Systems

3D polymer gel dosimetry was used in all studies within this thesis. Measurements have also been undertaken using additional 1D, 2D and 3D detector systems. These detector systems are briefly described in this chapter together with some other relevant measurement techniques.

2.2.1 1D Array

A linear detector array that holds 99 diodes, with a centre-to-centre distance of 5 mm and an active length of 49 cm, has recently been dosimetrically characterised (Ottosson et al., 2008) (Figure 5). The reproducibility of consecutive measurements, reproducibility over time, linearity, direction dependence and dose rate dependence was investigated. Output factor comparison was carried out and apart from a directional dependence of up to 10%, the results for the linear detector array showed good agreement with reference data. The largest observed output deviation was less than 1% for field sizes $\geq 4 \times 4$ cm^2. Correction factors for an over-sensitivity at low energies, due to low energy scatter, are embedded in the software.

This 1D diode array was used as a reference detector for the study described in Paper II.

Figure 5. A linear detector array, here mounted on a robot simulating respiratory-like motion.

2.2.2 2D Arrays

A number of 2D detector array systems are used in QC of radiotherapy. The electronic arrays, consisting of either diodes or ionisation chambers, vary in detector size and spacing but share the same design approach of being 2D dosimeters originally intended for irradiation with the beam central axis perpendicular to the detector plane. All of them can be used for verification of individual (segment) as well as integrated (composite) fields (Figure 6).

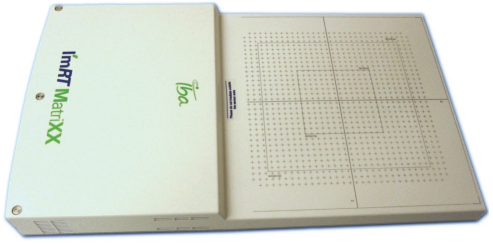

Figure 6. An example of a conventional 2D ion chamber array.

One example of the commonly used 2D array consists of 445 n-type diodes distributed over an area of 22 × 22 cm^2, with a center-to-center distance of 7.07 mm within the central 10 ×10 cm^2 region of the detector, and 14.14 mm in the remaining detector area. Each diode is 0.8 × 0.8 mm^2. During calibration of the system the diode outputs are corrected for variation in radiation sensitivity, and can be calibrated to be within ± 1% (Letourneau et al., 2004). Output factors measured for different field sizes with the central diode and a Farmer-type ionisation chamber agreed generally within 1% for field sizes ≥ 4 × 4 cm^2. Further, the dose-response relation was linear up to 3 Gy and a dose rate dependency of less than 2% was confirmed (Letourneau et al., 2004).

Several 2D detector arrays use ionisation chambers, arranged in lattice sizes from 27 × 27 to 32 × 32, with a minimum ion chamber center-to-center distance from 7.62 to 10 mm (Spezi et al., 2005). The output factors for field sizes from 5 × 5 cm^2 to 12 × 12 cm^2 have been measured to be within 1% of corresponding Farmer-type ionisation chamber measurements (Amerio et al., 2004). However, when comparing output factors for smaller field sizes obtained using reference detectors with smaller spatial resolution, the differences increased (Stasi et al., 2005). For field sizes in the range 3 × 3 cm^2 to 5 × 5 cm^2 a maximum difference of 1.9% was found, and for a 2 × 2 cm^2 field, a difference of 3.1% was observed between chamber array and reference detector data

(Stasi et al., 2005). The dose-response of ionization chamber arrays has been reported to be linear up to 5-10 Gy and have a dose rate dependency within 1% in the range of 0.5 to 6 Gy/min (Amerio et al., 2004, Stasi et al., 2005).

The detector spacing in the 2D array limits the spatial sampling of the radiation beam, and different recommendations of how to increase the resolution have been published (Spezi et al., 2006, Spezi et al., 2005, Poppe et al., 2007). For instance, data can be obtained from multiple beam deliveries with the 2D detector array in different positions. The array can for example be repositioned using a remote-controlled movement of the treatment couch.

A 2D ion chamber array was used as a reference detector for the study described in Section 4.3 (Ceberg et al. 2008).

A number of 2D arrays have been developed for volumetric dose verification of rotational therapy techniques, used in combination with an add-on gantry angle sensor. An ion chamber array was recently investigated and a relatively large variability in response as a function of gantry angle (up to 11%), specifically in angle ranges between 91°–110° and 269°–260°, was found (Wolfsberger et al., 2010). To correct for the angular dependency, a new calibration method was developed. By using a reference phantom that matches the geometry of the 2D array but without the internal structure, and a reference detector, which has no measurable angular dependency, a calibration factor was defined as the ratio of these measurements. When the 2D array measurement was corrected using this calibration factor the angular dependency was decreased to approximately 1% (for fields other than AP fields) (Wolfsberger et al., 2010).

2.3 Alternative 3D Dosimetry Methods

Together with polymer gel dosimeters other 3D and "quasi"-3D dosimetry system have been introduced to the radiotherapy area. Some of them are presented in this chapter.

2.3.1 Reconstructed Patient Dose Distribution

One possible way to carry out volumetric dose verification is to use the measurements obtained from a 2D detector system to reconstruct a 3D dose distribution.

A 2D detector assembly can be mounted directly onto the gantry, for instance in the wedge slot of the linear accelerator (Venkataraman et al., 2009). By using this transmission device real-time dose measurements can be acquired of all fields and arcs during treatment delivery. Based on these 2D fluence measurements in conjunction with

patient CT information, a reconstructed dose distribution in 3D can be utilized.

Another method that reconstructs a 3D dose distribution from 2D data is electronic portal imaging device (EPID) transmission-dosimetry. A novel method using EPID transmission-dosimetry to perform 3D EPID dosimetry has recently been introduced (Wendling et al., 2009). The dose was reconstructed within the patient volume in multiple planes parallel to the EPID for each gantry angle. By summing the 3D dose grids of all beams, the 3D dose distribution for the treatment was obtained. This 3D back-projection method has been further modified to make it applicable to volumetric modulated arc therapy (Mans et al., 2010). A connection between the treatment machine and the EPID acquisition software has been used to obtain gantry angle-resolved dosimetric information.

The total EPID 3D dose distribution of a VMAT delivery is a summation of all 3D dose distribution of all individual frames, each derived by the back-projection method, where the transmission is estimated from the CT data. Corrections for the transmission through the couch, and the EPID arm displacement due to gravity, are applied to each individual frame. In addition, a correction for the EPID sensitivity is applied to the total 3D dose. Good agreement between EPID reconstructed and planned dose distributions has been reported (Mans et al., 2010), which shows the potential for a 3D dose verification of a VMAT delivery using EPID dosimetry.

A novel method unlike the two previously mentioned, in the way that the detector is not moving with the gantry, consist of two orthogonal 2D detector arrays (Sadagopan et al., 2009). This bi-planar diode array is placed on the couch and consists of a cylindrical PMMA phantom with the two orthogonal 2D detector boards inside (Figure 7). A 3D dose array is obtained using TPS calculated depth dose data and interpolation of data measured in the two planes. One plane, the so called “main board” has a measurement area of 20 × 20 cm^2 and the other plane consists of two “wings” covering 20 × 10 cm^2 each. The planes are aligned +50° (main board) and -40º (wings) from the vertical plane. Due to the orthogonal arrangement of the detector arrays it is ensured that the dose modulation information is not lost regardless of the beam incidence angle. The detector system has in total 1069 *p*-type cylindrical silicone diodes covering the measurement area. The diode size is 1 mm in diameter and 0.05 mm thick and the centre-to-centre distance is 5 mm in a central 6 × 6 cm^2 region of the detector and 10 mm in the remaining measurement area.

Recently, the bi-planar diode detector was characterized, demonstrating dose response linearity, dose rate independence and good reproducibility

(Nilsson, 2007, Sadagopan et al., 2007, Xue, 2007). However, a number of correction factors have to be applied to the measured data to allow conversion to absorbed dose. For instance, the measurements have to be corrected for the intrinsically varying sensitivity of the diodes, the temperature variation during calibration and measurements, and the directional dependence, both for the gantry angle and the diodes' position along the phantom's longitudinal axis. The directional dependency decreased from approximately ± 3% to less than ± 2% using a correction factor obtained from an average from 21 randomly selected diode measurement (Feygelman et al., 2009).

Rotational, depth, and field-size correction factors are obtained from standard beam irradiations and applied on a segment-by-segment basis to every individual diode. Correction factors are embedded in the software and are neither editable by, nor visible to, the end user. The dose-errors would have ranged from -4.7% to 0.8% without these corrections (Feygelman et al., 2009). With the corrections and under optimal conditions, e.g. with no beams incident along the detector boards and provided no steep dose gradient are present, 99.8% of the diodes read within 3% of the expected value.

The detector system has tools for a semi empirical volumetric dose calculation which uses data from incident rays that are traced from the source through the phantom. Any ray will intercept at least one, and usually both, detector planes, yielding one or two measured dose points along that ray. The system then renormalizes the treatment planning system (TPS) calculated depth dose along the same ray to fit the measurement points, and uses those data to reconstruct the dose in 3D.
The system samples data only during the dose pulse. All channels are read simultaneously and reset after each pulse. The synchronization of dose delivery and measurements adds a temporal dimension to the acquired data, which means that each segment of an IMRT plan can be associated with an individual dose measurement. For rotational treatments using conventional linacs, additional gantry angle information is obtained from an independent inclinometer mounted on the gantry.

The bi-planar diode array detector was used for absorbed dose measurements in the study described in Paper V.

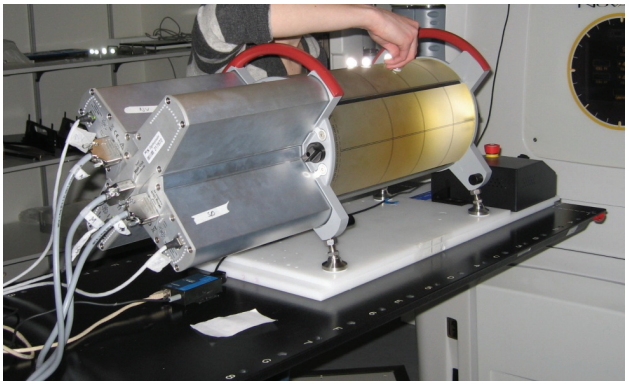

Figure 7. A bi-planar diode detector array, here positioned on a moving platform simulating respiratory-like motion.

2.3.2 Radiochromic Plastic Dosimetry System

A novel 3D dosimetry system consisting of a radiocromic plastic dosimeter and an optical-computed tomography (optical CT) scanner for absorbed dose read out has been suggested (DOSGEL 2006, Brady et al., 2010). The plastic is doped with leuco dye, which is a dye whose molecules may acquire two forms; one that is clear (colourless) and one that appear colourful. Once the plastic is irradiated the change in colour is proportional to absorbed dose (Adamovics and Maryanski, 2004). Published data showed that the dose response was linear up to 50 Gy and no photon energy dependence (1.25 – 18 MV) or dose rate dependency (1–6 Gy min^{-1} up to 5 Gy) was found (Adamovics and Maryanski, 2006).

The collected data, i.e. the optical projections, for the optical-CT technique can be acquired in different ways. One way is to scan a laser across the dosimeter, which is detected by a photodiode detector. Another way is to let a broad light field pass through the dosimeter and be collected by a charged coupled device (CCD). The principles optical CT is the same as for the x-ray CT, achieving a 3D reconstruction using filtered back-projection (Wuu and Xu, 2010).

This plastic/optical CT 3D dosimetry system has further advantages such as the plastic being insensitive to oxygen and of solid texture, allowing measurements without the requirement of an external container. In addition, some optical CT scanners are capable of acquiring a complete 3D data set within five minutes (Brady et al., 2010). However, the samples are limited in size and with a density different from water, which reduces its capability to be used in the form of anthropomorphic phantoms. Leuco-dyed plastic dosimeters (Figure 8)

have become commercially available, and further developments in this area are to be expected.

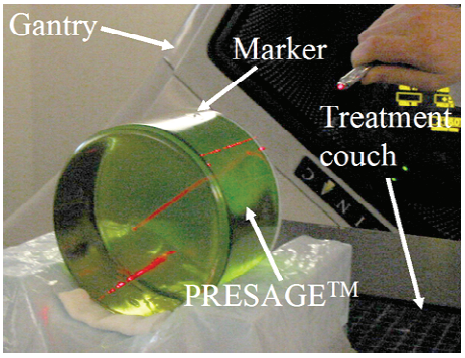

Figure 8. The Radiochromic plastic 3D dosimeter. Photo Courtesy of Mark Oldham, Duke University Medical Center.

3 Materials and Methods

3.1 Polymer Gel Manufacturing, Irradiation and Read-out

3.1.1 Compositions and Manufacturing

Two types of normoxic polymer gels have been investigated in the studies included in this thesis. Both types of gel were mixed in a fume cupboard, under normal levels of oxygen. The ingredients were always ultra pure deionised water (resistivity > 18.2 MΩcm), gelatine (swine skin, 300 bloom, Sigma Aldrich), monomers and an antioxidant. The gelatine, which was used as a matrix substance, was mixed with water in room temperature and the mixture was heated to 45°C for the gelatine to completely dissolve. Up to this point the manufacturing procedure was the same for both types of polymer gel. For the nMAG gel type (Papers I, II and III) the heat was then turned off and the Methacrylic acid (MAA) (~99% titration, Sigma Aldrich) was added when the mixture temperature had decreased to 35°C. After approximately another 10 minutes the Tetrakis(hydroxymethyl)phosphonium (THP) antioxidant (techn. ~80% in water, Sigma Aldrich) was added.

For the nPAG type gel (Papers I, II, IV and V) the Acrylamide (AA) (electrophoresis grade, ≥ 99%, powder, Sigma Aldrich) was added to the 45°C mixture. When the monomers had completely dissolved (after about 30 minutes), the N,N'-methylene-bis-acrylamid (BIS) (electrophoresis grade, ≥98%, powder, Sigma Aldrich) was added. After the BIS was dissolved the solution was left to cool down to 35°C before the THP was added.

The gel was then poured into phantoms and glass vials and were left in the dark to set at room temperature. Even if an oxygen scavenger is used, oxygen contamination will affect the polymerization process (Sedaghat et al., 2010). Thus, it is preferable to use phantom material with no or low oxygen permeability (Oldham et al., 1998, Bonnett et al., 1999). Glass containers were used in all studies in this thesis.

3.1.2 Irradiation

The irradiation was carried out approximately 24 hours after the gel was manufactured. Each experiment typically included a larger gel phantom (see applications, Section 3.3) and a number of glass vials (15 ml, Ø 1.5 cm, length 6 cm), which were filled with gel from the same batch. The vials were used for confirmation of linearity of the absorbed dose response, but also for evaluation of absorbed dose response

characteristics. In all studies, the vials were irradiated at 3 cm depth in a 30 × 30 × 30 cm^3 water phantom. The source-to-surface distance (SSD) was 100 cm, the gantry angle 90º and field size 20 × 20 cm^2.

3.1.3 Read-out and Data Processing

Read-out was carried out approximately 20 hours after irradiation, using a 1.5 T MRI scanner (Siemens Symphony, Siemens Medical Solutions, Germany).

Due to the temperature dependency of R2 (e.g. Spevacek et al., 2001, De Deene et al., 2007, De Deene et al., 2006a) the gel phantoms and vials were stored in the scanning room for about four hours before scanning to ensure temperature equilibration within the gel volumes.
The gels were centrally positioned in the head coil (receiver), and scanned using the body coil as transmitter. A 32-echo multi-spin-echo sequence was used for both nMAG and nPAG gels, with inter echo times (TE) of 10.6 ms and 25 ms, respectively. The repetition time (TR) was at least 4000 s for all acquisitions. The voxel sizes were 1.0 × 1.0 × 3.0 mm^3 and two acquisitions were averaged for each scan.

For the quantification of T2, multi spin echo (MSE) sequences were used (De Deene and Baldock, 2002). The signal, S, decays mono-exponentially with time To obtain T2, a number of signal images were collected at various echo times (TE) (equation 1).:

$$S = S_0 \cdot e^{-\left(\frac{TE}{T2}\right)} + C \qquad (1)$$

In the above equation, S_0 is the signal at TE = 0, and C is the background value. Chi-square fits, optimized using the Levenberg-Marquardt algorithm, was used to obtain T2 . All T2 calculations in this thesis were undertaken using in-house developed software (Karlsson et al., 2003).

The response of the irradiated gel phantoms was converted to relative absorbed dose using background subtraction and normalization in a region of homogenous dose (Bjoreland et al., 2008).

The background value was obtained in a container of the same size as the gel phantom, rather than a vial, as it has previously been shown that the cooling history of the gel plays an important role in determining the absorbed dose (De Deene et al., 2007, Dumas et al., 2006). To keep the temperature history after fabrication as similar as possible for the gel dosimeter phantoms, the dose response vials and the background phantom were all stored together during the entire fabrication-irradiation-and-read out-chain.

MATLAB 7.4.0 was used for all image processing, 3D rendering and 3D gamma evaluation. A box-filter (3 × 3 × 3) was applied to the gel arrays and the inner surface of the container was used for alignment of measured and calculated data. Data arrays were linearly interpolated to 1 × 1 × 1 mm^3 cubic voxel size to enable 3D gamma evaluation (Papers IV and V, section 3.2.3).

3.2 Gel Dosimeter Characteristics

As stated previously, the overall aim of this thesis was to use gel dosimetry for absorbed dose verification in 3D of complex radiotherapy delivery techniques such as volumetric arc therapy and dynamic MLC-tumour tracking delivery. Before this could be carried out, the uncertainty from parameters that would possibly affect the dose response in these situations, including dose rate and fractionation dependency, was estimated.

3.2.1 Uncertainty Analysis

Factors such as dose rate or fractionation- dependent response and a temperature dependent response may have an influence on the accuracy on the measured absorbed dose. If the gel phantoms have cooled down at different rates before irradiation, an additional inaccuracy has to take into account. Furthermore, during MR scanning, possible dose inaccuracies originate from dose-related imaging artifacts and a scanning temperature-dependent response. Controlling all these factors by using "good practice" will decrease the uncertainty of the polymer gel dosimetry experiment (Karlsson, 2007, Baldock et al. 2010).

In the clinical applications presented in this thesis, the nPAG system, containing 3% AA, 3% BIS and 5% gelatine, was used and evaluated at an absorbed dose level of 3-4 Gy. For this gel system, an uncertainty analysis regarding the measured absorbed dose was carried out following the Guide to the expression of uncertainty in measurement (GUM) (ISO, 2008). The uncertainty distributions were assumed to be normally distributed, and all uncertainties were assumed to be uncorrelated. The uncertainties were estimated and evaluated based on published data.

3.2.2 Fractionation Dependency

In advanced dynamic radiotherapy, the gel dosimeter will be exposed to fractionated irradiation and a varying dose rate. In a series of feasibility studies preparing for the pre-clinical applications, the dose response of the gel dosimeter to fractionated irradiation was therefore investigated. In the first of these studies, the dose response of the gel was recorded for

four different fractionation schemes. A total dose of 10 Gy was delivered in fractions of 0.25, 0.5, 1 and 2 Gy (Paper I). The beam was turned off for approximately 70 s between two subsequential fractions, which was considered as a clinically relevant time between individual beams for a conventional treatment.

In addition, the fractionation dependency was evaluated using beam-on and beam-off periods corresponding to a respiratory gating delivery (Paper II). Vials filled with nPAG or nMAG gel were irradiated, using gated delivery with 12 MU/beam or delivering the entire dose in one fraction. The vials receiving gated delivery were irradiated every 6.5 s, simulating a normal breathing period. The gel response for total absorbed doses between 0.5 and 4.0 Gy was investigated for the two types of delivery.

3.2.3 Motion-related Dose rate Dependency

Preparatory feasibility studies were also carried out with the aim to investigate possible effects on dose response stemming from the dose rate variation in the gel caused by the motion in and out of the beam (Paper II). One phantom was irradiated in a static position and one was irradiated during a respiratory-like motion with a 12 mm peak-to-peak motion extent.

The motion, corresponding to a representative chest wall movement during respiratory gating, was achieved using an in-house designed and built BERT (Breathing simulation Equipment in Radiotherapy) robot (Figure 5, Section 2.2.1). The motion could be varied in amplitude, frequency and curve pattern using 54 two-dimensional vectors containing information about position and velocity. A respiratory-like motion could be mimicked, with plateaus corresponding to the end-inspiration and end-expiration breathing phases. Additionally, the BERT robot was mounted on a fixation device designed for Varian couches and the position of the moving platform was verified using the Varian real-time positioning management system (RPM, Varian Medical Systems).

To isolate the effect from possible dose rate dependency caused by the motion in and out of the beam, the dose profile from a gel irradiated under motion was compared with the dose profile from a static gel irradiation, mathematically convolved with the motion function. Thus, any deviation between the convolved and measured data (in motion) would suggest an additional effect caused by dose rate dependence. The motion function was calculated from the velocity and position vectors controlling the respiration robot. For dosimetric verification of the

dynamic gel data, measurements using a linear diode array (described in Section 2.2.1) were also carried out.

During a dynamic MLC tumour tracking delivery, possible dosimetric uncertainties arise from the estimation of the actual target position, possible delay between target motion detection and beam repositioning and output variations due to e.g. dissimilar head-scatter conditions during off-axis irradiation. Before verifying a treatment with the tumour-tracking system adapted to an advanced radiotherapy delivery technique, a feasibility study was carried out in a simplified set-up with a circular beam and a 1D motion parallel to the MLC trajectory (Ceberg et al., 2008b). Additional measurement of the same delivery was carried out using a 2D ion chamber array (described in Section 2.2.2).

3.2.4 Theoretical Modelling

In order to develop the understanding of the dose rate- and fractionation-dependency of the gel dosimeter, the basic dose response characteristics were studied theoretically. For this purpose, a compartment model was developed (Paper III) in order to model the effects of dose rate and fractionation schemes on the resulting R2 values.

In this model, the protons in the gel were divided into different pools, or compartments, (Figure 9). Initially, before radiation, all protons are contained in the first compartment. As the radiation induced polymerization proceeds, protons are transferred from one compartment to another (Lepage et al., 2001).

The polymerization process is quite complex (Fuxman et al. 2004), and it is not trivial to establish well-defined proton compartments. Known steps in the polymerisation process were omitted for simplicity. The first generation model used here included two competing processes to be able to reproduce the observed effects of dose rate and fractionation scheme (De Deene et al., 2006a, Karlsson et al., 2007). Two basic compartments were assumed; one containing mobile protons associated to monomers, water and the gel matrix, and one containing protons associated to growing polymers and the resulting polymer network. Further, the second compartment was divided into three sub-compartments.

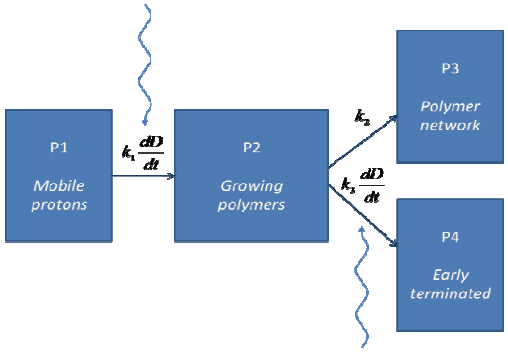

Figure 9. The compartment model used in the study. P1-P4 denotes the four different proton pools. The k-values are the transfer coefficients and the light blue arrows indicate irradiation.

In this model, at time t = 0, all protons were contained in compartment P1. When exposed to irradiation, protons were transferred to compartment P2, and further on to compartments P3 and, during radiation, P4. At a sufficient time after the irradiation has stopped, compartment P2 is empty, and all protons originally transferred from compartment P1 are located in compartments P3 and P4 (Figure 10). The model was fitted to a set of measurements using nMAG gel dosimeters exposed to different dose levels and fractionation schemes. A set of differential equations describing the transfer between different compartments were solved using MATLAB, and the resulting distribution of protons in the different compartments was then used to calculate an average R2 value, which was compared to the corresponding measured R2 value.

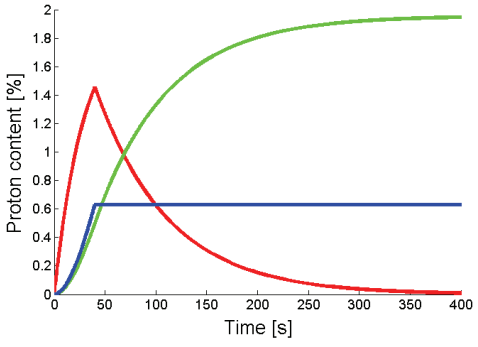

Figure 10. An illustration of how the proton content in each compartment varies during time. When irradiation starts the protons in P1 are transferred to P2 (red curve) and further to P3 (green curve). During irradiation protons are also transferred from P2 to P4 (blue curve).

3.3 3D Verification of Advanced Radiotherapy

Two advanced radiotherapy deliveries were dosimetrically verified in 3D for the first time; a VMAT delivery (Paper IV) and a breathing adapted VMAT delivery using a DMLC-based tumour-tracking system (Paper V). In both studies the VMAT technique was RapidArc (Varian Medical Systems) and the same nPAG gel formula, mixing and storing gel procedures, linear accelerator, MR read-out parameters, calibration method and 3D data analysis program were used.

The dose distributions obtained from the gel measurements were compared with dose distributions calculated using the TPS or Monte Carlo simulations, or with measurements using other detector systems. All these different methods are connected with various difficulties and related uncertainties, with the result that there is no undisputable "gold standard" in these comparisons. However, one may presume that a good agreement between several different, independent methods is in itself an indication of the accuracy of their predictions.

3.3.1 Verification of Volumetric Arc Therapy

For this study, an 18 MV VMAT prostate treatment plan was created using a beta version of the pre-clinical RapidArc optimizer (Paper IV). The target dose was 3.3 Gy, delivered using a clockwise arc rotation from 210° to 150° and an output that varied between 200 and 600 MU min^{-1} during the rotation. The resolution of the dose array was originally $2.5 \times 2.5 \times 2.5$ mm^3 but it was subsequently re-sampled by interpolation to $1 \times 1 \times 1$ mm^3 in order to match the resolution in the second study. These dose arrays were then exported as DICOM objects, and imported into in-house developed MATLAB programs for further analysis.

Three identical cylindrical gel phantoms were used. The delivery was repeated twice, irradiating the first two phantoms. The third phantom was used to obtain an R2 background value.

Comparisons were also made with Monte Carlo calculations. The Monte Carlo calculations reported in Paper IV were carried out using the VIMC-arc code developed at the BC cancer center in Vancouver (Bush et al., 2008) system. VIMC-arc is based on the well documented radiation transport codes BEAMnrc (Rogers et al., 1995), particle DMLC (Keall et al., 2001), and DOSXYZnrc (Walters et al., 2009) or VMC++ (Kawrakow and Fippel, 2000). The linac model in VIMC-arc, which was tuned to reproduce the 18 MV photon beam of a Varian 21EX, has previously been tested and verified for open beams, absolute dose calculations including sliding window IMRT, sliding window IMRT profiles as well as RapidArc dose distributions (Bush et al., 2008 and Gagne et al., 2008). For the beam used in this work, the agreement

between calculations and measurements is better than 1%. The input to VIMC-arc consisted of a RapidArc plan and a patient model exported as a DICOM dataset from the treatment planning system. In the simulations, the RapidArc delivery was built up by a sequence of 176 static gantry positions and corresponding apertures according to the plan produced by the TPS. The statistical uncertainty of the MC simulation was kept within 1%. The resulting absorbed dose distribution were converted to dose-to-water using the appropriate mass-stopping power ratios and re-exported in DICOM format for further analysis in MATLAB. The resolution of the 3D dose distribution array was originally $5 \times 5 \times 5$ mm^3 but it was re-sampled by interpolation to $1 \times 1 \times 1$ mm^3 in order to facilitate the comparisons with the other data arrays.

4.5.2 Verification of Breathing Adapted VMAT

For this study, a 6 MV VMAT lung plan was made in the clinical treatment planning system, Eclipse version 8.6 (Paper V). The plan was designed for a target dose of 4 Gy, a 358º arc rotation and an output of up to 600 MU min^{-1}. The resulting dose array, with a resolution of $1 \times 1 \times 1$ mm^3, was exported as before as DICOM objects for further analysis in MATLAB.

To simulate lung tumour movement, a programmable motion platform (Standard Imaging, Inc) was set to carry out sinusoidal motion in the superior–inferior (SI) direction with a peak-to-peak distance of 20 mm during a period of 4 s. This motion platform was used instead of the BERT robot for two reasons; i) a lung tumour motion rather than a breast tumour (chest wall) motion was simulated, and ii) the platform on BERT was not able neither to carry nor move the bi-planar diode array detector (27 kg).

The target motion related to the leaf trajectory was more complicated than in the feasibility study. The VMAT plan was optimized using a 45º collimator rotation, thus a non-parallel leaf trajectory motion component was included. To enable the plan for DMLC tracking, the jaws were forced to set 6×6 cm^2 to avoid covering the moving target during delivery. A pre-clinical real-time 3D DMLC-tracking system was used for tumour-tracking.

Verification measurements were made with four identical gel phantoms, as well as the bi-planar diode array described in Section 2.3.1. The delivery was carried out in the following four set-up modes: i) the detector in motion and the tracking system disconnected, ii) the detector at rest and the tracking system disconnected, iii) the detector at rest and the tracking system connected and iv) the detector in motion and the tracking system connected.

By evaluating the difference between the measurement during motion and the static measurement for each detector system, any possible discrepancy compared to the TPS was excluded and, thus, the DMLC tracking performance was isolated.

The static measurements performed with the tracking system disconnected, were, however, used for dosimetric verification of the VMAT plan. Further, by comparing the two static measurements, with and without a connected tracking system, the dose difference due to the transmission dose leakage could be evaluated.

In addition, direct measurement comparisons of the gel dosimeter and the bi-planar diode array were carried out (Figure 11). Both data sets were normalised to the dose at the isocentre.

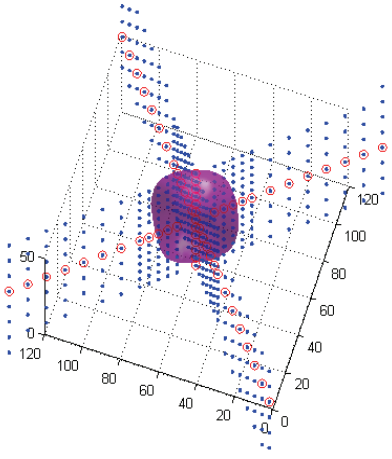

Figure 11. An overlay of the gel measurement and the positions of the diodes in the bi-planar detector array.

3.3.2 Analysis of 3D Dose Distributions

For basic analyses, the dose distribution arrays were compared voxel-by-voxel, resulting in a dose difference array that could be evaluated with respect to mean value and standard deviation. Relative dose difference histograms and dose-volume histograms were used to present the results from these comparisons.

When comparing 3D dose distributions, however, both dosimetric and spatial accuracy need to be considered, and in general these two dimensions are interrelated. The gamma-index (γ) is a parameter designed to describe the combined spatial and dosimetric performance

(Low et al. 1998), and can be used as an evaluation tool when comparing two dose distributions.

All gamma evaluations carried out in the studies in this thesis have been applied in 3D (Papers IV and V). For visualisation, an illustration of how the γ index evaluation tool works for 2D dose distributions is presented in figure 12.

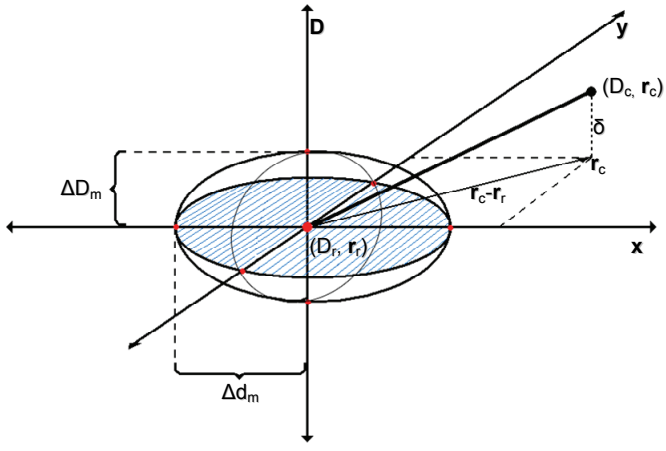

Figure 12. An illustration of the γ index concept. The reference dose and position is denoted by (D_r, $\mathbf{r}_r$) and the compared dose and position is denoted by (D_c, $\mathbf{r}_c$). The ellipsoid represents the given acceptance criteria. (Drawing by Sacha af Wetterstedt)

The two dose distributions to be evaluated are here denoted as "reference" and "compared". The evaluation is based on two acceptance criteria; the maximum allowed dose difference ΔD_m, and the maximum allowed distance-to-agreement (DTA) Δd_m (Figure 12). The combined acceptance criterion is represented by an ellipsoid defined by

$$1 = \sqrt{\frac{\Delta r^2}{\Delta d_M^2} + \frac{\Delta D^2}{\Delta D_M^2}} \qquad (2)$$

where

$\Delta r = \left| \mathbf{r} - \mathbf{r}_r \right|$

and

$\Delta D = D(\mathbf{r}) - D(\mathbf{r}_r)$

In order for the "compared" dose distribution to match the "reference" dose at the reference point $\mathbf{r}_r$, it is required that at least one point on the ellipsoid surface defined by

$$\Gamma(\mathbf{r}_r, \mathbf{r}_c) = \sqrt{\frac{r^2(\mathbf{r}_r, \mathbf{r}_c)}{\Delta d_M^2} + \frac{\delta^2(\mathbf{r}_r, \mathbf{r}_c)}{\Delta D_M^2}}, \qquad (3)$$

where

$r(\mathbf{r}_r, \mathbf{r}_c) = |\mathbf{r}_c - \mathbf{r}_r|$

and

$\delta = D(\mathbf{r}_c) - D(\mathbf{r}_r)$,

lies within the ellipsoid defined in Eq. 3. The γ index is defined as the $\Gamma(\mathbf{r}_m, \mathbf{r}_c)$ value at the position $\mathbf{r}_c$ for the "compared" dose distribution where it is minimal.

When calculating a γ distribution, finite area segments composing a matrix are given their respective γ index value; 0 corresponding to an exact match between measured and calculated dose and 1 being the point at which the given tolerance is precisely met. Values above 1 represent points where the tolerance has been exceeded.

4 Results and Discussion

4.1 Uncertainty Analysis

An uncertainty analysis was carried out for the nPAG-type of gel used in the two studies verifying a VMAT delivery and a breathing adapted VMAT delivery (Papers IV and V). The combined standard uncertainty for the nPAG gel system was found to be about 5% for the absorbed dose interval 3-4 Gy (Table 1). The figures were calculated (Type A: noise and T2 calculation) or estimated (Type B: all other) according to GUM and a relative evaluation as suggested by Karlsson (Karlsson, 2007). Most of the Type B uncertainties were estimated from the results published by De Deene et al. (2006a). Uncertainties were separated into the three main groups based on the procedures involved in a gel measurement : preparation, irradiation and scanning (Table 1).

		Uncertainty (1SD) %
Preparation	• spatial & temporal stability	1
	• temperature during storage	0.5
Irradiation	• contraction of the volume	0.5
	• dose rate and fractionation	0.5
	• temperature during irradiation	0.5
MRI scanning	• artefacts	2.5
	• T2 calculation	1.5
	• stochastic noise	3
	• temperature during scanning	3.5
	Combined standard uncertainty	5

Table 1. Summary of uncertainties in an nPAG experiment.

The relatively low uncertainty levels given in Table 1 has been achieved by using a "good practice" strategy (Karlsson, 2007, Baldock et al., 2010), which has minimized the effects of influencing parameters in every step of the procedure. In addition, longer MRI acquisition times have been used, which has improved the signal-to-noise ratio.

The estimated uncertainties are valid under the specified circumstances and should not be assumed to have general applicability. The mentioned uncertainties vary significantly between different gel systems, which means that each new gel composition and read-out has to be characterized.

4.2 Fractionation Dependency

For the gel systems investigated, the R2 dose response for a given total absorbed dose increased with an increased number of sequential beams (Paper I). This fractionation dependency was particularly pronounced for the nMAG dosimeter (Figure 13a).

The ratio between the absorbed dose responses for a fractionation scheme of 0.5 Gy per beam-on and the single beam irradiation increased for the nMAG system with increased amount of the monomer MAA (Figure 13b). Furthermore, the effect increased with increased total dose and with increased number of beams. The fractionation dependency for the nPAG (3%/AA/3%BIS) was relatively small (Figure 13b).

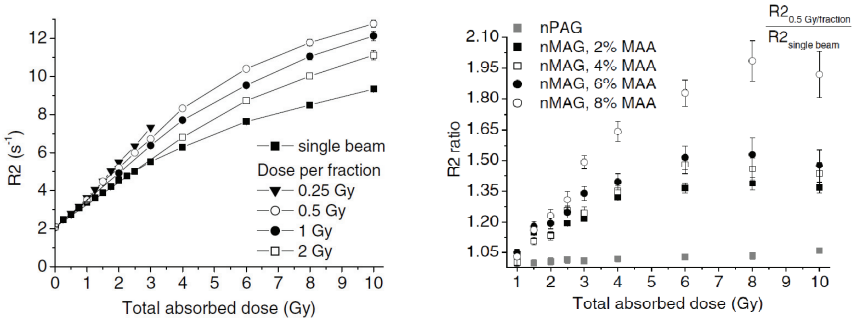

(a) **(b)**

Figure 13 a) R2 dose response for nMAG samples (2% MAA) irradiated to absorbed doses of up to 10 Gy. When the total dose was delivered in sequential beams the R2 dose response for the total absorbed dose increased with increased number of beams. **b)** The effect of different amount of MAA, normalised to a single dose irradiation. Corresponding nPAG data is included for comparison.

To investigate the magnitude of the fractionation dependency during a typical respiratory gating delivery a corresponding beam-on and beam-off scheme using various gel compositions was evaluated.

It was found that the nPAG dosimeter was to prefer when verifying a gated treatment (Papers I and II). The difference in R2 for the gel samples that received gated delivery compared to when the dose was given in a single irradiation was less than 1% for nPAG and approximately 4% for nMAG, for absorbed doses up to 2 Gy (Figure 14). The maximum difference in R2 was 1.2% for nPAG and 9.0% for nMAG, occurring for the highest investigated dose.

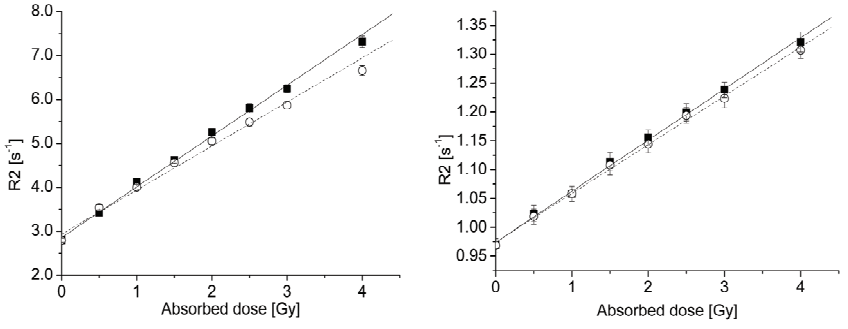

(a) **(b)**

Figure 14. R2 dose response for **a)** nMAG and **b)** nPAG vials irradiated to absorbed doses up to 4 Gy. Two sets of samples for each gel were irradiated during a single beam delivery (empty circles) or during gated delivery with 12 MU every 6.5 s (black squares).

It was thus verified that there is a large fractionation effect on the dose response for the nMAG system. Furthermore, when the interval between beam-on sequences was decreased, i.e. the irradiation approached a single beam delivery, the fractionation effect decreased. A possible radio-chemical explanation is that the mean radical concentration is proportional to the mean dose rate during the total irradiation, and thus the mean R2 values approach each other for the measurements of the gated and un-gated deliveries.

4.3 Motion-related Dose rate Dependency

The data obtained under respiratory-like motion showed good agreement between dynamic gel measurements, convolved static gel data and measurements carried out using the linear diode array LDA (Figure 15).

All dynamic 80–20% penumbra widths agreed within 1 mm. Additionally, the difference between the full width at half-maximum (FWHM), i.e. the profile width at a 50% absorbed dose level, was within 1 mm for the calculated convolved data and the measured dynamic data for both gel systems. Thus, the dose response of both investigated gel dosimeters (nMAG and nPAG) can be considered to be invariant during motion (Paper II).

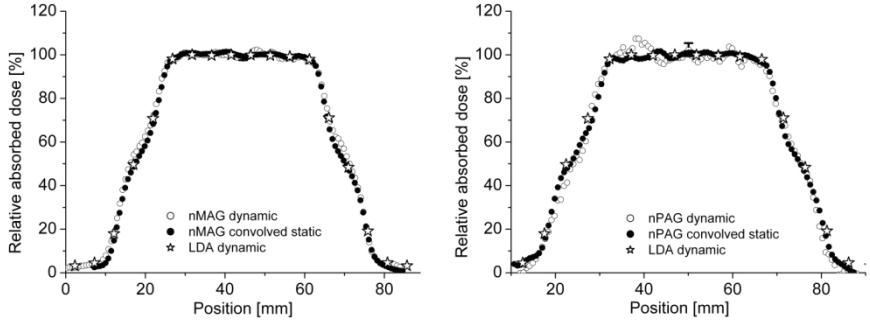

(a) **(b)**

Figure 15. Relative absorbed dose profiles from the (a) nMAG and (b) nPAG during respiratory-like motion in and out of the beam (empty circles). Also included is corresponding LDA data (stars) and convolved data (black circles).

As a next step the performance of the dynamic MLC-tumour tracking system was investigated. The motion introduced a significant dose-blurring when the tracking system was disconnected, as expected (Figures 16a and 16b). When the tracking system was connected good agreement was observed between the static and tracked measurements (Figures 16a and 16c). The distance between the 50% absorbed dose contour of the static and tracked gel-measurements was less than 1 mm for 96% of the points along the contour (maximum distance 1.4 mm). The absorbed dose in planes through the depth of dose maximum in the static and tracked gels were compared using gamma evaluation with a 3%/3mm criteria. A 91% and 82% pass ratio was obtained in the region containing absorbed doses greater than 80% and 20%, respectively. Most of the dose points failing the gamma criteria were located in the penumbra region, and could possibly be attributed to motion induced dose-smearing effects.

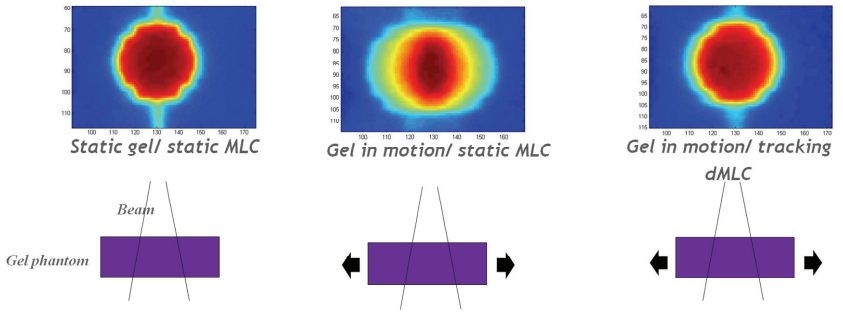

a) **b)** **c)**

Figure 16. Dose distributions measured using gel dosimetry with and without the DMLC-tumour tracking connected.

Overall, the measurements carried out using a 2D ion chamber array agreed well with the gel measurements (Figure 17). However, due to the limited spatial resolution of the 2D array a detailed comparison was not possible.

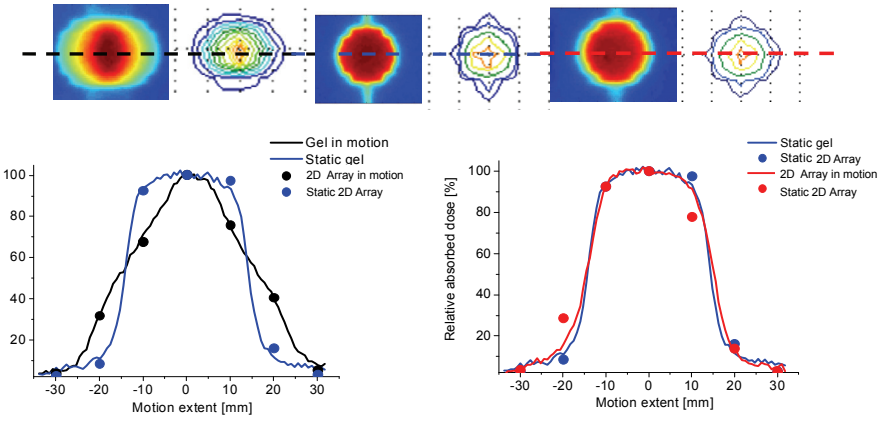

a) **b)**

Figure 17. Relative absorbed dose profiles extracted from nPAG (lines) and 2D ion chamber array (dots) measurement data, performed with the detectors in motion or in a static position a) Tracking system disconnected. Detector moving (black) and in a static position (blue). b) Tracking system connected. Detector moving (red) and in a static position (blue).

4.4 Theoretical Modelling

In order to gain further insight into the fractionation and dose rate dependency of the gel dosimeter a theoretical investigation was undertaken (Paper III). A compartment model was developed and fit to measured data. In the first experiment, the model was fit to a series of measurements with the nMAG gel exposed to different dose levels using different fractionation schemes. The results showed a very good agreement between the measured and calculated data (Figure 18).

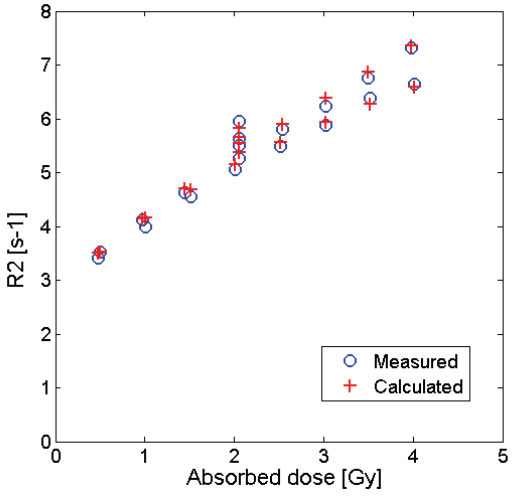

Figure 18. The difference between calculated R2 values (red crosses) and measured R2 values (blue circles) was on average 1.1 ± 1.6% (1SD) for the experiments with nMAG gels irradiated with different fractionation patterns.

For an absorbed dose of 2 Gy, variations in R2 of up to 16% can be expected depending on fractionation scheme. This fractionation dependency for the nMAG dosimeter, which was also reported in Papers I and II, indicates that the nMAG gel is not a suitable dosimeter for verification of respiratory gating.

The model was also used to simulate irradiations with fractionation schemes more relevant to an IMRT delivery. The irradiations were all delivered within the same total time and to the same total absorbed dose, with the goal to compare the resulting calculated R2 values. The calculations showed that the R2 value remained nearly the same for the different fractionation schemes, given that a given total dose was delivered during a given total time.

Additionally, the model was fit to a set of measurements using nPAG gel dosimeters exposed to different dose levels at two different dose rates. The resulting R2 calculations together with the measured data are presented in Figure 19. Although these experiments are still preliminary, the results presented here show that the same simplified, mechanistic modeling may be used to predict the gel dosimeter response both to fractionated irradiation and dose rate variations.

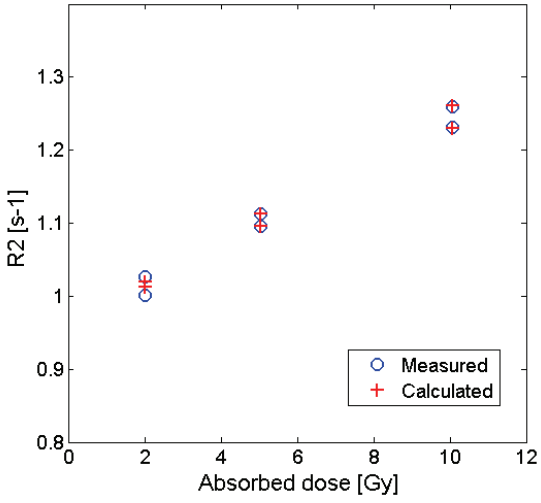

Figure 19. Calculated R2 values (red crosses) and measured R2 values (blue circles) for the nPAG gels irradiated at different dose rates.

The model may be further developed to include more processes which will provide improved understanding of the observed dependencies on dose rate and fractionation (Paper III).

4.5 Verification of Dynamic and Breathing Adapted Radiotherapy

As shown above, polymer gel has been found to be a suitable detector for dose measurements under motion since the dose response is not influenced by dose rate variation due to the motion in and out of the beam. Consequently 3D dose verifications of dynamic and breathing adapted radiotherapy could be carried out without correction for such effects.

4.5.1 Verification of Volumetric Arc Therapy

Polymer gel was used for verification of the absorbed dose delivery using a VMAT technique (RapidArc). Additionally, MC simulated dose distributions were calculated using the VIMC-Arc software for verification of the TPS calculated dose distributions.

Overall, there was close agreement between the expected RapidArc dose distribution (TPS) and the 3D gel measured data (Paper IV). In addition, the MC data confirmed the TPS accuracy. Thus, no discrepancies between the planned dose delivery and the actual delivery were observed.

To illustrate the good result an overlay of the three volumes, each enclosed by the 90% isodose surface, was projected into a 3D view (Figure 20). Good agreement was observed for all isodose levels compared in two slices representing a medium (Figure 21a) and highly modulated dose distribution (Figure 21b). Both slices were obtained in regions more than 15 mm from the normalization volume. In the region with a very highly modulated dose distribution and thus steep dose gradients, the agreement of the dose profiles is still within 3% (Figure 21c).

The relative absorbed dose differences were calculated voxel-by-voxel for all volumes investigated, including the repeated gel measurement. All dose volume comparisons showed good agreement with a mean difference smaller than 1% and a standard deviation within 2.5% (1SD).

Three dimensional gamma evaluations resulted in high pass rates within the dose volume defined by the 50% and 90% isodose surfaces. More than 95% of the TPS points were within 3%/3 mm of both the gel measurement and the MC simulated data.

Three dimensional gamma evaluations were also carried out using stricter gamma criteria (1%/2mm) within the entire irradiated volume to investigate potential differences between TPS and each verification method in more detail. Within the treated volume, in one particular region, a relative calculated overdosage on the order of 3–5% was found in the TPS as compared to both the gel measurement and the MC simulations. Since the gamma criteria were very strict this result may be of no clinical relevancy. Nevertheless, considering the agreement of the two verification methods, this result indicated that the TPS calculations were inaccurate in this region.

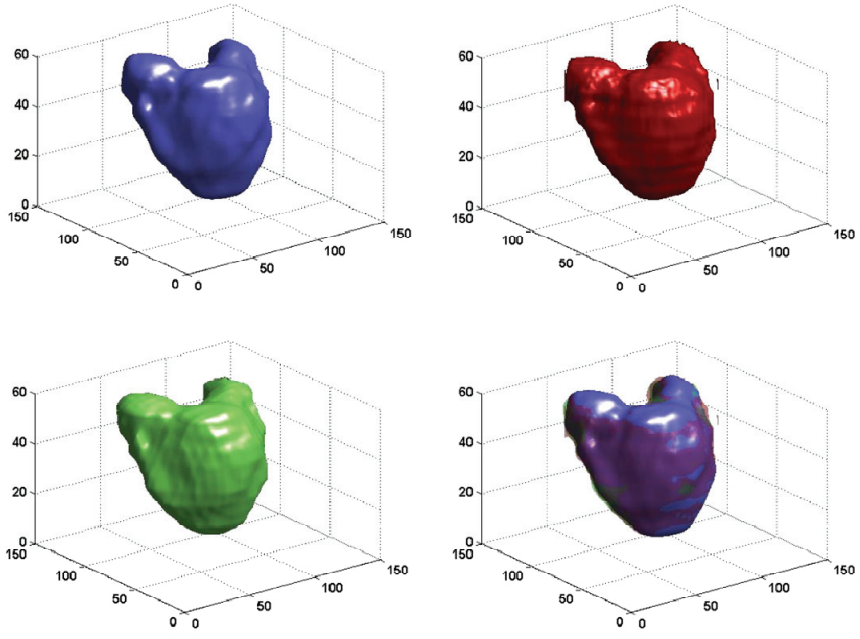

Figure 20. The 90% isodose surface projected into a 3D view for (top left) the RapidArc^{TM} TPS data, (top right) the gel measurement and (bottom left) the MC simulation. An overlay of all three volumes is presented in (bottom right) where the gel and Monte Carlo surfaces are transparent. The unit on all axes is millimetres. It should be noted that the dissimilar surface structures, such as stripes on the gel measurement volume and the slightly checked pattern on the MC-calculated volume, derive from the different original resolutions.

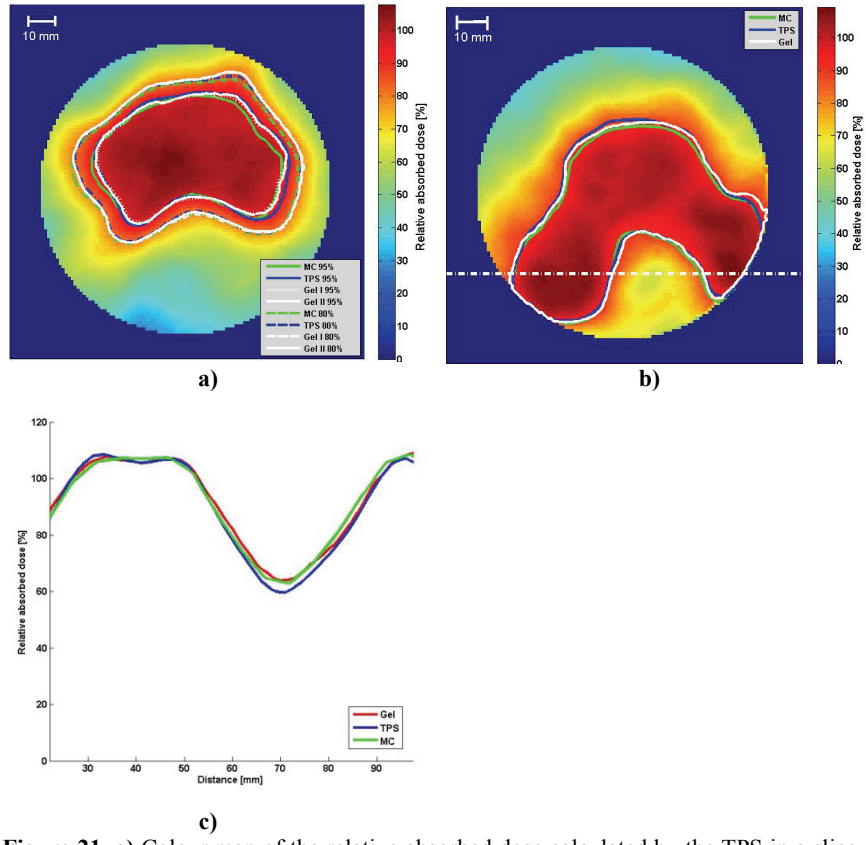

Figure 21. a) Colour map of the relative absorbed dose calculated by the TPS in a slice away from the normalization volume. The overlaid 80% and 95% isodose lines are data from the two gel measurements (white lines), MC simulations (green lines) and TPS calculations (blue lines). **b)** Colour map of the relative absorbed dose calculated by the TPS. The overlaid 90% isodose lines are extracted from the gel measurement (white line), MC simulations (green line) and TPS calculations (blue line). Profiles extracted across a region with steep dose gradients, along the white dotted line, are plotted in (c). **c**) Relative absorbed dose profiles extracted along the white dotted line in (b). The profiles are extracted from the gel measurement (red line), the MC simulation (green line) and the TPS calculations (blue line).

4.5.2 Verification of Breathing Adapted VMAT

The performance of a pre-clinical DMLC-tumour tracking system during a VMAT delivery was dosimetrically verified using 3D polymer gel and a bi-planar diode array.

When investigating the absorbed dose volumes from the static and tracked gel measurements, the results showed that the DMLC-tracking system correctly accounts for target motion during intensity modulated arc therapy (Paper V). To illustrate the good tracking performance an overlay of the measured 90% isodose surfaces of the static and tracked gel measurement was presented (Figure 22a). The worst case scenario, if the motion is not taken into account, i.e. the static measurement compared to the moving non-tracked gel, resulted in an underdosage of the target volume (Figure 22b).

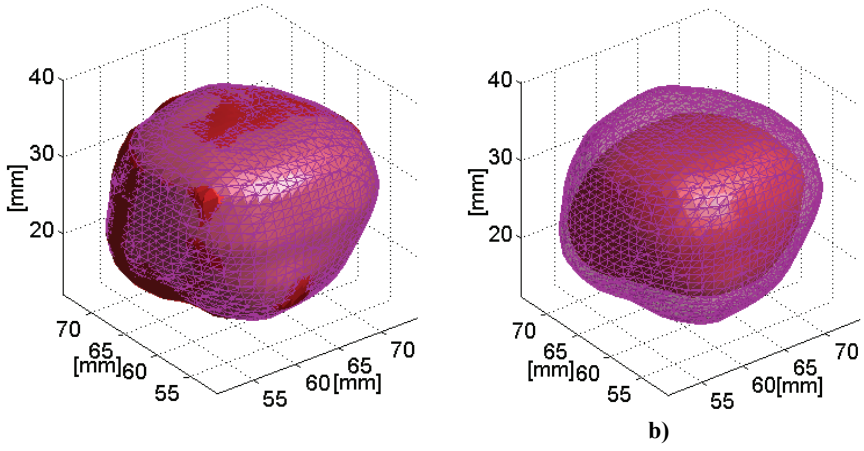

a) **b)**

Figure 22. The 90% isodose surface overlay of the gel measurements obtained in static mode (wire framed pink volumes) and gel measurements obtained during motion (red volumes). The good agreement between the static and tracked measurements is presented in **a)**. The smaller red non-tracked volume in **b)** visualizes the reduction of the 90% isodose volume due to motion.

The differences were calculated voxel-by-voxel within the volume of interest (VOI) enclosed by the 90% isodose surface (VOI_{90}). The dose difference was within 2% for 97.1% of the voxels (Figure 23a). This result should be compared with the case where the motion was not accounted for, where only 26.6% of the voxels were within 2% dose difference (Figure 23b).

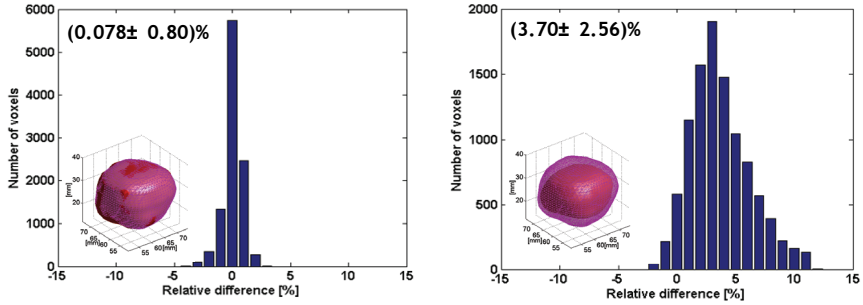

a) Static *vs.* motion (tracking connected), VOI_{90}

b) Static *vs.* motion (tracking disconnected), VOI_{90}

Figure 23. The distribution of voxel-by-voxel deviations between the different gel measurement sets within the volumes enclosed by the 90% isodose surface. The number of voxels is plotted against the difference in relative dose between the two analyzed volumes. Note the different scale of the ordinates.

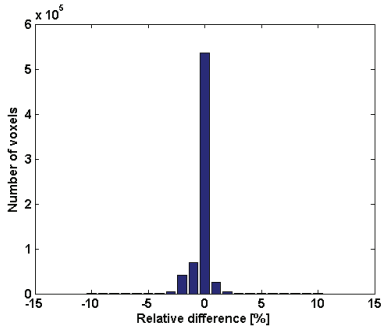

Figure 24.
Static (tracking disconnected) *vs.* static (tracking connected), $VOI_{20\text{-}50}$. The distribution of voxel-by-voxel deviations between the different gel measurements within the volume enclosed between the 20% and 50% isodose surfaces. The number of voxels is plotted against the difference in relative dose between the two analyzed volumes.

No contribution due to leakage was found in the investigated low dose volumes for the two static measurements, with and without the tracking system connected (Figure 24).

The gel measurement was compared with the results obtained with the bi-planar diode array during the DMLC-tracking delivery. The tracked measurements were overlaid and three orthogonal dose profiles through the gel and the array detector system were presented (Figure 25). The relative dose differences between the two measurements were evaluated by selecting each gel measurement point from the 3D gel arrays at the position corresponding to each diode location in the bi-planar diode array. Very good agreement was observed, with a mean value of the differences equal to (0.23 ± 2.5)% (1SD).

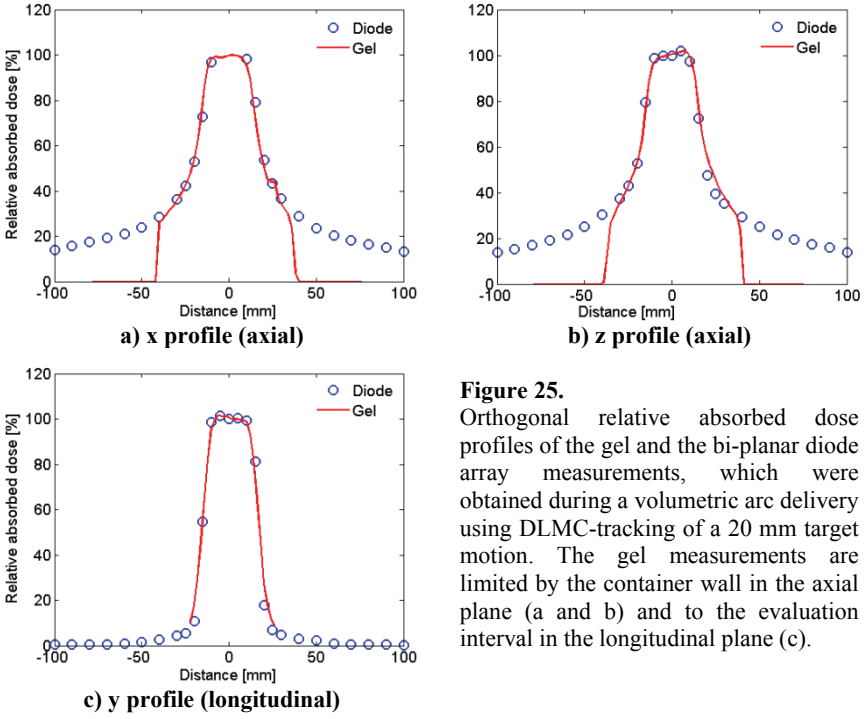

a) x profile (axial)

b) z profile (axial)

c) y profile (longitudinal)

Figure 25.
Orthogonal relative absorbed dose profiles of the gel and the bi-planar diode array measurements, which were obtained during a volumetric arc delivery using DLMC-tracking of a 20 mm target motion. The gel measurements are limited by the container wall in the axial plane (a and b) and to the evaluation interval in the longitudinal plane (c).

This study verified that a VMAT treatment of a moving target was delivered with greatly improved conformity when real-time DMLC-tracking was incorporated. The delivery was verified using both gel dosimetery and a bi-planar diode array, showing that that the DMLC-based tumour-tracking delivery system successfully accounted for respiratory-like target motion. The comparison of the measurements obtained with the two dosimetry systems showed a surprisingly good agreement which add extra confidence to the tracking performance technology used in this work.

5 Conclusions

Dosimetric verification of advanced radiotherapy, involving clinical and pre-clinical delivery techniques have been studied within the scope of this thesis. Polymer gel measurements and measurements using 1D, 2D and quasi-3D detector systems, as well as MC simulations were used for verification.

Owing to a more pronounced fractionation dependency for nMAG type gel, it was concluded that nPAG should be used for verification of dynamic dose deliveries such as for example respiratory gated radiotherapy (Papers I and II). The result from a kinetic simulation using a compartment model indicated, however, that this may be overcome if the total delivery time was kept constant using different fractionation schemes. This is for example the case during an IMRT delivery and the total fractionation effect may thus be reduced, allowing the gel to be used for accurate dose verification (Paper III).

Irradiating the gel dosimeter under respiratory-like motion, using an in-house designed and built breathing simulated motion device, showed no influence of the dose rate variation related to motion in and out of the beam. The gel measurements agreed very well with data obtained using a 1D reference detector as well as mathematically convolved data (Paper II).

Gel dosimetry and MC simulation were used for a 3D verification of a VMAT treatment plan and delivery. Very good agreement was observed for 3D comparisons of all datasets (TPS calculations, gel measurement and MC simulation). It was thus successfully demonstrated that the VMAT plan was accurately calculated and delivered as planned. Furthermore, the repeated gel measurements showed excellent consistency, indicating a highly reproducible delivery (Paper IV).

The ability of the pre-clinical dynamic MLC-tracking system to account for 20 mm target motion during radiotherapy was investigated using polymer gel (nPAG), 2D ion chamber array and bi-planar diode detector measurements. Both a feasibility experiment, using a basic, simplified delivery set up, and a VMAT delivery were investigated. Good agreement in absorbed dose was found between the static and tracked measurements (Paper V). It was thus verified that this very complex treatment was delivered with greatly improved conformity when applying the real-time DMLC-tracking during a VMAT delivery.

It has been demonstrated that polymer gel dosimetry can be used for verification of complex dynamic radiotherapy deliveries and breathing adapted radiotherapy. This was achieved by, in every step of the procedure, minimizing the known uncertainties of the dosimeter. Reproducible measurements in good agreement with conventional detector systems and theoretical methods has been presented. In conclusion, it has been shown that polymer gel is a robust tool for relative 3D dosimetry, suitable for verification and benchmarking of highly complex and dynamic radiotherapy techniques.

Future Development

Polymer gel dosimetry of today has been shown to be useful for 3D verification measurement for various novel delivery techniques. Still, additional applications and further development to improve the properties of the dosimeter should be carried out. Some future aspects are listed below:

- To develop an anthropomorphic phantom including both low-density gel and normal-tissue density gel, simulating a thorax phantom.

- To use a detector insert in the gel phantom, providing an independent, time resolved, and accurate absorbed dose measurement, to which the gel measurement can be normalised.

- To use compartment models to increase the understanding of the polymerisation process and by simulations find the optimal gel-type for different measurements.

- Dose painting and various interplay effects are two situations in modern radiotherapy, where high resolved 3D absorbed dose measurement using polymer gels may contribute to the understanding of the new techniques.

- As demonstrated in this thesis, 3D polymer gel dosimetry is of great value when introducing new techniques. The closely related method of radiochromic plastic has the potential to simplify some of the steps included in the measurement procedure. This will be further investigated.

Popular Scientific Summary in Swedish

En cancerpatient kommer till sjukhuset för att genomgå en strålbehandlig. Sjukhusets personal tar bilder av patienten och identifierar tumörens placering och utbredning. Bilderna läggs in i ett datorprogram, som i sin tur simulerar en strålbehandling. Strålningsapparaten, dvs. linjäracceleratorn, har flera justerbara parametrar; strålfältets storlek, vinkeln på den infallande strålen och strålningens energi m fl. Genom att simulera olika inställningar på dessa parametrar kan behandlingen optimeras. Varje patient får på så sätt sin individuella behandlingsplan.

Innan patienten lägger sig på britsen inför bestrålningen verifieras behandlingen genom kontrollmätningar. Stråldosen, som mäts på den plats där patienten kommer att befinna sig, uppmäts med en detektor placerad i ett medium med samma densitet som mänsklig vävnad. Det finns flera olika typer av detektorer, men de allra flesta mäter dosen som ska ges till patienten i en punkt eller i ett plan. I denna studie har en geldosimeter utvecklats och använts för att mäta dosen under avancerade bestrålningsförhållanden. Gelen, vars egenskaper förändras vid bestrålning, är unik i sitt slag; dels kan dosen mätas i en hel volym, dels integreras dosen över tiden vilket möjliggör mätningar under dynamiska förhållanden.

Då tumören befinner sig i området kring bröstkorgen, t ex vid lung- eller bröstcancer, rör sig tumören pga. att patienten andas. För att undvika att tumören rör sig ut ur strålfältet används stora marginaler. En sådan åtgärd innebär att tumören alltid är i strålfältet trots patientens andningsrörelser, men också att mängden bestrålad frisk vävnad ökar. För att minska dosen till frisk vävnad, t ex till hjärta och lungor, har nya behandlingsmetoder tagits fram. Dessa andningsanpassade strål-behandlingar ställer antingen in linjäracceleratorn så att den strålar endast då patientens tumör är i strålfältet alternativt så följer strålen tumören i dess rörelse. På så sätt kan strålfältet anpassas till tumörens storlek och frisk omkringliggande vävnad bättre klarar sig undan strålningen.

Enligt Cancerfonden kommer var tredje svensk diagnostiseras med cancer under deras levnadstid. Ungefär hälften av dem får gå igenom strålbehandling. För att bemöta detta, har utvecklingen av avancerade bestrålningstekniker accelererat under de senaste tio åren. Idag kan patienter behandlas med tekniker där strålfältet roterat kring patienten samtidigt som strålfältet ändrar både storlek och intensitet, och detta samtidigt som hänsyn tas till patientens andningsrörelser.

Det som däremot inte utvecklats lika snabbt som behandlingsteknikerna är de detektorsystem med vilka vi kontrollmäter behandlingar med innan de ges till patienten.

I denna studie har flera gelsystem först undersökts för att se om de passar för att mäta dosen som levereras med dessa avancerade bestrålningstekniker. Efter olika tester togs den bäst lämpade gelen fram och dosmätningar av andningsanpassade rotationsbestrålningar har genomförts. Dessa mätresultat har jämförts med resultat uppmätta med andra system (fast gelen har varit den enda som mätt med hög upplösning i tre dimensioner), beräkningar och simuleringar. All data stämmer överrens, vilket visar att gelen är en bra detektor. Dessutom visar resultaten presenterade i denna avhandling på att stråldosen till patienter som ska få avancerad dynamisk strålbehandling faktiskt är enligt planerna. När nya tekniker ska introduceras i kliniken kan gel dosimetern bidra med unika mätdata för att säkerställa en korrekt behandling.

Acknowledgements

This study was financially supported by the Swedish Cancer Society and the Cancer Foundation at Skåne University Hospital in Malmö.

Det är min fulla övertygelse att det aldrig hade blivit en avhandling om det inte vore för en hel drös med hjälpsamma, inspirerande, smarta, glada, uthålliga, kritiska och optimistiska människor i min omgivning. Tack till alla er vänner och kolleger!

Tack till mina fantastiska handledare;

Sven – för att du innehar den förträffliga egenskapen att vara simultant smart och ödmjuk! Tack för din totala tillit och för att du alltid fått mig att känna mig bra på det jag gör, t.o.m. när jag sprängde micron på labbet. Och för att du viker dig dubbel när du skrattar!

Helen – för ditt energiska sätt och positiva hållning. För att du alltid ställer upp i alla lägen. Du har lyckats med konsttycket att vara en närvarande handledare trots Malmö – Canburra avståndet det sista året. Nåväl, du kan ha hur goda handledar-egenskaper som helst, det är ändå din vänskap jag värderar högst.

Professor Sören, tack för att du alltid tar dig tid, för att din kontorsdörr alltid står välkomnande på glänt. Tack för alla bra och trevliga pratstunder både om och bortom jobb.

Thanks to all my co-authors all over the world; from Sweden, Copenhagen, Vancouver, Sherbrook, Sydney and Stanford. This thesis would be very thin without you. Extra thanks to you Clive, Tina and Stephen for introducing me to optical scanning at Sydney University.

Tack Uppfinnar-Jocke I, II och III, dvs. Rolf, Henrik och Robert på Medicinsk Tekniska Avdelningen för ett innovativt och roligt samarbete som resulterade i en cool andningssimulerande robot.

Tack all personal på strålbehandlingen och på MR-skannern ”Symphony” på DC. För att det bara har varit glada miner trots att jag kommit och stökat med mina geler i tid och otid, och för att ni drog i väg med mig på er personalfest mitt under nattliga experiment!

Tack alla goa doktorandkolleger för dessa nöjsamma år! Ni är definitionen av trivselfaktorn. Extra tack till mina forskargrupps-kollegor: Fredrik - för givande diskussioner, trevliga resor och för att du alltid fixar saker och ting åt mig, och Anna - för exemplarisk undervisning i labbet och sköna bastueftermiddagar. Min roomie Calle, tack för underhållning och inte minst för att du fick mitt skrivbord att framstå som ordningsamt bredvid ditt.

Tack Anju min vän. Tänk att vi började vår första dag i Lund bredvid varandra, och att vi nu doktorerar bredvid varandra. Vad vi än väljer att göra i framtiden, så vet jag att det är bredvid varandra.

Tack kära Åke och Anita, för att ni ställer upp som ni gör, speciellt nu i slutspurten. Utan er hjälp med allt vad familjelivet kräver hade jag kommit till kapitel 2 vid det här laget, max.

Tack Mamma och Pappa! Ni har övertygat mig att allt är möjligt om man vill. Nu råkade det bli en doktorsavhandlig, det kunde lika gärna bli något helt annat, (eller inget alls), och ni hade varit lika glada för det. Tack för ert otroliga engagemang i allt stort som smått. Det betyder väldigt mycket för mig.

Tack lillasyster Jenny, min ögonsten och vårvind, för att du får mig att lyfta blicken och påminna mig om det allra viktigaste när det stundtals varit mycket jobb.

Tack underbara Nisse och Emma, för kuliga dagar när jag fått låna er från skolan och ni hjälpt mig med gelblandning på jobbet, och för alla andra fina dagar.

Tack min lilla Lisa, för att du gör mig glad varje dag. Hur mycket jag än läser är jag aldrig så nära svaren på alla frågor jag någonsin haft, som när jag tittar in i dina stora blå.

Tack för allt CC, min livskamrat och man…...du får polstjärnan att blekna.

References

ADAMOVICS, J. & MARYANSKI, M. (2004) A new approach to radiochromic three-dimensional dosimetry-polyurethane. *Journal of Physics: Conference Series.*, 172-175.

ADAMOVICS, J. & MARYANSKI, M. J. (2006) Characterisation of PRESAGE: A new 3-D radiochromic solid polymer dosemeter for ionising radiation. *Radiat Prot Dosimetry,* 120**,** 107-12.

ALEXANDER, A. S., WELLS, D., BERRANG, T., PARSONS, C., MYDIN, A., SHAFFER, R., WONG, F., SAYERS, D. & OTTO, K. (2008) Volumetric Arc Therapy (VMAT) Reduces Treatment Time Compared to Conventional IMRT (cIMRT) While Maintaining Similar Plan Quality in Whole Pelvic Gynecologic Radiotherapy. *International Journal of Radiation Oncology*Biology*Physics,* 72**,** S366-S366.

AMERIO, S., BORIANO, A., BOURHALEB, F., CIRIO, R., DONETTI, M., FIDANZIO, A., GARELLI, E., GIORDANENGO, S., MADON, E., MARCHETTO, F., NASTASI, U., PERONI, C., PIERMATTEI, A., SANZ FREIRE, C. J., SARDO, A. & TREVISIOL, E. (2004) Dosimetric characterization of a large area pixel-segmented ionization chamber. *Med Phys,* 31**,** 414-20.

APPLEBY, A. (1999) The radiation chemical basis of gel dosimetry. *In: 1st International Workshop of Radiation Therapy Gel Dosimetry.* Lexington, Kentucky.

BALDOCK, C., DEENE, Y. D., DORAN, S., IBBOTT, G., JIRASEK, A., LEPAGE, M., MCAULEY, K. B., OLDHAM, M. & SCHREINER, L. J. (2010) TOPICAL REVIEW Polymer gel dosimetry. *Physics in Medicine and Biology,* 55**,** R1-R63.

BJORELAND, A., LINDVALL, P., KARLSSON, A., GUSTAVSSON, H., BACK, S. A., KARLSSON, M. & BERGENHEIM, T. A. (2008) Liquid ionization chamber calibrated gel dosimetry in conformal stereotactic radiotherapy of brain lesions. *Acta Oncol,* 47**,** 1099-109.

BONNETT, D. E., FARAJOLLAHI, A. J. & HARDING, P. F. (1999) An investigation into phantom wall materials for polymer gel phantoms. *In: Proceedings of the 1st International Workshop of Radiation Therapy Gel Dosimetry, Lexington, Kentucky*.

BRADY, S. L., BROWN, W. E., CLIFT, C. G., YOO, S. & OLDHAM, M. (2010) Investigation into the feasibility of using PRESAGE/optical-CT dosimetry for the verification of gating treatments. *Phys Med Biol,* 55**,** 2187-201.

BUSH, K., TOWNSON, R. & ZAVGORODNI, S. (2008) NOTE Monte Carlo simulation of RapidArc radiotherapy delivery. *Physics in medicine and biology,* 53**,** N359-N370.

CEBERG, S., GAGNE, I., GUSTAFSSON, H., SCHERMAN, J. B., KORREMAN, S. S., KJAER-KRISTOFFERSEN, F., HILTS, M. & BACK, S. A. (2010) RapidArc treatment verification in 3D using polymer gel dosimetry and Monte Carlo simulation. *Phys Med Biol,* 55**,** 4885-98.

CEBERG, S., KARLSSON, A., GUSTAVSSON, H., WITTGREN, L. & BÄCK, S. Å. J. (2008a) NOTE Verification of dynamic radiotherapy: the potential for 3D dosimetry under respiratory-like motion using polymer gel. *Physics in medicine and biology,* 53**,** N387-N396.

CEBERG, S., KEALL, P., GUSTAVSSON, H., NORDSTRÖM, F., ZIMMERMAN, J., PERSSON, G., MEDIN, J., SAWANT, A., SVATOS, M., CATTELL, H., BÄCK, S. Å. J. & KORREMAN, S. (2008b) 4D tumour-tracking radiotherapy: a dosimetric and geometric verification using polymer gel [abstract]. *ESTRO27.* Göteborg, Sweden.

DE DEENE, Y., PITTOMVILS, G. & VISALATCHI, S. (2007) The influence of cooling rate on the accuracy of normoxic polymer gel dosimeters. *Physics in medicine and biology,* 52**,** 2719-2728.

DE DEENE, Y., VERGOTE, K., CLAEYS, C. & DE WAGTER, C. (2006a) The fundamental radiation properties of normoxic polymer gel dosimeters: a comparison between a methacrylic acid based gel and acrylamide based gels. *Phys. Med. Biol.,* 51**,** 653.

DE DEENE, Y., VERGOTE, K., CLAEYS, C. & DE WAGTER, C. (2006b) Three dimensional radiation dosimetry in lung-equivalent regions by use of a radiation sensitive gel foam: proof of principle. *Med Phys,* 33**,** 2586-97.

DOSGEL 2006. Fourth International Conference on Radiotherapy Gel Dosimetry. 2006. Sherbrooke.editors: M. Lepage, A. Jirasek, and L.J. Schreiner

DUAN, J., SHEN, S., FIVEASH, J. B., POPPLE, R. A. & BREZOVICH, I. A. (2006) Dosimetric and radiobiological impact of dose fractionation on respiratory motion induced IMRT delivery errors: a volumetric dose measurement study. *Med Phys,* 33**,** 1380-7.

DUMAS, E., LECLERC, G. & LEPAGE, M. (2006) Effect of container size on the accuracy of polymer gel dosimetry. *J. Phys.:Conf. Ser.,* 56**,** p239-241.

FALK, M., AF ROSENSCHOLD, P. M., KEALL, P., CATTELL, H., CHO, B. C., POULSEN, P., POVZNER, S., SAWANT, A., ZIMMERMAN, J. & KORREMAN, S. (2010) Real-time dynamic MLC tracking for inversely optimized arc radiotherapy. *Radiother Oncol,* 94**,** 218-23.

FEYGELMAN, V., FORSTER, K., OPP, D. & NILSSON, G. (2009) Evaluation of a biplanar diode array dosimeter for quality assurance of step-and-shoot IMRT. *J Appl Clin Med Phys,* 10**,** 3080.

FONG, P. M., KEIL, D. C., DOES, M. D. & GORE, J. C. (2001) Polymer gels for magnetic resonance imaging of radiation dose distributions at normal room atmosphere. *Phys Med Biol,* 46**,** 3105-13.

FUXMAN, A. M., MCAULEY, K. B. & SCHREINER, L. J. (2003) Modeling of Free-radical Crosslinking Copolymerization of Acrylamide and N,N'-Methylenebis(acrylamide) for Radiation Dosimetry. *Macromolecular Theory and Simulations,* 12**,** 647-662.

GAGNE, I. M., ANSBACHER, W., ZAVGORODNI, S., POPESCU, C. & BECKHAM, W. A. (2008) A Monte Carlo evaluation of RapidArc dose calculations for oropharynx radiotherapy. *Physics in medicine and biology,* 53**,** 7167-7185.

GIRAUD, P., YORKE, E., JIANG, S., SIMON, L., ROSENZWEIG, K. & MAGERAS, G. (2006) Reduction of organ motion effects in IMRT and conformal 3D radiation delivery by using gating and tracking techniques. *Cancer Radiother,* 10**,** 269-82.

HARALDSSON, P., KARLSSON, A., WIESLANDER, E., GUSTAVSSON, H. & BACK, S. A. (2006) Dose response evaluation of a low-density normoxic polymer gel dosimeter using MRI. *Phys Med Biol,* 51**,** 919-28.

HILTS, M., AUDET, C., DUZENLI, C. & JIRASEK, A. (2000) Polymer gel dosimetry using x-ray computed tomography: a feasibility study. *Phys Med Biol,* 45**,** 2559-71.

ISO (2008) JCGM 100:2008 (GUM 1995 with minor corrections) Evaluation of measurement data — Guide to the expression of uncertainty in measurement, Geneva, International Organisation for Standardisation.

JIN, J. Y., YIN, F. F., TENN, S. E., MEDIN, P. M. & SOLBERG, T. D. (2008) Use of the BrainLAB ExacTrac X-Ray 6D system in image-guided radiotherapy. *Med Dosim,* 33**,** 124-34.

JIRASEK, A., HILTS, M. & MCAULEY, K. B. (2010) Polymer gel dosimeters with enhanced sensitivity for use in x-ray CT polymer gel dosimetry. *Phys Med Biol,* 55**,** 5269-81.

KARLSSON, A. (2007) Characterization and Clinical Application of Normoxic Polymer Gel in Radiation Therapy Dosimetry Malmö, PhD Thesis Lund University (ISBN 978-91-628-7244-1).

KARLSSON, A., GUSTAVSSON, H., MÅNSSON, S., MCAULEY, K. B. & BÄCK, S. Å. J. (2007) Dose integration characteristics in normoxic polymer gel dosimetry investigated using sequential beam irradiation. *Physics in medicine and biology,* 52**,** 4697-4706.

KARLSSON, A., GUSTAVSSON, H., OLSSON, L. E. & BÄCK, S. Å. J. (2003) Image Processing Software for 3D Dose Evaluation in Gel Dosimetry. *World Congress on Medical Physics and Biomedical Engineering.*

KAWRAKOW I. & FIPPEL M. (2000) VMC++, a fast MC algorithm for radiation treatment planning *Proc. 13th Int. Conf. the Use of Computers in Radiotherapy (Heidelberg)* ed W Hamacher and T Bortfeld (Heidelberg: Springer)pp 126–8

KEALL, P. J. & BALDOCK, C. (1999) A theoretical study of the radiological properties and water equivalence of three types of gels used for radiation dosimetry. *Australas Phys Eng Sci Med***,** p.85-91.

KEALL, P. J., SIEBERS J. V., ARNFIELD M, KIM J. O. and MOHAN R. (2001) Monte Carlo dose calculations for dynamic IMRT treatments *Phys. Med. Biol.* **46** 929–41

KJAER-KRISTOFFERSEN, F., OHLHUES, L. & MEDIN, J. (2009) RapidArc volumetric modulated therapy planning for prostate cancer patients. *Acta Oncologica,* 48**,** 227-233.

KORREMAN, S., MEDIN, J. & KJÃ¦R-KRISTOFFERSEN, F. (2009) Dosimetric verification of RapidArc treatment delivery. *Acta Oncologica,* 48**,** 185-192.

KORREMAN, S. S., PEDERSEN, A. N., AARUP, L. R., NOTTRUP, T. J., SPECHT, L. & NYSTROM, H. (2006) Reduction of cardiac and pulmonary complication probabilities after breathing adapted radiotherapy for breast cancer. *Int J Radiat Oncol Biol Phys,* 65**,** 1375-80.

LANGEN, K. M. & JONES, D. T. (2001) Organ motion and its management. *Int J Radiat Oncol Biol Phys,* 50**,** 265-78.

LEPAGE, M., WHITTAKER, A. K., RINTOUL, L., BACK, S. A. & BALDOCK, C. (2001) The relationship between radiation-induced chemical processes and transverse relaxation times in polymer gel dosimeters. *Phys Med Biol,* 46**,** 1061-74.

LETOURNEAU, D., GULAM, M., YAN, D., OLDHAM, M. & WONG, J. W. (2004) Evaluation of a 2D diode array for IMRT quality assurance. *Radiother Oncol,* 70**,** 199-206.

LI, X. A., STEPANIAK, C. & GORE, E. (2006) Technical and dosimetric aspects of respiratory gating using a pressure-sensor motion monitoring system. *Med Phys,* 33**,** 145-54.

MANS, A., REMEIJER, P., OLACIREGUI-RUIZ, I., WENDLING, M., SONKE, J. J., MIJNHEER, B., VAN HERK, M. & STROOM, J. C. (2010) 3D Dosimetric verification of volumetric-modulated arc therapy by portal dosimetry. *Radiother Oncol,* 94**,** 181-7.

MARYANSKI, M. J., GORE, J. C., KENNAN, R. P. & SCHULZ, R. J. (1993) NMR relaxation enhancement in gels polymerized and cross-linked by ionizing radiation: a new approach to 3D dosimetry by MRI. *Magn Reson Imaging,* 11**,** 253-8.

MCCARTER, S. D. & BECKHAM, W. A. (2000) Evaluation of the validity of a convolution method for incorporating tumour movement and set-up variations into the radiotherapy treatment planning system. *Phys Med Biol,* 45**,** 923-31.

MÅNSSON, S., KARLSSON, A., GUSTAVSSON, H., CHRISTENSSON, J. & BÄCK, S. Å. J. (2006) Dosimetric verification of breathing adapted radiotherapy using polymer gel. *Journal of Physics: Conference Series,* 56**,** 300.

NILSSON, G. (2007) SU-FF-T-135: Delta4 – A New IMRT QA Device [Abstract]. *Med Phys,* 34**,** 2432.

NOVOTNY, J., JR., SPEVACEK, V., DVORAK, P., NOVOTNY, J. & CECHAK, T. (2001) Energy and dose rate dependence of BANG-2 polymer-gel dosimeter. *Med Phys,* 28**,** 2379-86.

OHARA, K., OKUMURA, T., AKISADA, M., INADA, T., MORI, T., YOKOTA, H. & CALAGUAS, M. J. (1989) Irradiation synchronized with respiration gate. *Int J Radiat Oncol Biol Phys,* 17**,** 853-7.

OLDHAM, M., BAUSTERT, I., LORD, C., SMITH, T. A. D., MCJURY, M., WARRINGTON, A. P., LEACH, M. O. & WEBB, S. (1998) An investigation into the dosimetry of a nine-field tomotherapy irradiation using BANG-gel dosimetry. *Phys Med Biol,* 43**,** 1113-1132.

OLSSON, L. E., BÄCK, S. Å. J., MAGNUSSON, P. & HARALDSSON, P. (1998) 3D Dosimetry using gels and MRI in Imaging in Radiation Therapy. IN ED, J., HAZLE, D. & BOYER, A. L. (Eds.) *AAPM Monograph No 24.*

OTTO, K. (2008) Volumetric modulated arc therapy: IMRT in a single gantry arc. *Medical Physics,* 35**,** 310-318.

OTTOSSON, W., NORDSTRÖM, F., CEBERG, S. & BACK, S. A. (2008) Characterization and evaluation of a diode array detector system for dynamic and convetional radiotherapy. *ESTRO 27th.* Göteborg, Sweden.

PALMA, D., VOLLANS, E., JAMES, K., NAKANO, S., MOISEENKO, V., SHAFFER, R., MCKENZIE, M., MORRIS, J. & OTTO, K. (2008) Volumetric Modulated Arc Therapy (VMAT) for Delivery of Prostate Radiotherapy: Reduction in Treatment Time and Monitor Unit Requirements Compared to Intensity Modulated Radiotherapy. *International Journal of Radiation Oncology*Biology*Physics,* 72**,** S312-S312.

PEDERSEN, A. N., KORREMAN, S., NYSTROM, H. & SPECHT, L. (2004) Breathing adapted radiotherapy of breast cancer: reduction of cardiac and pulmonary doses using voluntary inspiration breath-hold. *Radiother Oncol,* 72**,** 53-60.

POPESCU, C., OLIVOTTO, I. A., BECKHAM, W. A., ANSBACHER, W., ZAVGORODNI, S., SHAFFER, R., WAI, E. S. & OTTO, K. (2010) Volumetric Modulated Arc Therapy Improves Dosimetry and Reduces Treatment Time Compared to Conventional Intensity-Modulated Radiotherapy for Locoregional Radiotherapy of Left-Sided Breast Cancer and Internal Mammary Nodes. *International Journal of Radiation Oncology, Biology, Physics,* 76**,** 287-295.

POPPE, B., DJOUGUELA, A., BLECHSCHMIDT, A., WILLBORN, K., RUHMANN, A. & HARDER, D. (2007) Spatial resolution of 2D ionization chamber arrays for IMRT dose verification: single-detector size and sampling step width. *Phys Med Biol,* 52**,** 2921-35.

ROGERS DW., FADDEGON B A, DING G X, MA CM,WE J & MACKIE T R (1995) BEAM: a Monte Carlo code to simulate radiotherapy treatment units *Med. Phys.* **22** 503–24

SADAGOPAN, R., BENCOMO, J., MARTIN, R., BALTER, P., VEDAM, S. & NILSSON, G. (2007) TU-D-M100F-04: Characterisation, Commissioning and Evaluation of DELTA4 IMRT QA System [Abstract]. *Med Phys,* 34**,** 2560.

SADAGOPAN, R., BENCOMO, J. A., MARTIN, R. L., NILSSON, G., MATZEN, T. & BALTER, P. A. (2009) Characterization and clinical evaluation of a novel IMRT quality assurance system. *J Appl Clin Med Phys,* 10**,** 2928.

SAWANT, A., VENKAT, R., SRIVASTAVA, V., CARLSON, D., POVZNER, S., CATTELL, H. & KEALL, P. (2008) Management of three-dimensional intrafraction motion through real-time DMLC tracking. *Med Phys,* 35**,** 2050-61.

SEDAGHAT, M., BUJOLD, R. & LEPAGE, M. (2010) Impact of oxygen in the accuracy and precision of normoxic polymer gel dosimeters. *Journal of Physics: Conference Series***,** 83-87.

SEPPENWOOLDE, Y., SHIRATO, H., KITAMURA, K., SHIMIZU, S., VAN HERK, M., LEBESQUE, J. V. & MIYASAKA, K. (2002) Precise and real-time measurement of 3D tumor motion in lung due to breathing and heartbeat, measured during radiotherapy. *Int J Radiat Oncol Biol Phys,* 53**,** 822-34.

SHAFFER, R., MORRIS, W. J., MOISEENKO, V., WELSH, M., CRUMLEY, C., NAKANO, S., SCHMULAND, M., PICKLES, T. & OTTO, K. (2009) Volumetric modulated Arc therapy and conventional intensity-modulated radiotherapy for simultaneous maximal intraprostatic boost: a planning comparison study. *Clin Oncol (R Coll Radiol),* 21**,** 401-7.

SPEVACEK, V., NOVOTNY, J., JR., DVORAK, P., NOVOTNY, J., VYMAZAL, J. & CECHAK, T. (2001) Temperature dependence of polymer-gel dosimeter nuclear magnetic resonance response. *Med Phys,* 28**,** 2370-8.

SPEZI, E., ANGELINI, A. L. & FERRI, A. (2006) A multiple acquisition sequence for IMRT verification with a 2D ion chamber array. *Med Dosim,* 31**,** 269-72.

SPEZI, E., ANGELINI, A. L., ROMANI, F. & FERRI, A. (2005) Characterization of a 2D ion chamber array for the verification of radiotherapy treatments. *Phys Med Biol,* 50**,** 3361-73.

STASI, M., GIORDANENGO, S., CIRIO, R., BORIANO, A., BOURHALEB, F., CORNELIUS, I., DONETTI, M., GARELLI, E., GOMOLA, I., MARCHETTO, F., PORZIO, M., SANZ FREIRE, C. J., SARDO, A. & PERONI, C. (2005) D-IMRT verification with a 2D pixel ionization chamber: dosimetric and clinical results in head and neck cancer. *Phys Med Biol,* 50**,** 4681-94.

SUH, Y., SAWANT, A., VENKAT, R. & KEALL, P. J. (2009) Four-dimensional IMRT treatment planning using a DMLC motion-tracking algorithm. *Phys Med Biol,* 54**,** 3821-35.

TACKE, M. B., NILL, S., KRAUSS, A. & OELFKE, U. (2010) Real-time tumor tracking: automatic compensation of target motion using the Siemens 160 MLC. *Med Phys,* 37**,** 753-61.

TEKE, T., BERGMAN, A. M., KWA, W., GILL, B., DUZENLI, C. & POPESCU, I. A. (2010) Monte Carlo based, patient-specific RapidArc QA using Linac log files. *Med Phys,* 37**,** 116-23.

WENDLING, M., MCDERMOTT, L. N., MANS, A., SONKE, J. J., VAN HERK, M. & MIJNHEER, B. J. (2009) A simple backprojection algorithm for 3D in vivo EPID dosimetry of IMRT treatments. *Med Phys,* 36**,** 3310-21.

VENKATARAMAN, S., MALKOSKE, K. E., JENSEN, M., NAKONECHNY, K. D., ASUNI, G. & MCCURDY, B. M. (2009) The influence of a novel transmission detector on 6 MV x-ray beam characteristics. *Phys Med Biol,* 54**,** 3173-83.

WALTERS B. R., KAWRAKOW I. & ROGERS D. W. (2009) DOSXYZnrc users manual *National Research Council of Canada Report PIRS-794 rev B*

WOLFSBERGER, L. D., WAGAR, M., NITSCH, P., BHAGWAT, M. S. & ZYGMANSKI, P. (2010) Angular dose dependence of Matrixx TM and its calibration. *J Appl Clin Med Phys,* 11**,** 3057.

WONG, J. W., SHARPE, M. B., JAFFRAY, D. A., KINI, V. R., ROBERTSON, J. M., STROMBERG, J. S. & MARTINEZ, A. A. (1999) The use of active breathing control (ABC) to reduce margin for breathing motion. *Int J Radiat Oncol Biol Phys,* 44**,** 911-9.

WUU, C.-S. & XU, Y. (2010) How to perform dosimetry with Optical CT. *Journal of Physics: Conference Series***,** 200-209.

XUE, T. (2007) SU-FF-T-436: Using a 3D Diode Array System to Verify 3D Dose Distribution [Abstract] *Med Phys,* 34**,** 2502.

YORKE, E. D., WANG, L., ROSENZWEIG, K. E., MAH, D., PAOLI, J. B. & CHUI, C. S. (2002) Evaluation of deep inspiration breath-hold lung treatment plans with Monte Carlo dose calculation. *Int J Radiat Oncol Biol Phys,* 53**,** 1058-70.

ZIMMERMAN, J., KORREMAN, S., PERSSON, G., CATTELL, H., SVATOS, M., SAWANT, A., VENKAT, R., CARLSON, D. & KEALL, P. (2009) DMLC motion tracking of moving targets for intensity modulated arc therapy treatment: a feasibility study. *Acta Oncol,* 48**,** 245-50.

Paper I

IOP Publishing Physics in Medicine and Biology

Phys. Med. Biol. **52** (2007) 4697–4706 doi:10.1088/0031-9155/52/15/021

Dose integration characteristics in normoxic polymer gel dosimetry investigated using sequential beam irradiation

A Karlsson[1], H Gustavsson[1], S Månsson[1], K B McAuley[2] and S Å J Bäck[1]

[1] Department of Medical Radiation Physics, Lund University, Malmö University Hospital, Sweden
[2] Department of Chemical Engineering, Queen's University, Kingston, ON, K7L 3N6, Canada

E-mail: anna.karlsson@med.lu.se

Received 9 May 2007, in final form 15 June 2007
Published 18 July 2007
Online at stacks.iop.org/PMB/52/4697

Abstract

Dose integration properties were investigated for normoxic polymer gels based on methacrylic acid (nMAG) and acrylamide/*N*, *N*′-methylenebisacrylamide (nPAG). The effect of sequential irradiation was studied for different fractionation schemes and varying amounts of methacrylic acid for the nMAG gels. Magnetic resonance imaging (MRI) was used for read out of the absorbed dose response. The investigated gels exhibited a dependence on the fractionation scheme. The response when the total dose was divided into fractions of 0.5 Gy was compared with the response when the total dose was delivered in a single fraction. The slope of the R2 versus the absorbed dose response decreased when the absorbed dose per fraction was increased. Also, for higher amounts of methacrylic acid in the nMAG system the difference in the response increased. For gels containing 2, 4, 6 and 8% methacrylic acid, the R2 versus the absorbed dose response increased by 35, 37, 63 and 93%, respectively. Furthermore, the effect of the fractionation was larger when a higher total absorbed dose was given. The effect was less pronounced for the investigated nPAG, containing 3% acrylamide and 3% *N*,*N*′-methylenebisacrylamide, than for the nMAG systems. Consequently, this study indicates that the nPAG system has preferable beam integration characteristics compared with the nMAG system.

1. Introduction

Polymer gel dosimetry has been used for measurements of absorbed dose distributions in a complete volume with high spatial resolution in several studies (e.g. Gustavsson *et al* (2003), Vergote *et al* (2004), Papagiannis *et al* (2006)). A number of gel formulations

Table 1. Gel compositions investigated in this study. The residual amount was ultra-pure deionized water.

	nMAG	nPAG
Gelatine	8% w/w	5% w/w
Methacrylic acid	2%, 4%, 6%, 8% w/w	–
Acrylamide/*N*, *N*′-methylenebisacrylamide	–	3%/3% w/w
Tetrakis(hydroxymethyl)phosphonium chloride	2 mM	5 mM

have been investigated and evaluated (Lepage *et al* 2001a, De Deene *et al* 2002a, 2002b). In common for all polymer gel dosimetry systems are the polymerization induced locally by free radical products of water radiolysis. The polymerization alters various physical and chemical properties of the polymer gel system. The 3D absorbed dose map can, for example, be read out using MRI, optical and x-ray computed tomography (CT) or ultrasound. In order to assess the quality of a gel dosimeter to be used for radiotherapy dosimetry, a number of properties, such as dose resolution (Baldock *et al* 2001), temporal and spatial stability, beam quality dependence, dose-rate dependence and temperature dependence during manufacturing, irradiation and evaluation should be characterized. Polymer gels with added oxygen scavengers which obviate the need to exclude oxygen from the manufacturing process, the so-called normoxic polymer gels, were introduced by Fong *et al* (2001). Recent studies have contributed to the characterization of normoxic polymer gel dosimeters (Gustavsson *et al* 2004a, Venning *et al* 2005, De Deene *et al* 2006, 2007). The aforementioned properties vary significantly between different gel systems. Consequently, each new gel composition has to be characterized. To verify complex radiotherapy treatments with several beam segments or a combination of external therapy and brachy therapy the dosimetry system used should be a dose integrating system, independent of the fractionation scheme. Polymer gel dosimeters have generally been considered to be fully dose integrating dosimetry systems (De Deene and Baldock 2004). The aim of this study was to investigate the dose integration properties for normoxic polymer gels based on methacrylic acid (MAA) (nMAG) and acrylamide (AA)/*N*, *N*′-methylenebisacrylamide (BIS) (nPAG). The effect of sequential irradiation was investigated for different fractionation schemes and varying amounts of MAA. MRI was used for the read out of the absorbed dose response.

2. Methods

2.1. Gel preparation

In this study, five normoxic polymer gel compositions were investigated (table 1). Tetrakis(hydroxymethyl)phosphonium (THP) was used as an oxygen scavenger. The gels were mixed in a fume cupboard, under normal levels of oxygen. All gels were prepared using gelatine (swine skin, 300 bloom, Sigma Aldrich), THP (techn. ∼80% in water, Sigma Aldrich) and ultra-pure deionized water (resistivity >18.2 MΩ cm). For both the nMAG and the nPAG types of gels the gelatine was added to the water at room temperature, which was then heated to 45 °C. The mixture was kept at this temperature until the gelatine had melted completely after approximately 30 min. For the nMAG gel type, the heat was then turned off and when the mixture temperature had cooled to 35 °C the methacrylic acid (∼99% titration, Sigma Aldrich) was added. After approximately another 10 min the THP was added. For the nPAG gel type, the acrylamide (electrophoresis grade, ⩾99%, powder, Sigma Aldrich)

was added to the 45 °C gelatine and water mixture. After approximately 30 min when the acrylamide had completely dissolved, the BIS (electrophoresis grade, ⩾98%, powder, Sigma Aldrich) was added. After the BIS was dissolved, the solution was left to cool down to 35 °C before the THP was added. The solutions were stirred continuously through the entire mixing procedure. The gels were poured into 15 ml screw-top glass vials and left to set at room temperature (approx. 20 °C) overnight.

2.2. Irradiation

All gel samples were irradiated using an Elekta Sli (Sweden) linear accelerator. The vials were irradiated with 18 MV photons at the depth of dose maximum, in a 30 × 30 × 30 cm^3 water phantom, in order to ensure a homogenous absorbed dose over the sample. A beam size of 20 × 20 cm^2 was used and the SSD was 100 cm. Five different fractionation schemes were used: 0.25, 0.5, 1, 2 and 4 Gy per fraction. The beam was turned off for approximately 70 s between two sequential beams, which was considered as a clinically relevant time between individual beams. The dose rate at the position where the vials were irradiated was 5.1 Gy min^{-1}.

2.3. Output linearity of the linear accelerator

The dose response per monitor unit was investigated for the 18 MV beam used for the gel measurements. A cylindrical ionization chamber (NE 2571 Farmer, 0.6 cm^2) was placed at the isocenter at a depth of 10 cm in a water-filled phantom (21 × 21 × 28 cm^3). The setup followed the recommendations for measurement of the absorbed dose in the standard dosimetry protocol, IAEA TRS-398 (International Atomic Energy Agency 2000). The collimator settings for the measurements were 10 × 10 cm^2. Readings were recorded for monitor units ranging from 1 to 900 MUs.

2.4. Magnetic resonance imaging and evaluation

MRI was undertaken approximately 24 h after the irradiation, using a Siemens Symphony 1.5 T scanner (Siemens Medical Solutions, Germany). The samples were stored at room temperature between irradiation and scanning to ensure temperature equilibration. The gels were scanned using a 32-echo multiple spin echo sequence, with a repetition time of 4000 ms and voxel size of 1.0 × 1.0 × 3.0 mm^3. The inter echo time was set to 10.6 ms for the nMAG gels. For the nPAG gel the inter echo time was increased to 20.0 ms. Two acquisitions were averaged for each scan and the total acquisition time was approximately 24 min. Data processing was carried out using an in-house written software routine run under IDL (Interactive Data Language, Research Systems Inc., Boulder, CO, USA) (Karlsson *et al* 2003). For evaluation of the absorbed dose response the linear regions of R2 versus the absorbed dose curves were used. In this study, all slopes of the R2 versus the absorbed dose response curves have been assessed from the linear region in the low dose area of the response. All linear fits to assess the slopes had r^2 values higher than 0.994.

3. Results

The deviations in ionization per monitor unit were within ±0.4% for the monitor unit settings used in this study (figure 1). The output linearity was found to be of the same magnitude as reported for other linear accelerators (cf Hansen *et al* (1998), Cheng and Das (2002),

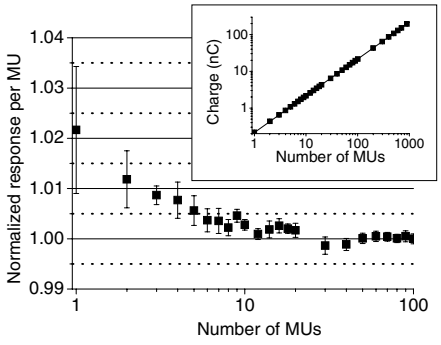

Figure 1. The response per monitor unit versus the number of monitor units for the 18 MV beam, Elekta Sli, normalized to the 100 MU measurement. A minimum of 23 MUs, 0.25 Gy, per beam was used. The uncertainty bars represent the spread from repeated measurements (1 SD).

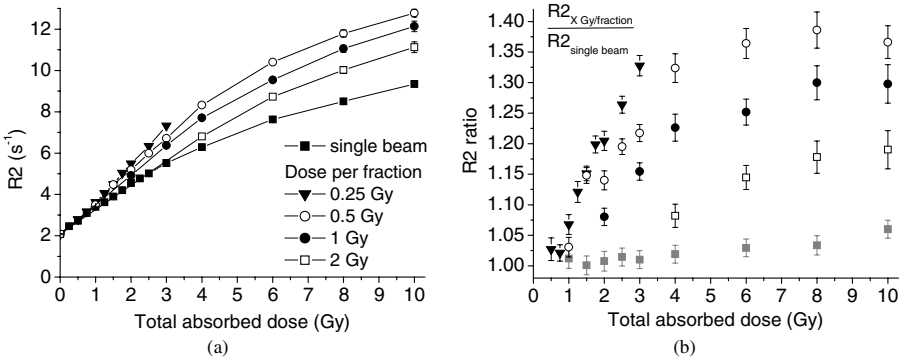

Figure 2. (a) The R2 dose response for nMAG samples (2% MAA) irradiated to absorbed doses of up to 10 Gy. When the total dose was delivered in sequential beams the R2 dose response for the total absorbed dose increased with an increased number of beams. In most cases the uncertainty bars, one standard deviation (1 SD) in the R2 map, were smaller than the symbols and therefore not visible. The lines were included as a visual aid. (b) The same result as in (a) normalized to the single-beam irradiation. The result for the nPAG (3%AA/3%BIS) was also included (■). The uncertainty bars correspond to 1 SD in the R2 map. The different fractionation schemes are denoted with the same symbols in (a) and (b).

Aspradakis *et al* (2005)). Thus, no effect of varying output linearity was expected and no corrections were undertaken.

For both the nMAG and the nPAG system the R2 versus absorbed dose response was found to be dependent on the fractionation scheme used (figures 2(a) and 3). The effect was larger when a higher total dose was given (figures 2(b) and 3).

For the nMAG system the slope of the R2 versus the absorbed dose response decreased in an exponential way when the dose per fraction was increased (figure 4). Although on a different time scale, this resembles the dose-rate dependence reported by De Deene *et al* (2006).

For the nMAG system, the difference in slopes of the dose response curves, when the dose was given in 0.5 Gy fractions compared to a single beam, was increased when higher

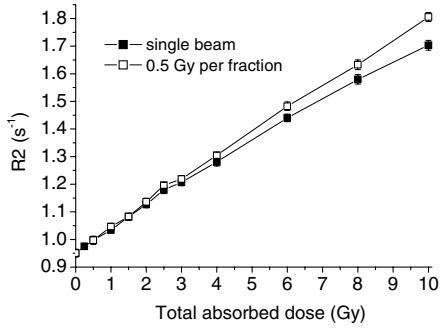

Figure 3. R2 versus the total absorbed dose for the nPAG (3%AA/3%BIS). The lines were included as a visual aid. The uncertainty bars correspond to 1 SD in the R2 map. In most cases the uncertainty bars were smaller than the symbols and therefore not visible.

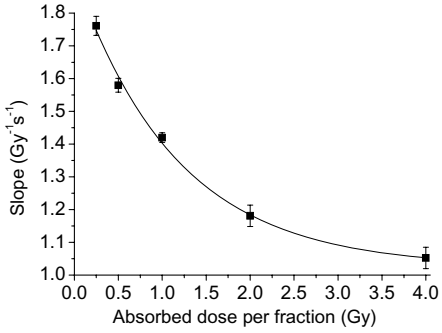

Figure 4. The slope of the dose response for the various fractionation schemes versus the dose per fraction for the nMAG dosimeter (2% MAA). The approximately linear regions in the low dose area of R2 versus absorbed dose curves were used when the slopes were estimated. Further, the uncertainty bars correspond to 1 SD of the linear fits from which the slopes were obtained. The exponential curve was included in the figure as a visual aid.

concentrations of MAA were used (figure 5). The increases were 35, 37, 63 and 93% for gels containing 2, 4, 6 and 8% MAA, respectively. The increased slope ratios point out the dependence on the amount of MAA in the gel recipe.

4. Discussion

As described by Appleby (1999), free-radical-induced chain polymerization can be considered as a four-step process involving radical generation, chain initiation, propagation and termination. The gel systems studied consist of approximately 90% by weight of water, and therefore the response to the absorbed dose is mainly based on reactions initiated by the radiation chemistry of water. The free radicals are generated through radiolysis of water (Johns and Cunningham 1980), which is followed by an initiation step in which many of these radicals react with monomers to form free radicals with one monomer unit. The resulting radicals then add monomer units to the end of the chain via propagation reactions. The radical generation, initiation and propagation processes for the two gel systems investigated in this

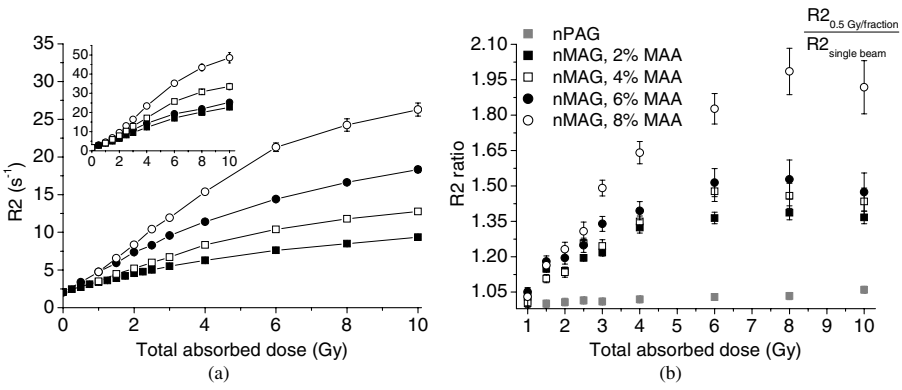

Figure 5. (a) R2 dose response for nMAG (2% MAA (filled), 4% MAA (open), 6% MAA (insert, filled), 8% MAA (insert, open)) irradiated to absorbed doses of up to 10 Gy. The data for the gels that contained 6% and 8% MAA were inserted in (a) in order to utilize a more suitable dynamic range for the R2-values considering the response of the 2% and 4% MAA gels. The total dose was divided into fractions of 0.5 Gy (circles) or delivered using a single beam (squares). When the amount of MAA was increased, the ratio between the absorbed dose responses for the 0.5 Gy/fraction scheme and the single beam irradiation was increased. In most cases the uncertainty bars, one standard deviation (1 SD) in the R2 map, were smaller than the symbols and therefore not visible. The lines were added as a visual aid. (b) The same result as in (a) normalized to the single beam irradiation. The result for the nPAG (3%/AA/3%BIS) was also included. The uncertainty bars correspond to 1 SD in the R2 map.

study are very similar, except that the nPAG system involves two monomers (the acrylamide monomer and the *N*, *N*′-methylenebisacrylamide crosslinker) and the nMAG system has only one monomer (the methacrylic acid monomer).

In both systems, chain growth stops through termination and chain transfer processes. Termination occurs when two free radicals meet, and either a combination or disproportionation reaction occurs. Both modes of termination result in the destruction of the free radicals so that further propagation cannot occur. In the termination-by-combination process, the two growing free radical chains combine to form a single long polymer chain, with the two free radical electrons participating in a new covalent chemical bond. In the termination-by-disproportionation process, two dead polymer molecules are formed after one of the free radicals abstracts (steals) a hydrogen atom near the free radical on the other chain, leading to a new covalent bond between the carbon at the end of the first chain and the abstracted hydrogen. The new unpaired electron, which is left behind when the hydrogen atom is abstracted, leads to the formation of a carbon–carbon double bond at the end of the second chain, which consumes both free radicals. In methacrylic acid and acrylamide systems the kinetic parameters for the biomolecular termination processes, i.e., combination and disproportionation, have been reported to be of similar magnitudes and are relatively small (Gromov *et al* 1980, Matuszewska-Czerwik and Polowinski 1998, Seabrook *et al* 2005). This indicates that the differences in fractionation scheme dependence for the two systems could not be explained by differences in the kinetics of the bimolecular termination processes.

In the chain transfer process, a polymeric radical abstracts a hydrogen atom from another molecule (a hydrogen atom that is not near a radical chain end). A covalent bond forms between the abstracted hydrogen and the growing polymer chain, consuming the free radical at the end of the original chain. A new free radical is produced on the species

from which the hydrogen atom was abstracted. In cases where the new free radical that is generated is able to initiate new polymerization reactions, then chain transfer reactions have little influence on the polymerization rate, and the main outcome is that short dead polymer molecules are created. However, when the new radical that is generated is quite stable, so that it is unable to (or slow to) initiate further polymerization, then a lower polymerization rate is obtained. Stable radicals that do not initiate further polymerization are capable of bimolecular termination with propagating radicals, which can further reduce the polymerization rate. Fuxman *et al* (2003, 2005) used chain transfer reactions with gelatine and the formation of stable gelatine radicals to explain the reduction in monomer consumption rates that are observed in PAG dosimeters (Lepage *et al* 2001b) when higher gelatine concentrations are used. Reactions between radicals and THP may also be important in normoxic dosimeters. Recently, De Deene *et al* (2006) showed that nPAG and nMAG dosimeters behave very differently in response to increases in gelatine concentrations. Unlike nPAG dosimeters, in which higher gelatine levels lead to lower NMR dose sensitivity (De Deene *et al* 2006) due to lower polymerization rates, in nMAG dosimeters increasing gelatine levels actually increase the NMR dose sensitivity (De Deene *et al* 2006) because growing polymethacrylic acid chains do not readily undergo chain transfer to gelatine and gelatine is important for precipitation of polymethacrlyic acid chains from solution (McAuley 2006, De Deene *et al* 2006).

Radical generation rate (i.e. dose rate) has an important influence on the rate of free radical polymerization reactions (Appleby 1999). Higher rates of radical generation lead to higher concentrations of radicals. Since propagation and chain transfer reactions involve one polymeric radical, the rates of these reactions are proportional to the radical concentration. Chain termination reactions (by combination and by disproportionation) involve reactions between two free radicals and, as a result, the rates of these termination reactions are proportional to the *square* of the radical concentration. When radical concentrations are doubled, the rates of propagation and chain transfer reactions increase by a factor of 2, whereas the rates of bimolecular termination reactions increase by a factor of 4. This is the reason for the dose-rate dependence in nMAG, which has been observed by De Deene *et al* (2006) and in this study. Since the dominant means of radical consumption in nMAG is bimolecular termination, generating a higher concentration of radicals over a shorter time (i.e. a higher dose rate) will result in a reduction in the average lifetime for free radicals and to less polymer formation. On the other hand, in nPAG where chain transfer to gelatine appears to be the dominant means for radical consumption (Fuxman *et al* 2003, McAuley 2006), increasing the radical concentration has very little influence on the average lifetime for a free radical and the average chain length that is obtained before a radical is consumed.

The fractionation dependence observed for nMAG in this study is related to the dose-rate effect. When radicals are generated in short bursts, followed by a period without irradiation, each burst of radicals results in a short period of high radical concentration and fast bimolecular termination. As the concentration of radicals drops between the radiation pulses, the rate of termination decreases. If the same total dose is delivered using smaller dose fractions, the same total number of radicals is generated by radiolysis of the water, but the total amount of bimolecular termination that occurs is smaller, because the radical concentration during each burst is smaller. As a result, less polymer forms if the total dose is delivered all at once, rather than in smaller fractions. Unfortunately, this fractionation dependence reveals that nMAG is not a good integrating dosimeter.

The influence of the fractionation dependence on clinical dosimetric verification will depend on the choice of calibration method. This was demonstrated with a simulated example for the nMAG system with 2% MAA (figure 6). The results from the gel measurements

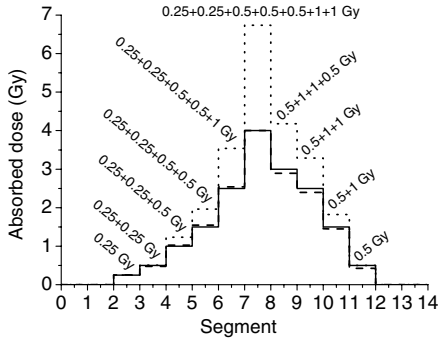

Figure 6. A simulated example of absorbed dose profiles for the nMAG system with 2% MAA. The figures in the graph denote the hypothetical fractionation scheme for the segments of the absorbed dose profile. The solid line represents the true absorbed dose. The absorbed dose profile obtained using gel vial calibration (method I, dotted line) was compared with the absorbed dose profile obtained using a relative calibration (method II, dashed line).

(figure 2(a)) were used for the calculations that corresponded to gel vial calibration (method I) or relative calibration, i.e. assuming a linear dose response and knowledge of the dose in a normalization point (method II). The difference between the true absorbed dose and the estimated absorbed dose when the gel system was calibrated according to method I was approximately 70% in the simulated high dose area. Using method II, the difference between the true and the estimated absorbed dose was within 3% for all segments of the absorbed dose profile (figure 6). Naturally, this method will be most accurate at the normalization dose level. In this simulated example normalization was performed at the target dose level (4 Gy). The effect of the fractionation dependence increased with increased total absorbed dose. Hence, using higher absorbed doses will increase the uncertainty related to fractionation dependence.

In order to minimize the fractionation dependence when using the nMAG system, the concentration of MAA should be reduced to a minimum and the total absorbed dose should be as low as possible. However, lowering the amount of MAA will reduce the sensitivity and the dose resolution of the system (Baldock *et al* 2001, Gustavsson *et al* 2004b). In practice this means that the nMAG gel systems are not suitable for clinical dosimetry. The nPAG system has preferable beam integration characteristics compared with the nMAG system. The differences in slopes of the dose response curves when the dose was given in 0.5 Gy fractions compared to a single fraction were 35% and 12% for the nMAG (2% MAA) and nPAG systems, respectively. Again, the slopes were evaluated in the approximately linear regions in the low dose area of the R2 versus absorbed dose curves.

It is likely that altering the time interval will have an influence on the degree of fractionation dependence. The difference between the dose rate and the fractionation dependence might be seen as an indication of that. Further investigations would be of great interest, especially regarding verification of intensity-modulated radiotherapy (IMRT) and breathing-adapted radiotherapy (BART).

5. Conclusion

For the polymer gels investigated in this study the absorbed dose response was found to be dependent on the fractionation scheme. The R2 versus the absorbed dose response was increased when the dose per fraction was decreased. A dependence on the concentration

of MAA was observed for the nMAG system. A higher concentration of MAA led to a more pronounced dependence on the fractionation scheme. Furthermore, the effect of the fractionation was larger when a higher total absorbed dose was given for both the nMAG and the nPAG system. However, this study indicates that the nPAG system has preferable beam integration characteristics compared with the nMAG system.

The influence of the fractionation dependence in clinical dosimetry will depend on the choice of calibration method. Relative calibration will lead to a much smaller measurement error.

Acknowledgments

The financial support of the Swedish Cancer Society (4726-B04-03XAC) and the Cancer Foundation at Malmö University Hospital is acknowledged.

References

Appleby A 1999 The radiation chemical basis of gel dosimetry *Proc. 1st Int. Workshop of Radiation Therapy Gel Dosimetry (Lexington, Kentucky)*

Aspradakis M M, Lambert G D and Steele A 2005 Elements of commissioning step-and-shoot IMRT: delivery equipment and planning system issues posed by small segment dimensions and small monitor units *Med. Dosim.* **30** 233–43

Baldock C, Lepage M, Back S A, Murry P J, Jayasekera P M, Porter D and Kron T 2001 Dose resolution in radiotherapy polymer gel dosimetry: effect of echo spacing in MRI pulse sequence *Phys. Med. Biol.* **46** 449–60

Cheng C W and Das I J 2002 Comparison of beam characteristics in intensity modulated radiation therapy (IMRT) and those under normal treatment condition *Med. Phys.* **29** 226–30

De Deene Y and Baldock C (ed) 2004 *Third Int. Conf. on Radiotherapy Gel Dosimetry, J. Phys.: Conf. Series* **3**

De Deene Y, Hurley C, Venning A, Vergote K, Mather M, Healy B J and Baldock C 2002a A basic study of some normoxic polymer gel dosimeters *Phys. Med. Biol.* **47** 3441–63

De Deene Y, Pittomvils G and Visalatchi S 2007 The influence of cooling rate on the accuracy of normoxic polymer gel dosimeters *Phys. Med. Biol.* **52** 2719–28

De Deene Y, Venning A, Hurley C, Healy B J and Baldock C 2002b Dose-response stability and integrity of the dose distribution of various polymer gel dosimeters *Phys. Med. Biol.* **47** 2459–70

De Deene Y, Vergote K, Claeys C and De Wagter C 2006 The fundamental radiation properties of normoxic polymer gel dosimeters: a comparison between a methacrylic acid based gel and acrylamide based gels *Phys. Med. Biol.* **51** 653–73

Fong P M, Keil D C, Does M D and Gore J C 2001 Polymer gels for magnetic resonance imaging of radiation dose distributions at normal room atmosphere *Phys. Med. Biol.* **46** 3105–13

Fuxman A M, Mcauley K B and Schreiner L J 2003 Modeling of free-radical crosslinking copolymerization of acrylamide and N, N′-methylenebis(acrylamide) for radiation dosimetry *Macromolecular Theory Simulations* **12** 647–62

Fuxman A M, Mcauley K B and Schreiner L J 2005 Modelling of polyacrylamide gel dosimeters with spatially non-uniform radiation dose distributions *Chem. Eng. Sci.* **60** 1277–94

Gromov V F, Galperina N I, Osmanov T O, Khomikovskii P M and Abkin A D 1980 Effect of solvent on chain propagation and termination reaction rates in radical polymerization *Eur. Polym. J.* **16** 529–35

Gustavsson H, Back S A, Medin J, Grusell E and Olsson L E 2004a Linear energy transfer dependence of a normoxic polymer gel dosimeter investigated using proton beam absorbed dose measurements *Phys. Med. Biol.* **49** 3847–55

Gustavsson H, Ck S, Lepage M, Rintoul L and Baldock C 2004b Development and optimization of a 2-hydroxyethylacrylate MRI polymer gel dosimeter *Phys. Med. Biol.* **49** 227–41

Gustavsson H, Karlsson A, Back S A, Olsson L E, Haraldsson P, Engstrom P and Nystrom H 2003 MAGIC-type polymer gel for three-dimensional dosimetry: intensity-modulated radiation therapy verification *Med. Phys.* **30** 1264–71

Hansen V N, Evans P M, Budgell G J, Mott J H L, Williams P C, Brugmans M J P, Wittkamper F W, Mijnheer B J and Brown K 1998 Quality assurance of the dose delivered by small radiation segments *Phys. Med. Biol.* **43** 2665–75

International Atomic Energy Agency 2000 Absorbed Dose Determination in External Beam Radiotherapy: An International Code of Practice for Dosimetry based on Standards of Absorbed Dose to Water *Technical Report Series* No 398. (Vienna)

Johns H E and Cunningham J R 1980 *The Physics of Radiology (American Lecture Series)* (Springfield, IL: Charles C Thomas)

Karlsson A, Gustavsson H, Olsson L and Back S A 2003 Image processing software for 3D dose evaluation in gel dosimetry *Proc. World Congress on Medical Physics and Biomedical Engineering (Sydney, Australia, 24–29 Aug)*

Lepage M, Jayasakera P M, Back S A J and Baldock C 2001a Dose resolution optimization of polymer gel dosimeters using different monomers *Phys. Med. Biol.* **46** 2665–80

Lepage M, Whittaker Andrew K, Rintoul L, Ck S and Baldock C 2001b The relationship between radiation-induced chemical processes and transverse relaxation times in polymer gel dosimeters *Phys. Med. Biol.* **46** 1061–74

Matuszewska-Czerwik J and Polowinski S 1998 Template photopolymerization of methacrylic acid-VI. Homo- and copolymerization *Eur. Polym. J.* **34** 557–9

McAuley K B 2006 Fundamentals of polymer gel dosimeters *J. Phys.: Conf. Ser.* **56** 35–44

Papagiannis P, Pantelis E, Georgiou E, Karaiskos P, Angelopoulos A, Sakelliou L, Stiliaris S, Baltas D and Seimenis I 2006 Polymer gel dosimetry for the TG-43 dosimetric characterization of a new 125I interstitial brachytherapy seed *Phys. Med. Biol.* **51** 2101–11

Seabrook S A, Pascal P and Tonge M P 2005 Termination rate coefficients for acrylamide in the aqueous phase at low conversion *Polymer* **46** 9562–74

Venning A J, Hill B, Brindha S, Healy B J and Baldock C 2005 Investigation of the PAGAT polymer gel dosimeter using magnetic resonance imaging *Phys. Med. Biol.* **50** 3875–88

Vergote K, De Deene Y, Duthoy W, De Gersem W, De Neve W, Achten E and De Wagter C 2004 Validation and application of polymer gel dosimetry for the dose verification of an intensity-modulated arc therapy (IMAT) treatment *Phys. Med. Biol.* **49** 287–305

Paper II

IOP PUBLISHING PHYSICS IN MEDICINE AND BIOLOGY

Phys. Med. Biol. **53** (2008) N387–N396 doi:10.1088/0031-9155/53/20/N02

NOTE

Verification of dynamic radiotherapy: the potential for 3D dosimetry under respiratory-like motion using polymer gel

S Ceberg, A Karlsson, H Gustavsson, L Wittgren and S Å J Bäck

Department of Medical Radiation Physics, Lund University, Malmö University Hospital, Sweden

E-mail: sofie.ceberg@med.lu.se

Received 3 July 2008, in final form 20 August 2008
Published 30 September 2008
Online at stacks.iop.org/PMB/53/N387

Abstract

Following the implementation of advanced treatment procedures in radiotherapy, there is a need for dynamic dose verification in 3D. Gel dosimetry could potentially be used for such measurements. However, recently published data show that certain types of gels have a dose rate and fractionation dependence. The aim of this study was to investigate the feasibility of using a polymer gel dosimeter for dose verification of dynamic radiotherapy. To investigate the influence of dose rate dependence during respiratory-like motion in and out of the beam, a respiration robot together with two types of gel systems (normoxic methacrylic acid gel (nMAG) and normoxic polyacrylamide gel (nPAG)) were used. Reference measurements were obtained using a linear diode array (LDA). Expected results, if there was no influence of the dose rate variation, were calculated by convolving the static irradiated gel data with the motion function controlling the robot. To investigate the fractionation dependence, the gels were irradiated using gated and ungated deliveries. Magnetic resonance imaging was used to evaluate the absorbed dose response of the gel. The measured gel data coincided well with the LDA data. Also, the calculated data agreed well with the measured dynamic gel data, i.e. no dose rate dependence due to motion was observed. The difference in the R2 response for the gels receiving ungated and gated, i.e. fractionated, deliveries was less than 1% for the nPAG and 4% for the nMAG, for absorbed doses up to 2 Gy. The maximum difference was 1.2% for the nPAG and 9% for the nMAG, which occurred at the highest given dose (4 Gy). The investigated gels were found to be feasible detectors for dose measurements under respiratory-like motion. For dose verification of dynamic RT involving gated delivery, e.g. breathing-adapted radiotherapy, relative absorbed dose evaluation should be used in order to minimize the effects of fractionated irradiation.

(Some figures in this article are in colour only in the electronic version)

1. Introduction

The desire to increase the conformity of the dose distribution in external radiotherapy has resulted in advanced treatment procedures, for instance techniques using intensity-modulated beams and arcs, or breathing-adaptive radiotherapy (BART) (Otto 2008, Li *et al* 2008, Keall *et al* 2006). The advantage of these techniques is the increased possibility of delivering a high absorbed dose to the target volume while minimizing the dose to normal tissues. However, the dosimetric and geometric uncertainties associated with small fields, steep dose gradients and target motion remain to be evaluated in detail. For instance, in the case of respiratory motion, experimental data have until now been obtained using ionization chambers, diode arrays or film, in order to determine the dosimetric impact of the smearing effect due to the motion (Wiersma and Xing 2007, Li *et al* 2006, Duan *et al* 2006). Aiming under measurement conditions, as similar to the clinical case as possible, and having a respiratory-induced target motion during volumetric-modulated arc therapy delivery in mind, there is a need for 3D dose verification methods. Polymer gel dosimetry is an attractive 3D dosimetric system that could potentially be used for this purpose (De Deene 2002, Gustavsson *et al* 2003, Vergote *et al* 2004, Isbakan *et al* 2007). Recently published data indicate that the dose response of certain types of polymer gels depends on the dose rate and fractionation scheme (De Deene *et al* 2006, Karlsson *et al* 2007). This could limit the usefulness of gels for dose verification of dynamic radiotherapy. In the case of measurements during respiratory-like motion, a certain region in the gel will experience a gradually varying dose rate while it is moving in and out across the penumbra region of the beam. Furthermore, if the gel dosimeter is irradiated using BART such as respiratory gating, the irradiation will be fractionated since the beam is turned on and off during gated delivery. Dose rate and fractionation dependence on the absorbed dose response are most probably caused by the same chemical phenomena, although on different time scales (Karlsson 2007, Karlsson *et al* 2007).

The aim of this study was, therefore, to investigate the feasibility of using a 3D gel dosimeter for dose verification of dynamic radiotherapy. In order to estimate the magnitude of the possible dose rate and fractionation dependences, the effects were isolated during the experiments. A respiration robot together with two types of normoxic polymer gel system was used. To validate the gel measurements, a linear diode array (LDA) was used as a reference detector system. Additionally, expected results were calculated by convolving the static irradiated gel data with the motion function controlling the respiration robot.

2. Methods and materials

2.1. Gel preparation

In this study, two normoxic polymer gel systems were used: normoxic methacrylic acid gel (nMAG), based on 2% w/w methacrylic acid (∼99% titration, Sigma Aldrich), and normoxic polyacrylamide gel (nPAG), based on 3% w/w acrylamide (electrophoresis grade, ⩾99%, powder, Sigma Aldrich) and 3% w/w *N*,*N*′-methylenebisacrylamide (electrophoresis grade, ⩾98%, powder, Sigma Aldrich). In both systems, gelatine (swine skin, 300 bloom, Sigma Aldrich) was used as the matrix substance and tetrakis(hydroxymethyl)–phosphonium chloride (techn. ∼80% in water, Sigma Aldrich) was used as an oxygen scavenger (table 1). The remaining constituent was ultra-pure deionized water (resistivity > 18.2 MΩ cm). The gel preparation has been described elsewhere (Karlsson *et al* 2007). The gelatine and water were mixed in room temperature and then heated to 45 °C to completely dissolve the gelatine. For the nPAG system, the monomers were added at this temperature before cooling down, but

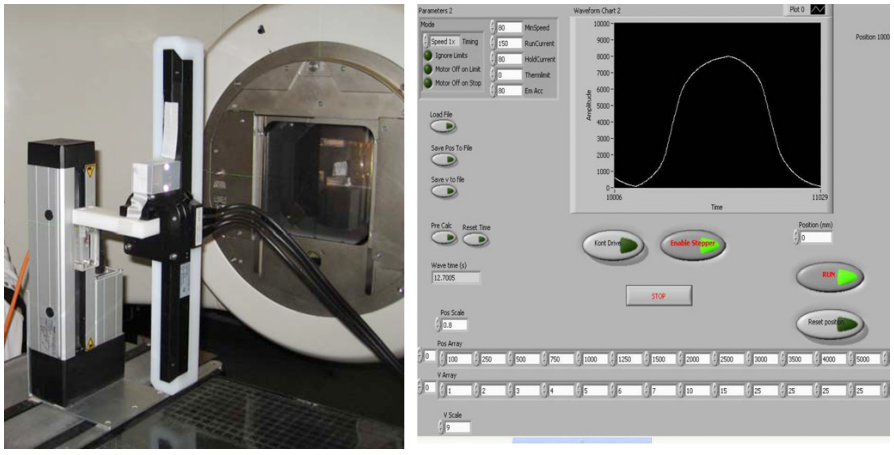

Figure 1. The robot simulated the respiration motion, here shown with the LDA detector attached to the moving platform (left). The RPM system (Varian) was used to monitor the position of the platform. The motion was generated using a step motor, controlled by an in-house-developed software (right) in which the motion parameters such as amplitude, frequency and curve pattern were defined.

Table 1. Gel compositions.

Gel ingredients	nPAG	nMAG
Gelatine	5% w/w	8% w/w
Monomers	3%/3% w/w acrylamide/*N*, *N*′ methylenebisacrylamide	2% w/w methacrylic acid
Tetrakis(hydroxymethyl)-phosphonium chloride	10 mM	2 mM
Ultra-pure deionized water	89% w/w	90% w/w

for the nMAG system the monomer was added after the mixture temperature had decreased to 35 °C. The gels were prepared under normal levels of oxygen, and the solutions were stirred continuously through the entire mixing procedure. Ten minutes before the gel was poured into bottles and vials, the oxygen scavenger was added. The phantoms were left to set in the dark at room temperature for about 24 h before irradiation.

2.2. The respiration robot

A respiration robot, simulating the respiratory motion of the thorax region, was designed and constructed. The motion was generated using a step motor, controlled by a computer program (LabVIEW 7.1), which allowed setting of several motion parameters such as amplitude, frequency and curve pattern. Based on 54 two-dimensional vectors containing information about position and velocity, a typical breathing pattern was generated (figure 1). A gel phantom was positioned on a platform attached to the motion generator. To enable measurements using a LDA, the platform was replaced by a special holder. To remain stable during motion, the robot was mounted on to a fixation equipment designed for Varian couches. In this study,

the respiration robot software was programmed to produce a motion pattern with a 12 mm amplitude during a 12.7 s cycle. To mimic a respiratory-like motion, more time was spent at the extreme positions of the platform. Plateaus corresponding to the end-inspiration and end-expiration breathing phases were thus simulated. The position of the respiration robot was verified using the real-time positioning management system (RPM, Varian Medical Systems).

2.3. Radiation delivery and dose measurement

2.3.1. Linear accelerator output linearity in a gating mode. The linear accelerator (Clinac 2100C/D, Varian Medical Systems) output linearity is checked regularly as part of the department's quality assurance program. Additionally, to confirm that the linear accelerator delivered the same dose in the gating mode as when giving the total number of monitor units (MU) in a single irradiation, the output from gated and ungated beams was investigated using a cylindrical ionization chamber (Farmer 2571, 0.6 cm^3, Nuclear Enterprise). The chamber was placed at 10 cm depth in a water-filled phantom and irradiated using a 10×10 cm^2 6 MV photon beam. During gated irradiation, a respiration robot trigged the accelerator to deliver 10 MU during each beam-on, determined by an adjustable gating window defined by the RPM system. Twenty 10 MU beams were delivered in the gating mode and readings were recorded for each beam. Conventional ungated beams were delivered with the MU ranging from 1 to 250 for comparison.

2.3.2. Motion-induced dose rate variation. To investigate the effect of the dose rate variation in the gel caused by the motion in and out of the beam, two identical 250 ml gel phantoms from the same batch for each gel system were irradiated to a target dose of 2 Gy. One phantom was irradiated in a static position and one was irradiated during the 12 mm periodical vertical motion. The linear accelerator was set to deliver 300 MU min^{-1} and the measurements were undertaken using a 5×5 cm^2 6 MV photon beam at a 90° angle to the vertical motion. A dose profile from the static phantom was convolved with a motion function calculated from the velocity and position vectors controlling the respiration robot. The convolved data were then compared with the measured dose profile from the moving phantom. For dosimetric verification of the dynamic gel data, measurement using a diode array was carried out. The linear detector array LDA-99 (IBA Dosimetry) consists of 99 Hi-pSi diodes with a center-to-center distance of 5 mm, i.e. an active length of 49 cm. The LDA response for a 5×5 cm^2 6 MV beam has been previously investigated regarding linearity and dose rate dependence (Ottosson *et al* 2008). Further, output factor comparison has been carried out with an ion chamber (Farmer 2577, 0.2 cm^3, Nuclear Enterprise) and depth–dose curves' comparisons with a PFD-3G diode (IBA Dosimetry). Since the largest observed deviation was below 1%, the LDA-99 detector was considered to be suitable to be used as a reference detector in this study. The LDA was attached to the respiratory robot with a 2.5 cm thick slab of polystyrene mounted on top of the array. The corresponding dose profiles from the gel measurements at mass density scaled depth were extracted from the gel phantom data. All irradiation parameters, such as the source-to-surface distance (SSD), beam size and simulated breathing pattern, were identical to the gel experiment. Two profiles were obtained using the LDA, one in the static mode and one during motion.

2.3.3. Fractionated dose induced by gated delivery. Gel vials were irradiated to investigate the possible beam fractionation effect on dose versus R2 response. To isolate the effect of fractionation dependence due to gated delivery alone, the respiration robot was disabled. Fourteen gel vials for each gel system were irradiated: seven undergoing gated delivery with

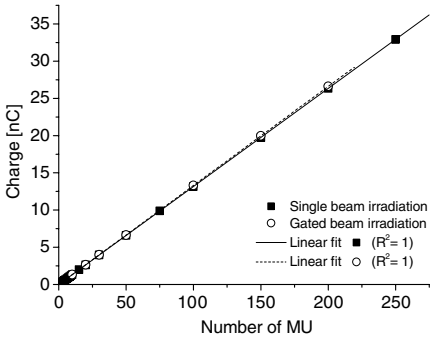

Figure 2. The accumulated charge in the gating mode compared to the charge collected from single beam irradiation. The gated irradiation was delivered in fractions of 10 MU/beam-on in the gating mode. Uncertainty bars represent the spread from repeated measurements (1 SD) and are smaller than the symbols and therefore not visible.

12 MU/beam and seven receiving the total dose in one fraction. The vials undergoing gated delivery were irradiated every 6.5 s, simulating a normal breathing period. The gel response for total absorbed doses between 0.5 and 4.0 Gy was investigated for the two types of delivery. To ensure a homogeneously absorbed dose, the vials were placed at 3 cm depth in a 30 × 30 × 30 cm^3 water phantom and irradiated using a 20 × 20 cm^2 6 MV photon beam. The linear accelerator was set to deliver 500 MU min^{-1}.

2.4. Magnetic resonance imaging

Approximately 24 h after irradiation, magnetic resonance imaging (MRI) of the gel was carried out using a 1.5 T MRI unit (Siemens Medical Systems) and a circularly polarized receive-only head coil. The protocol and set-up have been described elsewhere (Karlsson *et al* 2007). The images were acquired using a 32-echo multi-spin echo sequence with inter-echo spacing equal to 25 ms for the nPAG gel and 10.6 ms for the nMAG gel. The different inter-echo spacing times were chosen to obtain adequate coverage of the signal decay curve for the different gel types. The repetition time was 4000 ms and the voxel size was 1 × 1 × 3 mm^3. To obtain an accurate background signal, an identical but unirradiated gel phantom was scanned as well. The background phantoms were handled together with the irradiated phantoms during the whole process. In-house-developed software was used for image processing (Karlsson *et al* 2003).

3. Results and discussion

3.1. Linear accelerator output linearity in the gating mode

The readings for gated beams of 10 MU/beam-on coincided well with corresponding values for the ungated beams (figure 2). The deviation between the slopes was within 1% and the differences were less than 1% at all points. Thus, the linear accelerator output was confirmed to be the same in the gating mode as when giving the total number of monitor units in a single fraction.

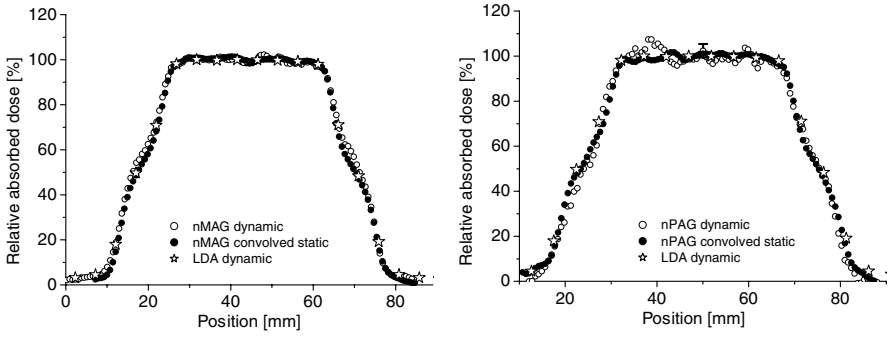

Figure 3. Relative absorbed dose profiles from the (a) nMAG and (b) nPAG during respiratory-like motion in and out of the beam. The uncertainty bar in the dynamic gel data corresponds to 1 SD of the relative absorbed dose in the flattened area. In the nMAG case, the uncertainty bar is of the same magnitude as the symbols and therefore not visible.

Table 2. Dose profiles data from static and dynamic measurements and calculated convolved data.

Detector system	nPAG			nMAG			LDA	
Absorbed dose profiles	Static	Dynamic	Convolved	Static	Dynamic	Convolved	Static	Dynamic
FWHM (mm)	51	51	51	52	54	53	53	54
80–20% penumbra width (mm)	3	10	11	3	11	11	5	11

3.2. Motion-induced dose rate variation

To investigate any potential invariance in absorbed dose due to the motion of the gel system in and out of the beam, the static gel profiles were convolved with the motion function controlling the respiration robot, and the measured dose profile from the moving phantom was compared with the mathematically convolved data. The dose profiles from the dynamic measurements coincided very well with the mathematically convolved measurements (figure 3). The 80–20% penumbra widths of the measured gel profiles, when the 12 mm periodical motion was applied, were verified using the LDA. All dynamic penumbra widths agreed within 1 mm (table 2). For both gel systems, the 80–20% penumbra widths of the convolved static gel profiles corresponded with the measured dynamic gel profiles (table 2). All reported penumbra widths are the average of both sides. Additionally, the difference between the full width at half-maximum (FWHM), i.e. the profile width at a 50% absorbed dose level, for the calculated convolved data and the measured dynamic data was within 1 mm for both gel systems. The flattened area was defined as 80% of the beam width, taken as the beam size minus the periodical motion extent. The standard uncertainty of the relative absorbed dose in the flattened area was 3.0% for the nPAG and 1.1% for the nMAG. The higher uncertainty of the nPAG can be attributed to the lower R2 dose sensitivity. Good agreement was observed between the dose profiles from the static gel measurements and the LDA data (figure 4). The FWHM of the static LDA profile concurred with the corresponding data for the static gel profiles. The largest deviation obtained between the LDA and gel measurements, 5 mm versus 3 mm, arises in the 80–20% penumbra widths of the static profiles (table 2).

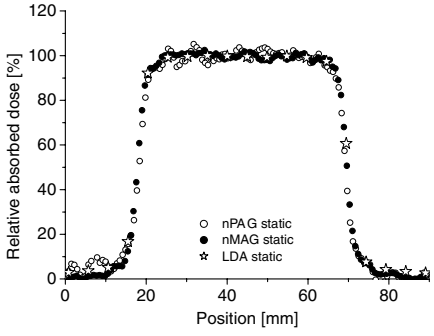

Figure 4. Relative absorbed dose profiles for the nPAG, nMAG and the LDA detector in the static mode.

This deviation can be explained by the difference in spatial resolution of the two detector systems. For the LDA, only one diode was positioned in the penumbra region during the static measurements. In comparison, when 12 mm periodical motion was introduced, there were more measurement points in the penumbra, and a better agreement was observed for the 80–20% penumbra widths. The set-up used to investigate dose rate effects differs from earlier published results where a number of samples were irradiated with different but constant dose rate levels (De Deene *et al* 2006). In the experiments carried out in this study, the same phantom is irradiated with varying dose rates in the penumbra region. Thus, the dose rate effect observed by De Deene will be implicit in these experiments, showing the summed effect in this particular clinical situation. Overall, good agreement was obtained between the dose profiles from the dynamic measurements carried out with the LDA and the dynamic gel measurements. Since the static data convolved with the motion function agreed very well with the measured dynamic profiles, the dose response of both investigated gel detectors can be considered to be invariant during motion under these experimental conditions. Thus, no influence of the dose rate variation owing to the motion in and out of the beam was detected.

3.3. Fractionated dose induced by gated delivery

To undertake a dose verification of dynamic radiotherapy, in particular using the gated BART technique respiratory gating, the fractionation dependence must be investigated. For this purpose, two different sets of samples for each investigated gel composition received gated and ungated irradiation. In order to simulate a clinically relevant gated treatment during a normal breathing period, the gel vials were irradiated with 12 MU every 6.5 s. The difference in R2 for the gel samples that received gated delivery with 12 MU/beam compared to when the dose was given in a single irradiation was less than 1% and 4% for nPAG and nMAG, respectively, for absorbed doses up to 2 Gy (figure 5). As a consequence of the different slopes for the response curves, the maximum difference in R2, i.e. 1.2% for nPAG and 9.0% for nMAG, occurred for the highest examined doses. In order to avoid systematic deviations due to the fractionation effect, the method of using a R2 versus dose response curve to calibrate a 3D gel measurement should be used with care. The calibration is strictly valid only for the particular fractionation scheme used, and large errors may be introduced if generalized to the complete irradiated gel volume. The effect will be considerably smaller if only a relative

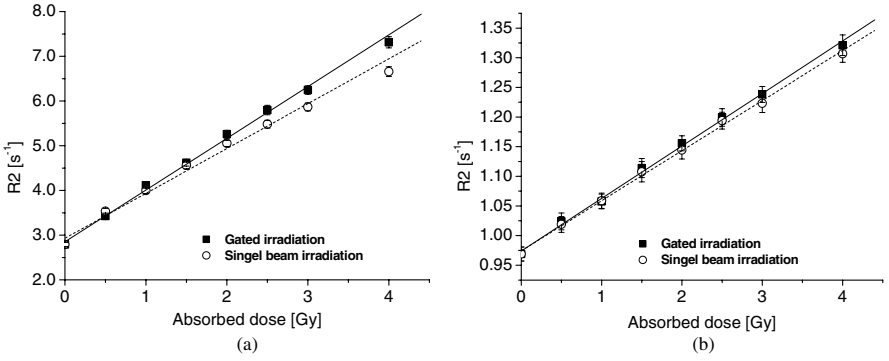

Figure 5. R2 dose response for (a) nMAG (2% MAA) and for (b) nPAG (3% AA, 3% BIS) vials irradiated to absorbed doses up to 4 Gy. The slopes for the linear fits were (a) 0.0112 (gated), 0.0095 (single beam) and (b) 0.0877 (gated), 0.0840 (single beam). Two sets of samples for each gel were irradiated during a single beam delivery or during gated delivery with 12 MU every 6.5 s. All measurements were carried out in the static mode. The uncertainty bars correspond to 1 SD in the R2 map, obtained from 78 pixels in each ROI. In the nMAG case, the uncertainty bars are smaller than the symbols at some points and therefore not visible.

evaluation is performed, provided that an approximately linear response is present within the examined dose interval (Karlsson *et al* 2007).

The fractionation effect is a consequence of the variation in mean radical concentration when different irradiation schemes are used. The radical concentration highly influences the rate of polymerization reactions, which are induced locally by free radical products of water radiolysis in all polymer gel dosimetry systems (Appleby 1999). During gated irradiation, i.e. fractionated beam delivery, the radicals are generated in short bursts, and the concentration drops between beam-on sequences. As a consequence, the mean radical concentration during the total irradiation (i.e. the time between beam-on for the first fraction and beam-off for the last fraction) will be lower with increased intervals between fractions. Since polymerization termination is proportional to radical concentration, termination will decrease and more polymers are formed, i.e. the R2 versus dose response increases with fractionated irradiation (Karlsson *et al* 2007, Karlsson 2007). The effect is larger for the nMAG system than for nPAG, since polymerization termination in nMAG mainly occurs through biomolecular termination, which is proportional to the square of the radical concentration. In the nPAG system, on the other hand, chain-transfer reactions, which are directly proportional to the radical concentration, dominate termination (Fuxman *et al* 2003, MacAuley 2006).

The results of this study verified the larger fractionation effect on the dose response for the nMAG system. Furthermore, since the mean radical concentration is proportional to the mean dose rate during the total irradiation, the effect is expected to decrease when the intervals between beam-on sequences are decreased, i.e. when the irradiation approaches single beam delivery. Previously published results were based on intervals of 70 s between beams (Karlsson *et al* 2007). In that study, the difference in R2 between fractionated and unfractionated irradiation at the 2 Gy level was approximately 20% for nMAG when the dose was given in 0.25 Gy fractions and approximately 13% for 0.5 Gy fractions. The total irradiation times were 520 s and 240 s, respectively. The corresponding values in this study were a 4% difference for a total dose of 2 Gy given in 0.12 Gy fractions, in a total irradiation

time of 105 s. The above data support the assumption of increased R2 versus dose response with increased total irradiation times. As expected, the observed differences are much smaller for the nPAG system.

4. Conclusion

To investigate the feasibility of using polymer gels for 3D dose verification of dynamic radiotherapy, two types of polymer gels were irradiated under respiratory-like motion. Measurements agreed very well with data obtained using a reference detector as well as mathematically convolved data. No influence of the dose rate variation related to motion in and out of the beam was observed. The investigated polymer gels are thus feasible detectors for dose measurements under respiratory-like motion. For dose verification involving gated delivery, relative absorbed dose evaluation should be used in order to minimize the effect of fractionated irradiation.

Acknowledgments

This study was financially supported by the Swedish Cancer Society and the Cancer Foundation at Malmö University Hospital. Rolf Vainonen, Henrik Hall and Robert Eskilsson at the Department of Biomedical Engineering at Malmö University Hospital are acknowledged for their help in constructing the breathing robot.

References

Appleby A 1999 The radiation chemical basis of gel dosimetry *Proc. 1st Int. Workshop of Radiation Therapy Gel Dosimetry (Lexington, KY)*

De Deene Y 2002 Gel dosimetry for the dose verification of intensity modulated radiotherapy treatments *Med. Phys.* **12** 77–88

De Deene Y, Vergote K, Claeys C and De Wagter C 2006 The fundamental radiation properties of normoxic polymer gel dosimeters: a comparison between a methacrylic acid based gel and acrylamide based gels *Phys. Med. Biol.* **51** 653–73

Duan J, Shen S, Fiveash J B, Popple R A and Brezovich I A 2006 Dosimetric and radiobiological impact of dose fractionation on respiratory motion induced IMRT delivery errors: a volumetric dose measurement study *Med. Phys.* **33** 1380–7

Fuxman A M, McAuley K B and Schreiner L J 2003 Modelling free-radical crosslinking copolymerization of acrylamide and N,N′-methylenebis(acrylamide) for radiation dosimetry *Macromol. Theor. Simul.* **12** 647–62

Gustavsson H, Karlsson A, Bäck S A, Olsson L E, Haraldsson P, Engström P and Nyström H 2003 MAGIC-type polymer gel for three-dimensional dosimetry: intensity-modulated radiation therapy verification *Med. Phys.* **30** 1264–71

Isbakan F, Ulgen Y, Bilge H, Ozen Z, Agus O and Buyuksarac B 2007 Gamma knife 3-D dose distribution near the area of tissue inhomogeneities by normoxic gel dosimetry *Med. Phys.* **34** 1623–30

Karlsson A 2007 Characterization and clinical application of normoxic polymer gel in radiation therapy dosimetry PhD Thesis Lund University (ISBN 978-91-628-7244-1)

Karlsson A, Gustavsson H, Månsson S, McAuley K B and Bäck S A 2007 Dose integration characteristics in normoxic polymer gel dosimetry investigated using sequential beam irradiation *Phys. Med. Biol.* **52** 4697–706 Epub 2007 July 18

Karlsson A, Gustavsson H, Olsson L and Bäck S A 2003 Image processing software for 3D dose evaluation in gel dosimetry *Proc. World Congress on Medical Physics and Biomedical Engineering (Sydney, Australia, 24–9 Aug)* ISBN 1877040142)

Keall P J, Cattell H, Pokhrel D, Dieterich S, Wong K H, Murphy M J, Vedam S S, Wijesooriya K and Mohan R 2006 Geometric accuracy of a real-time target tracking system with dynamic multileaf collimator tracking system *Int. J. Radiat. Oncol. Biol. Phys.* **65** 1579–84

Li G, Citrin D, Camphausen K, Mueller B, Burman C, Mychalczak B, Miller R W and Song Y 2008 Advances in 4D medical imaging and 4D radiation therapy *Technol. Cancer Res. Treat.* **7** 67–82

Li X A, Stepaniak C and Gore E 2006 Technical and dosimetric aspects of respiratory gating using a pressure-sensor motion monitoring system *Med. Phys.* **33** 145–54

McAuley K B 2006 Fundamentals of polymer gel dosimeters *J. Phys.: Conf. Ser.* **56** 35–44

Otto K 2008 Volumetric modulated arc therapy: IMRT in a single gantry arc *Med. Phys.* **35** 310–7

Ottosson W, Nordström F, Ceberg S and Bäck S 2008 Characterization and evaluation of a diode array detector system for dynamic and conventional radiotherapy *Accepted abstract to the 27th Conf. arranged by European Society for Therapeutic Radiology and Oncology (Göteborg, Sweden)*

Vergote K, De Deene Y, Duthoy W, De Gersem W, De Neve W, Achten E and De Wagter C 2004 Validation and application of polymer gel dosimetry for the dose verification of an intensity-modulated arc therapy (IMAT) treatment *Phys. Med. Biol.* **49** 287–305

Wiersma R D and Xing L 2007 Examination of geometric and dosimetric accuracies of gated step-and-shoot intensity modulated radiation therapy *Med. Phys.* **34** 3962–70

Paper III

Modelling the dose response of polymer gel dosimeters

Sofie Ceberg[1,2], Crister Ceberg[1], Martin Lepage[3], Helen Gustafsson[4], and Sven ÅJ Bäck[2]

[1]Department of Medical Radiation Physics, Lund University, Lund, Sweden
[2]Department of Radiation Physics, Skåne University Hospital, Malmö, Sweden
[3]Centre d'imagerie moléculaire de Sherbrooke, Département de médecine nucléaire et de radiobiologie, Université de Sherbrooke, Sherbrooke Québec, Canada
[4]Department of Medical Physics, ACT Health, Canberra, Australia

sofie.ceberg@med.lu.se

1. Introduction

Recently published data show that the polymer gel dosimeter has dose rate dependence (De Deene et al., 2006) and fractionation dependence (Karlsson et al., 2007). Since this may be of great importance for applications of gel dosimetry in dynamic radiotherapy, further investigations in this area are highly desirable.

In order to model the effects of dose rate and fractionation scheme on the measured R2-values, it is helpful to divide the protons of the gel into different pools, or compartments. As the radiation induced polymerization proceeds, protons are transferred from one compartment to another. Each compartment has its own specific R2-value, and the composite measure will then correspond to the average, weighted by the relative fraction of protons in each compartment. By creating such a compartment model, and fitting the transfer coefficients to measured R2-values, one may hopefully gain some new insight into the mechanisms of gel dosimetry in dynamic radiotherapy.

2. Materials and Methods

A simple model based on the assumption that magnetization in the gel dosimeter is exchanged rapidly between the different chemical species and water was useful in capturing the main effects responsible for the change of R2 as a function of the absorbed dose. In this model, the protons affecting the magnetic resonance signal and the R2-value of the gel were separated in mobile protons (*i.e.*, water protons and monomer protons), gelatin protons and polymer protons (see *e.g.* Baldock et al., 2010, Fuxman et al., 2005, Lepage et al., 2001). Each proton pool was assigned a specific relaxation rate and the weighted sum of the contribution from each pool was the measured R2-value. Upon absorption of a radiation dose, protons from the monomer pool are gradually transferred to the polymer pool. This approach was modified to

account for the termination of the polymerization by water free radicals *during* irradiation (Figure 1). To do this, we consider that the monomer protons ($P1_m$) are first transferred to a growing polymer pool (P2) with a transfer rate k_1. If irradiation stops, then all of the growing polymer will be transferred to a final polymer network proton pool (P4) with a transfer rate k_2. When water free radicals are abundant, (*i.e.*, during irradiation), there is a significant probability for early polymerization termination. Those polymer chains are transferred to an "early terminated" polymer proton pool with a transfer rate k_3. In this model, the water protons ($P1_w$) and the gelatin protons ($P1_g$) are spectators and remain constant throughout the process.

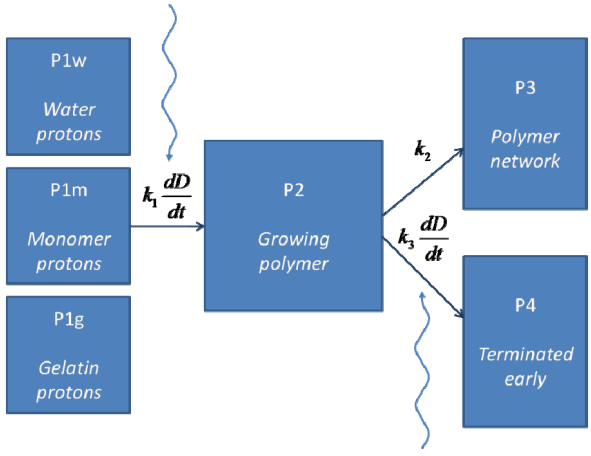

Figure 1. *Compartment model of the protons in a polymer gel dosimeter. Upon irradiation, the polymerization of monomers is initiated and protons are transferred from the monomer pool ($P1_m$) to the growing polymer pool (P2) with a rate constant k_1 times the dose rate. If polymerization proceeds with a rate constant k_2 these polymer chains become part of the polymer network (P3). If polymerization is terminated by water free radicals generated during irradiation, those polymer chains become part of a polymer pool terminated early (P4) with a rate constant k_3 times the dose rate. Each pool is characterized by a magnetic resonance transverse relaxation rate (R2).*

In mathematical terms, this model can be described by a simple set of linear differential equations:

$$\frac{dP1_m}{dt} = -k_1 \frac{dD}{dt} P1_m$$
$$\frac{dP2}{dt} = k_1 \frac{dD}{dt} P1_m - k_2 P2 - k_3 \frac{dD}{dt} P2$$
$$\frac{dP3}{dt} = k_2 P2$$
$$\frac{dP4}{dt} = k_3 \frac{dD}{dt} P2$$

This approach assumes the reactions obey zero-order kinetics but the main feature is that it includes two competing processes, which is a key component in order to be able to reproduce the observed effects of dose rate and fractionation scheme in gel dosimetry.

In this model, at time t=0, all protons are contained in compartment P1. When exposed to irradiation, protons are transferred to compartment P2, and further on to compartments P3 and, during radiation, P4. An example of how this model develops over time is displayed in Figure 3 below. At a sufficient time after irradiation has stoped, t_{sat}, compartment P2 is empty, and all protons originally transferred from compartment P1 are located in compartments P3 and P4. The apparent R2-value can then be calculated as:

$$R2_{fitted} = P1_{\mathrm{w}}R2_{1w} + P1_{\mathrm{g}}R2_{1g} + P1_{\mathrm{m}}(t_{sat})R2_{1m} + \mathrm{P3}(t_{sat})R2_{3} + \mathrm{P4}(t_{sat})R2_{4},$$

where $R2_{1w}$, $R2_{1g}$, $R2_{1m}$, $R2_3$ and $R2_4$ are the relaxation rates for the five proton pools in Fig.1.

The R2-value for compartments $P1_w$, $P1_g$ and $P1_m$ can be *derived* from an un-irradiated gel. In this model, it is assumed that compartment P4 contains small fragments of early terminated polymers and dissociated monomers, and that the R2-value for this compartment does not differ significantly from that of compartment $P1_m$. For simplicity, we set $R2_4$=$R2_{1m}$. The value of $R2_{1m}$ is set at $1.0s^{-1}$, $R2_{1w}$ is set at $0.5s^{-1}$ and $R2_{1g}$ is set at $39.2s^{-1}$. The R2-value for compartment P3, $R2_3$, and the three transfer coefficients, k_1-k_3, are fitting parameters. The initial values for $P1_w$, $P1_g$ and $P1_m$ are determined from the chemical composition of the nMAG dosimeter (2% methacrylic acid, 8% gelatine and 90% H_20) and are 92.43, 6.28 and 1.29, respectively. It is these 1.29% of protons that can be transferred from pool $P1_m$ to pool P2, and eventually to pools P3 or P4.

The dose rate- and fractionation dependencies are more pronounced for the metacrylic-based polymer gels (nMAG). Therefore, the model was fitted to a set of measurements using nMAG gel dosimeters exposed to different dose levels and fractionation schemes according to Table 1. The set of differential equations were solved using a Matlab program, and the resulting distribution of protons through the different compartments was then used to calculate the resulting R2-value according to equation (2), which was compared to the corresponding measured R2-value. This was done for the entire set of R2-measurements, and the fitting parameters were then adjusted iteratively in order to minimize the sum of the squared differences.

3. Results and discussion

The resulting R2-values from the calculations are presented (table 1). The measured and calculated data are plotted displayed in Figure 2.

#	t_{on} [s]	t_{off} [s]	n	Drate [Gy/s]	Dose [Gy]	MeasR2 [s^{-1}]	CalcR2 [s^{-1}]
1	6	0	1	0.084	0.50	3.53	3.53
2	12	0	1	0.084	1.01	4.00	4.16
3	18	0	1	0.084	1.51	4.56	4.69
4	24	0	1	0.084	2.01	5.05	5.15
5	30	0	1	0.084	2.52	5.48	5.57
6	36	0	1	0.084	3.02	5.87	5.93
7	42	0	1	0.084	3.52	6.38	6.27
8	48	0	1	0.084	4.02	6.65	6.58
9	1.44	4.06	4	0.084	0.48	3.42	3.51
10	1.44	4.06	8	0.084	0.97	4.12	4.14
11	1.44	4.06	12	0.084	1.45	4.62	4.71
12	1.44	4.06	17	0.084	2.05	5.26	5.38
13	1.44	4.06	21	0.084	2.54	5.80	5.89
14	1.44	4.06	25	0.084	3.02	6.24	6.39
15	1.44	4.06	29	0.084	3.50	6.76	6.87
16	1.44	4.06	33	0.084	3.98	7.31	7.35
17	1.44	9.5	17	0.084	2.05	5.50	5.54
18	1.44	15	17	0.084	2.05	5.63	5.65
19	1.44	37	17	0.084	2.05	5.95	5.83

Table 1. *The different dose levels and fractionation schemes used in the irradiation of nMAG gel dosimeters. The beam-on time in seconds is denoted t_{on} , t_{off} is the beam-off time in seconds, n is the number of fractions, Drate is the absorbed dose rate in Gy/s, Dose is the total given absorbed dose, MeasR2 is the measured R2-value in s^{-1}, and CalcR2 is the R2-value in s^{-1} calculated by the model after fitting the parameters.*

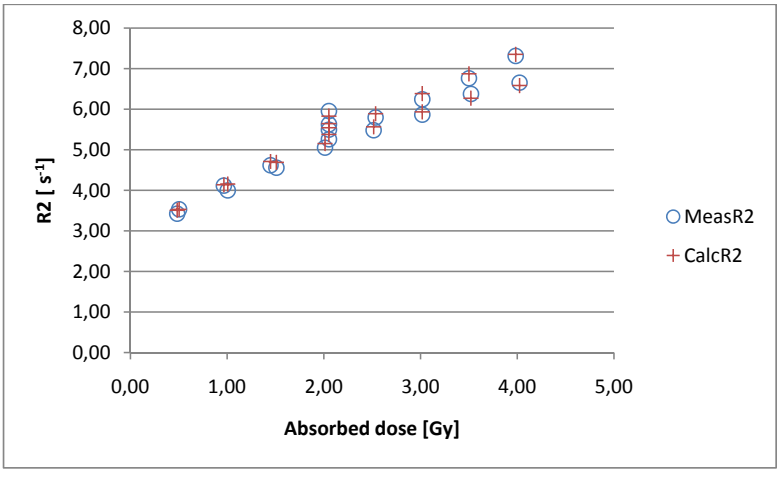

Figure 2. *Measured and calculated R2-values for the different irradiation schemes given in Table 1.*

4. Discussion

The compartment model is able to fit data from the nMAG dosimeter for different doses and different fractionation schemes. This confirms that the different R2-values for this dosimeter irradiated with different fractionation schemes is indeed due to a dose rate dependence. The difference between calculated and measured R2-values was on average 1.1±1.6% (1SD).

In particular, it was found in this study that for a given absorbed dose (2.0 Gy), the R2-value could differ up to 16% depending on the fractionation scheme (see Table 1), which indicates that the nMAG gel is not suitable for verification measurements for respiratory gating. This could be a major obstacle for gel dosimetry using the nMAG dosimeter in IMRT, since different parts of the irradiated volume in this case often experience different dose fractionation patterns. However, in this case the total irradiation time was also quite different, which is not the case in IMRT. Therefore, we have used the model to simulate irradiations with more clinically relevant fractionation schemes, all delivered within the same total time (80 s) and to the same total absorbed dose (2.0 Gy), with the goal to compare the resulting calculated R2-values. Three different fractionation schemes were used; i) one fraction of 40 s followed by 40 s without irradiation, ii) two fractions of 20 s separated by 20 s without irradiation, and iii) four fractions of 10 s with 10 s pauses. The dose rate is constant for all fractions at 0.05 Gy/s.

The results are displayed in Figure 3. The red curves show how the proton content of compartment P2 is built up during irradiation, and subsequently drained to compartments P3 and P4. According to the assumptions of the model, the transfer to P4 occurs only during irradiation, as shown by the blue curves. The green curves, finally, show how the proton content in the polymer pool, compartment P3, grows until it saturates as all available building blocks in P2 are consumed.

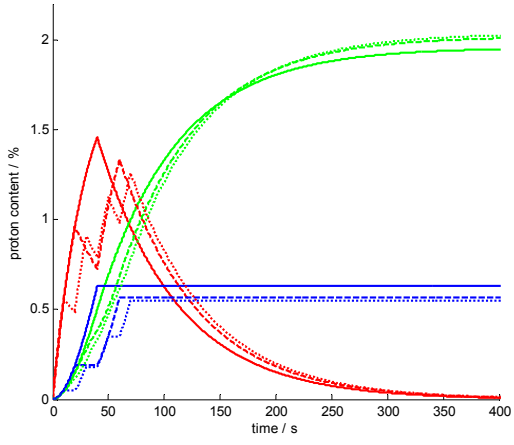

Figure 3. *The content of the compartments P2-P3 as a function of time after exposure to irradiation with different fractionations, solid curves one fraction of 40 s, dashed curves two fractions of 20 s, and dotted curves four fractions of 10 s each. The dose rate was constant at 0.05 Gy/s.*

This simulation indicates that the distribution across the different compartments is dependent on the fractionation scheme. However, the maximum difference between the calculated R2-values is now only 2%. It may, therefore, be hypothesized that the R2-value should remain nearly the same for different fractionation schemes, given that the same total dose is delivered during the same total time. The model can be used to generate similar hypotheses regarding for instance dose-rate dependence.

5. Conclusions

A compartment model has been designed to represent the polymerization process in the nMAG gel dosimeter and the termination of polymerization by water free radicals during irradiation. This model was used to fit measured R2-data for nMAG gel dosimeters exposed to irradiation with different fractionation schemes. The model was used to predict the behavior of a similar gel dosimeter exposed to irradiation according to a typical IMRT scenario. Based on the results, it is hypothesized that measured R2-values are approximately independent of the fractionation scheme, given that the same total dose is delivered during the same total time. This hypothesis will be tested by measurements in our further investigations.

References

Baldock C, Deene Y De, Doran S, Ibbott G, Jirasek A, Lepage M, McAuley K B, Oldham M and Schreiner L J. TOPICAL REVIEW Polymer gel dosimetry. Physics in Medicine and Biology 55 (2010) R1 – R63

De Deene Y, Vergote K, Claeys C, and De Wagter C. The fundamental radiation properties of normoxic polymer gel dosimeters: a comparison between a methacrylic acid based gel and acrylamide based gels. Physics in Medicine and Biology 51 (2006) 653 – 673

Fuxman A M, McAuley K B, and Schreiner L J. Modelling of polyacrylamide gel dosimeters with spatially non-uniform radiation dose distributions. Chemical Engineering Science 60 (2005) 1277 – 1293

Karlsson A, Gustavsson H, Månsson S, McCauley K B, and Bäck S Å J. Dose integration characteristics in normoxic polymer gel dosimetry investigated using sequential beam irradiation. Physics in Medicine and Biology 52 (2007) 4697 – 4706

Lepage M, Whittaker A K, Rintoul L, Bäck S Å J, and Baldock C. The relationship between radiation-induced chemical processes and transverse relaxation times in polymer gel dosimeters. Physics in Medicine and Biology 46 (2001) 1061 – 1074

Paper IV

IOP PUBLISHING PHYSICS IN MEDICINE AND BIOLOGY

Phys. Med. Biol. **55** (2010) 4885–4898 doi:10.1088/0031-9155/55/17/001

RapidArc treatment verification in 3D using polymer gel dosimetry and Monte Carlo simulation

Sofie Ceberg[1], Isabelle Gagne[2], Helen Gustafsson[1,3], Jonas Bengtsson Scherman[1,4], Stine S Korreman[4,5,6], Flemming Kjær-Kristoffersen[4], Michelle Hilts[2] and Sven Å J Bäck[1]

[1] Department of Medical Radiation Physics, Lund University, Skåne University Hospital, Malmö, Sweden
[2] BC Cancer Agency, Vancouver Island Centre, Victoria, Canada
[3] Department of Medical Physics, ACT Health, Canberra, Australia
[4] Department of Radiation Oncology, Rigshospitalet, Copenhagen, Denmark
[5] Niels Bohr Institute, Copenhagen University, Denmark
[6] Department of Human Oncology, University of Wisconsin-Madison, USA

E-mail: sofie.ceberg@med.lu.se

Received 22 April 2010, in final form 27 June 2010
Published 3 August 2010
Online at stacks.iop.org/PMB/55/4885

Abstract

The aim of this study was to verify the advanced inhomogeneous dose distribution produced by a volumetric arc therapy technique (RapidArc^{TM}) using 3D gel measurements and Monte Carlo (MC) simulations. The TPS (treatment planning system)-calculated dose distribution was compared with gel measurements and MC simulations, thus investigating any discrepancy between the planned dose delivery and the actual delivery. Additionally, the reproducibility of the delivery was investigated using repeated gel measurements. A prostate treatment plan was delivered to a 1.3 liter nPAG gel phantom using one single arc rotation and a target dose of 3.3 Gy. Magnetic resonance imaging of the gel was carried out using a 1.5 T scanner. The MC dose distributions were calculated using the VIMC-Arc code. The relative absorbed dose differences were calculated voxel-by-voxel, within the volume enclosed by the 90% isodose surface (VOI_{90}), for the TPS versus gel and TPS versus MC. The differences between the verification methods, MC versus gel, and between two repeated gel measurements were investigated in the same way. For all volume comparisons, the mean value was within 1% and the standard deviation of the differences was within 2.5% (1SD). A 3D gamma analysis between the dose matrices were carried out using gamma criteria 3%/3 mm and 5%/5 mm (% dose difference and mm distance to agreement) within the volume enclosed by the 50% isodose surface (VOI_{50}) and the 90% isodose surface (VOI_{90}), respectively. All comparisons resulted in very high pass rates. More than 95% of the TPS points were within 3%/3 mm of both the gel measurement and MC simulation, both inside VOI_{50} and VOI_{90}.

Additionally, the repeated gel measurements showed excellent consistency, indicating reproducible delivery. Using MC simulations and gel measurements, this verification study successfully demonstrated that the RapidArc™ plan was both accurately calculated and delivered as planned.

1. Introduction

RapidArc™ is a novel radiation therapy technique where the treatment is delivered during one or a few rotations of the linear accelerator gantry. The dose distribution from this type of volumetric arc therapy (VMAT) is modulated by simultaneously varying the MLC positions, the rotation speed of the gantry and the dose rate during the treatment (Otto 2008). RapidArc™ was first introduced clinically in 2008, and according to a number of planning comparison studies, the target–volume coverage and sparing of the normal tissue was better than or as good as conventional intensity modulated radiotherapy (IMRT) (Kjær-Kristoffersen *et al* 2009, Popescu *et al* 2010, Shaffer *et al* 2009, Palma *et al* 2008b). Additionally, the number of monitor units (MU) delivered and the treatment time were both decreased compared to IMRT calculated with the anisotropic analytical algorithm (AAA) in Eclipse (Palma *et al* 2008a, Alexander *et al* 2008).

Since the RapidArc™ optimization algorithm uses a stochastic element during the generation of the apertures, it is common to see plans with apertures including single isolated leaves and disconnected small segments. Furthermore, RapidArc™ plans are delivered dynamically with leaf and gantry motion up to approximately 1 cm and $2^{\circ}\ s^{-1}$, respectively. This kind of treatment delivery represents a new level of complexity, and a thorough dosimetric verification is therefore highly desirable.

RapidArc™ treatment planning calculations have previously been verified using Monte Carlo (MC) simulations (Bush *et al* 2008, Gagne *et al* 2008, Teke *et al* 2010), and complementary measurements are greatly needed. However, the advanced inhomogeneous 3D dose distribution produced by RapidArc™ is too complicated to verify by conventional means, such as single dose point measurements or 2D detector arrays. RapidArc™ deliveries have previously been verified using film dosimetry (Gagne *et al* 2008) and ion-chamber (Teke *et al* 2010). However, these authors suggest that a high-resolution 3D dose measurement system should be used.

The use of an independent 3D dosimetry method for benchmarking adds an extra safety layer in the quality assurance (QA) procedure not fully controlled by conventional techniques. This improves the patient safety and reduces the risk of systematic errors in the process when introducing new treatment regimes in the clinic.

In recently published work, dosimetric verification of RapidArc™ treatment delivery using a Scandidos Delta4 cylindrical diode array phantom was presented (Korreman *et al* 2009). The reported results showed very good agreement between the treatment planning system (TPS) and dose measurements, as well as reproducibility of consecutive deliveries. However, the Delta4 detector system is not a true independent 3D dosimeter as it interpolates measured data from only two planes to obtain a 3D matrix. During the interpolation, the Delta4 software system renormalizes the TPS-calculated depth dose along the ray between the planes to fit the measurement points, and uses that data to reconstruct the dose (Feygelman *et al* 2009). Additionally, the minimum center-to-center distance between the diodes is 5 mm in a central $6 \times 6\ cm^2$ region of the detector. Thus, a greater spatial resolution would be desirable, given the highly modulated dose distribution deliverable with RapidArc™.

The gel dosimetry research community has contributed to the dosimetric and geometric verification of several complex 3D dose distributions (Baldock *et al* 2010, Bjoreland *et al* 2008, Doran, 2009, Gustavsson *et al* 2003). Using 3D gel dosimetry, the absorbed dose can be obtained in the entire irradiated volume and furthermore, the response is independent of the direction of the incident radiation (Olsson *et al* 1998). In addition, the high-resolution gel system functions both as a phantom and a detector since the gel composition is nearly soft-tissue equivalent (Keall and Baldock, 1999). Recently published data have shown that polymer gels are feasible detectors for dose measurements under motion and that the dose response is not influenced by dose rate variation due to the motion in and out of beam (Ceberg *et al* 2008). As these dose rate variations are similar to those produced using varying gantry speed and continuous leaf motion, this normoxic polymer gel system should also be suitable for RapidArc^{TM} delivery verification.

The use of polymer gel dosimetry for the verification of an intensity modulated arc therapy (IMAT) has been reported (Yu 1995). Both the IMAT and the VMAT techniques use arc rotation and different MLC settings to generate a highly conformal dose distribution. However, using IMAT, both the fluence rate and the gantry speed are constant.

The aim of this study was to carry out a 3D verification of a RapidArc^{TM} treatment plan and delivery using 3D gel dosimetry and MC simulations. The rationale for this is that potential deviations between the gel and the TPS can be arbitrated with support from the MC simulations. Additionally, the reproducibility of the delivery was investigated by using repeated gel measurements.

2. Material and methods

The RapidArc^{TM} planning and delivery to the gel phantoms were done at Rigshospitalet in Copenhagen while the MC simulations were performed at the British Columbia Cancer Agency—Vancouver Island Center. The MC dose distributions were calculated using the VIMC-Arc code developed at the same center. The gel preparation, gel read-out and data analysis were carried out at Lund University, Skåne University Hospital in Malmö.

2.1. Gel preparation

In this study the normoxic polyacrylamide gel (nPAG) system was used. It is based on 3% w/w acrylamide (electrophoresis grade $\geqslant$99%, powder, Sigma Aldrich) and 3% w/w *N*, *N*′-methylenebisacrylamide (electrophoresis grade $\geqslant$98%, powder, Sigma Aldrich). Gelatine (swine skin, 300 bloom, Sigma Aldrich) was used as the matrix substance and tetrakis(hydroxymethyl)phosphonium chloride (techn. $\sim$80% in water, Sigma Aldrich) as an oxygen scavenger. The remaining constituent was ultrapure deionized water (resistivity $>$18.2 MΩ cm). The gelatine and water were mixed at room temperature and then heated to 45 °C until the gelatine was completely dissolved. The monomers were added before cooling the mixture to 35 °C. Ten minutes before the gel was poured into 1.3 liter flasks (Ø 10 cm, length 17 cm) and 15 ml vials (Ø 1.5 cm, length 6 cm), the oxygen scavenger was added. The gels were prepared under normal levels of oxygen and the solutions were stirred continuously throughout the entire mixing procedure.

Three identical 1.3 liter cylindrical glass containers and ten 15 ml glass vials were filled with the gel solution. The VMAT delivery was checked twice, using the first two flasks. The third flask was used to obtain a background value of R2 for the unirradiated gel. A large flask, rather than a small vial was needed for this, as it has previously been shown (Dumas *et al* 2006) that the cooling history of the gel plays an important role in determining

R2. The phantoms were left to set in the dark at room temperature for about 24 h before irradiation.

2.2. Treatment planning and RapidArc™ dose delivery

CT images of the gel phantoms were acquired using a spiral CT scanner (Sensation Open, Siemens Medical Systems). The slice thickness was 3 mm. The change in R2 caused by some 10 mGy to the gel detector from the CT scanning is considered to be negligible in relation to the far greater absorbed doses investigated in this study. The TPS (beta version pre-clinical RapidArc™ optimizer, Varian Medical Systems) was used to generate a RapidArc™ 18 MV prostate plan, with a clockwise arc rotation from 210° to 150°. The gantry rotation did not include the angles from directly below the couch in order to avoid beaming through the central couch rails. The prostate plan was made according to the standard design criteria used in our clinic, which have previously been published by Kjær-Kristoffersen *et al* (2009). The number of MU was 864 and the target dose was 3.3 Gy. A Clinac iX linear accelerator (Varian Medical Systems) was used to deliver the plan twice, using two of the identical gel phantoms. The collimator rotation was 46° and the output varied between 200 and 600 MU min^{-1} during the 300° rotation.

The vials were placed at 3 cm depth in a 30 × 30 × 30 cm^3 cubic water phantom and irradiated using a 20 × 20 cm^2 18 MV photon beam, with the linear accelerator set to deliver 600 MU min^{-1}.

All gel samples were stored in the dark at room temperature at all times.

2.3. Magnetic resonance imaging and image processing

Approximately 24 h after irradiation, magnetic resonance imaging (MRI) of the gel was carried out using a 1.5 T MRI unit (Siemens Symphony, Siemens Medical Systems). To avoid any temperature gradients in the gel phantoms during imaging, the containers were moved from storage in the dark and at room temperature into the MRI scanner room for about 4 h before imaging. The images were acquired using a 32-echo multi-spin echo sequence with an inter-echo spacing of 25 ms. The repetition time was 4000 ms and the voxel size was 1 × 1 × 3 mm^3. In-house developed software was used for T2 calculation (Karlsson *et al* 2003), and MATLAB 7.4.0 was used for image processing, 3D rendering and gamma evaluation. The raw data were smoothed with a 3×3×3 box-filter. The R2 data of the irradiated 1.3 liter gel phantoms were converted to relative absorbed dose using background subtraction and normalization in a region of homogenous dose (Bjoreland *et al* 2008).

2.4. Monte Carlo simulation

MC simulation of the 18 MV prostate RapidArc™ plan was performed at the BC Cancer Agency—Vancouver Island Centre using the VIMC-Arc (Bush *et al* 2008) system. VIMC-Arc is a fully automated system that currently enables MC simulation of 6 MV and 18 MV photon beam RapidArc™ plans exported from the TPS. Essentially, VIMC-Arc constructs the MC beam and patient models from a regular RapidArc™ DICOM dataset (i.e. patient CT images, plan, dose and structure files), simulates radiation transport using BEAMnrc (Rogers *et al* 1995), particle DMLC (Keall *et al* 2001, Siebers *et al* 2002), and DOSXYZnrc (Walters *et al* 2009) or VMC++ (Kawrakow and Fippel, 2000) radiation transport codes, collects the resulting dose and converts the dose into DICOM format for future import into the TPS. In VIMC-Arc, RapidArc™ deliveries are modeled through 176 static gantry positions, with the

Table 1. MC transport parameters used in the BEAMnrc/DOSXYZnrc/MLC simulations. AE (electrons) and AP (photons) are the particle production threshold energies. The ECUT (electron) and the PCUT (photon) are the transport cutoff energies in all the simulations.

MC parameter	Value
Voxel dimensions	$5 \times 5 \times 5$ mm^3
No of particles (est. mean std)	1.5×10^9 (0.8%)
AP/PCUT/AE/ECUT	0.010/0.010/0.7/0.7 MeV
Variance reduction	1. Azimuthal particle redistribution
	2. Directional bremstrahlung splitting ($\times$1000)

MLC leaves moving dynamically from one aperture to the next as recorded in the DICOM-plan file produced by the TPS. Each gantry angle is the average of the angles associated with the two corresponding bounding apertures.

Essential components of the VIMC-Arc system (6 MV and 18 MV photon beam, Varian 21EX linac) have been previously tested and verified. These include open field profiles, depth dose curves (Cranmer-Sargison *et al* 2004, Gagne and Zavgorodni, 2007), absolute dose calculations including sliding window IMRT (Popescu *et al* 2005), sliding window IMRT profiles (Stapleton *et al* 2005) as well as RapidArc^{TM} dose distributions (Bush *et al* 2008, Gagne *et al* 2008, Teke *et al* 2010, Li *et al* 2001). For the energy (18 MV) and field size (20×20 cm^2) used in this investigation, the calculated and measured dose distributions in water are within 1.0% for depths larger than d_{max}. Relevant MC transport parameters used in the MC simulation of the 18 MV prostate RapidArc^{TM} plan are summarized in table 1. The statistical uncertainty of the MC simulation was kept within 1%. As modern TPS report the absorbed dose as 'dose to water', the resulting MC 'dose to media' distribution obtained from DOSYXZnrc was converted to 'dose to water' using the ratio of mass stopping powers as outlined by Siebers *et al* (2000). As a final step, the MC dose-to-water distribution was converted into a DICOM compliant format.

2.5. Gamma evaluation in 3D

The treatment plan, the MC simulation and the measured relative absorbed dose volumes were aligned by matching the inner surface of the glass containers at the isocenter plane. There is a spatial unknown rotational uncertainty with regard to delivery, calculation and read-out. To avoid this uncertainty influencing the comparison of the matrices, the rotational shift was corrected for by visually matching the 90% isodose contour in the isocenter plane using the TPS as reference. Further, the investigated volume was truncated 5 mm immediately inside the wall of the container to avoid regions that potentially contain MR artifacts as well as inhomogeneities originating from the setting of the gel close to the glass. Since the TPS, the MC simulation and the gel data were acquired with different spatial resolutions (with voxel sizes of $2.5 \times 2.5 \times 2.5$ mm^3, $5 \times 5 \times 5$ mm^3 and $1 \times 1 \times 3$ mm^3, respectively), all dose distributions were linearly interpolated and re-sampled to $1 \times 1 \times 1$ mm^3 before the 3D gamma analysis. All dose matrices were normalized to 100% using the mean value in a $10 \times 10 \times 10$ mm^3 volume close to the isocenter in a region of homogeneous absorbed dose. The in-house developed 3D gamma evaluation method used was based on the theory by Low *et al* (1998) and was implemented into the MATLAB software environment (The MathWorks Inc.).

3. Results and discussion

The experimental gel dosimetry 3D measurements carried out in this study were used for verification of the absorbed dose delivery using a VMAT technique (RapidArc^{TM}). In addition, the MC-simulated dose distributions were calculated using the VIMC-Arc software to further investigate the TPS-calculated dose distributions. The use of MC as the gold standard TPS verification method in the RapidArc^{TM} setting is justified by several studies on VMAT verification (Bush *et al* 2008, Gagne *et al* 2008, Li *et al* 2001, Teke *et al* 2010). Thus, using these two methods of verification, gel and MC, discrepancies between the planned dose delivery and the actual delivery was investigated.

The gel vials irradiated to known doses were not used to obtain a gel calibration curve, but merely to assure the linearity of the gel dose response for this batch of gel. As the absorbed dose response of the polymer gel was confirmed to be linear in the relevant dose range (data not shown), the R2 data of the irradiated gel phantom could be directly translated to relative absorbed dose after subtracting the background signal. This method of evaluation, assuming a linear dose response, and using background subtraction, leads to a standard uncertainty in absorbed dose of approximately 3% (1SD) (Karlsson 2007).

3.1. Isodose lines and dose profiles

Overall, there was close agreement between the expected RapidArc^{TM} dose distribution (TPS) and the 3D gel-measured data. In addition, the MC confirmed the TPS accuracy as reported elsewhere (Bush *et al* 2008, Gagne *et al* 2008, Teke *et al* 2010, Li *et al* 2001). Furthermore, the RapidArc^{TM} delivery was found to be highly reproducible, confirming previously published data (Korreman *et al* 2009).

To illustrate the results, the TPS-calculated relative dose distribution in an axial plane, 15 mm from the normalization volume, is presented as a color map in figure 1, with the 80% and 95% isodose lines from the TPS, the MC simulation and the two gel measurements overlaid on the map. The deviation between the 95% isodose lines, which according to ICRU is considered to be the treated volume in a clinical case (ICRU 1999), is within 2 mm at all points.

A color map of a slice in a region with high modulation of the dose distribution and thus high dose gradients shows the relative dose distribution calculated by the TPS (figure 2(a)). The 90% isodose line from the TPS, the MC simulation and the gel measurement are overlaid. Since the repeated deliveries agree very closely (figure 1), only the result of the first gel measurement is shown. Relative absorbed dose profiles extracted along the dotted line are generally in good agreement (figure 2(b)). Deviations in profiles in the order of 3% are observed between the TPS and the gel measurement in the low dose region, and deviations of up to 1.5% in a high dose region. MC simulations agree well with the gel measurement in the low dose region. The selected slice is representative for regions involving steep dose gradients (figure 2(a)).

3.2. Cumulative dose volume histograms

Cumulative dose volume histograms (DVH) for the RapidArc^{TM} TPS plan, the MC-calculated and gel-measured dose matrices for the volume enclosed by the 90% isodose surface (volumes illustrated in figure 3) are shown in figure 4(a). Within the volume of interest, VOI_{90}, the relative absorbed dose differences were calculated voxel-by-voxel for TPS versus gel, TPS versus MC and MC versus gel (A versus B corresponds to $A_{voxel(i)}$–$B_{voxel(i)}$). The deviations

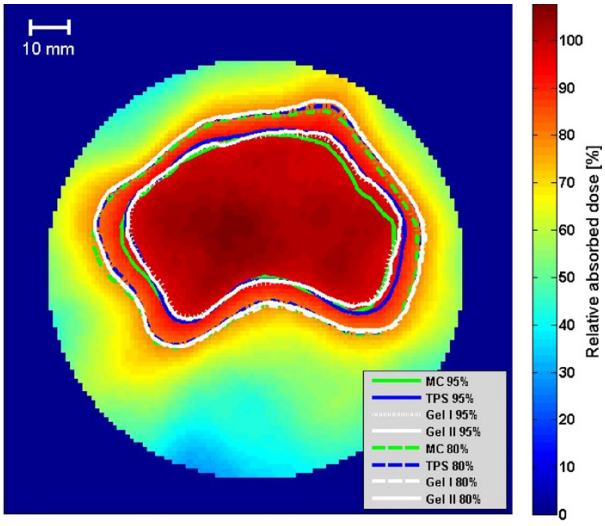

Figure 1. Color map of the relative absorbed dose calculated by the TPS in a slice away from the normalization volume. The overlaid 80% and 95% isodose lines are data from the two gel measurements (white lines), MC simulations (green lines) and TPS calculations (blue lines).

between the repeated deliveries were investigated in the same way. All investigated dose volume comparisons showed good agreement with a mean value within 1% and a standard deviation within 2.5% (1SD) (figure 4(b)). The mean value and standard deviation were $(0.39 \pm 0.92)\%$ for the deviations between the repeated deliveries, i.e. gel measurement I versus gel measurement II. The corresponding numbers for the TPS versus gel and TPS versus MC comparisons were $(-0.34 \pm 2.1)\%$ and $(0.65 \pm 2.5)\%$, respectively. The deviation between the two RapidArc^{TM} verification methods, MC versus gel, was $(-0.99 \pm 2.5)\%$. No skewed distributions were found, and no general systematic deviations were observed.

3.3. 3D gamma analysis

Additionally, 3D gamma analysis comparing the TPS and gel measurement, as well as the TPS and MC simulations, was carried out within the volumes of interest enclosed by the 50% isosurface (VOI_{50}) and the 90% (VOI_{90}) isosurface, respectively. The 3D gamma analysis was also used to investigate differences between the two consecutive deliveries and the two different verification methods, MC and gel. All comparisons were done with the gel measurement I. The gamma criteria 3%/3 mm and 5%/5 mm were used and high pass rates were obtained for all cases (table 2). More than 95% of the TPS points were within 3%/3 mm of both the gel measurement and the MC simulation data in the dose volume defined by the 50% and 90% isodose surfaces. The outcome agrees with recently published results, which show good agreement between the MC-simulated dose distribution compared with RapidArc^{TM} TPS-calculated doses (Bush *et al* 2008, Gagne *et al* 2008, Teke *et al* 2010), and which show good agreement between the TPS and RapidArc^{TM} dose measurements, as well as reproducibility of consecutive deliveries (Korreman *et al* 2009, Nicolini *et al* 2009).

In order to identify regions with potential deviations between the TPS calculations and each verification method, 3D gamma evaluation was carried out using stricter criteria,

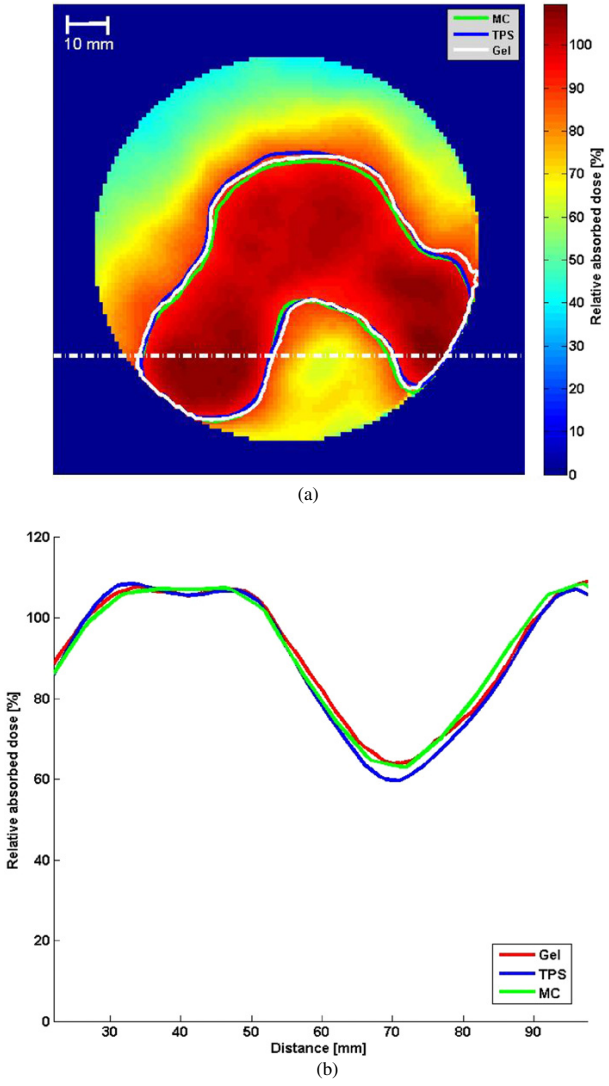

Figure 2. (a) Color map of the relative absorbed dose calculated by the TPS. The overlaid 90% isodose lines are extracted from the gel measurement (white line), MC simulations (green line) and TPS calculations (blue line). Profiles extracted across a region with steep dose gradients, along the white dotted line, are plotted in (b). (b) Relative absorbed dose profiles extracted along the white dotted line in (a). The profiles correspond to the gel measurement (red line), the MC simulation (green line) and the TPS calculations (blue line).

1%/2 mm, in the entire irradiated volume, $VOI_{container}$. This volume was defined by the interior of the cylindrical bottle and limited by the field edges in the longitudinal direction. Overall, the highest pass rate was obtained for the TPS versus MC evaluation (80%) over the TPS versus gel evaluation (70%). In the gamma evaluation, A versus B corresponds to

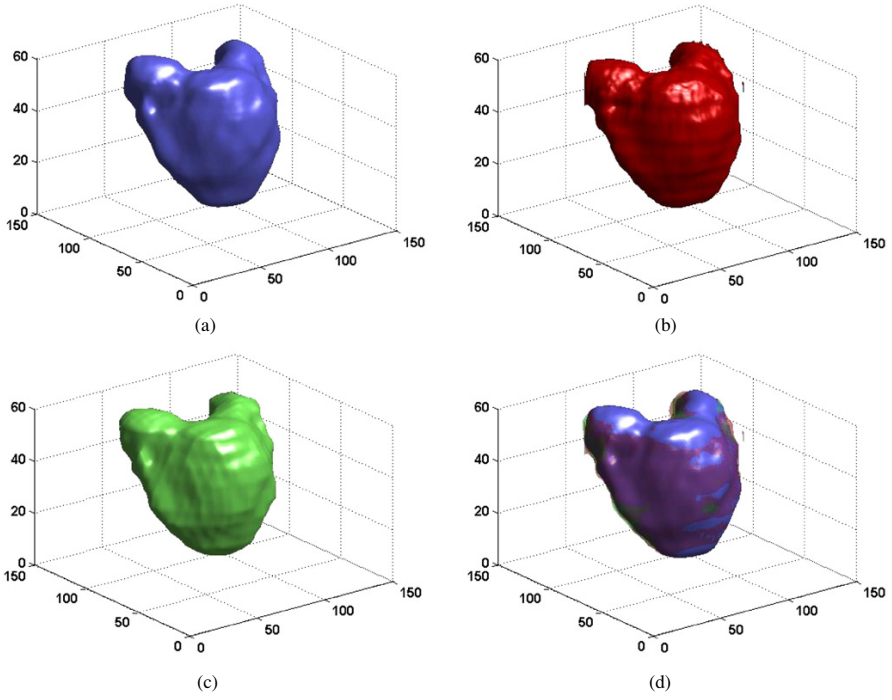

Figure 3. The 90% isodose surface projected into a 3D view for (a) the RapidArc^{TM} TPS, (b) the gel measurement and (c) the MC simulation. An overlay of all three volumes is presented in (d) where the gel and Monte Carlo surfaces are transparent. The unit on all axes is millimeters. It should be noted that the dissimilar surface structures, such as stripes on the gel measurement volume and the slightly checked pattern on the MC-calculated volume, derive from the different original resolutions. (a) TPS. (b) Gel measurement. (c) MC simulation. (d) Overlay of all three volumes.

Table 2. Pass rates obtained from 3D gamma analysis of repeated gel measurements, TPS versus gel measurement, TPS versus MC simulations and gel measurement versus MC. For each pair of compared dose distributions, four gamma volumes (3D version of 'gamma map') were obtained using gamma criteria of 5%/5 mm and 3%/3 mm, and investigating the volumes enclosed by the 50% and 90% isosurface, respectively.

	50% isodose volume		90% isodose volume	
Volume of interest	γ <1 for	γ <1 for	γ <1 for	γ <1 for
Gamma criteria	3%/3 mmDTA	5%/5 mmDTA	3%/3 mmDTA	5%/5 mmDTA
Gel versus repeated gel	99.9%	100%	100%	100%
TPS versus gel	97.5%	99.9%	98.9%	100%
TPS versus MC	98.2%	100%	95.2%	100%
MC versus gel	96.1%	100%	95.6%	99.9%

A = reference data and B = evaluated data. In one particular region, a relative calculated over-dosage on the order of 3–5% was found in the TPS as compared to both the gel

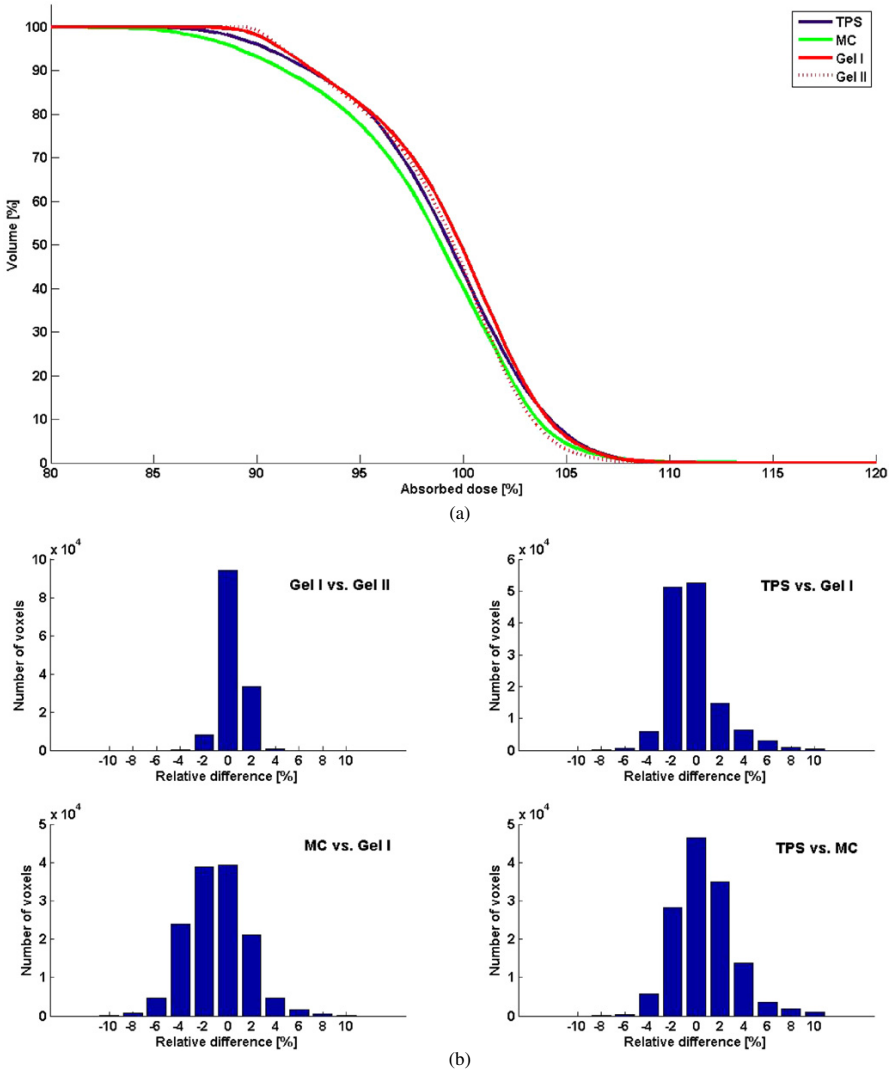

Figure 4. (a) RapidArc^{TM} TPS plan MC-calculated and gel-measured cumulative dose volume histogram (DVH) for the 90% isodose volume. (b) The distribution of voxel-by-voxel deviations between the different datasets within the volumes enclosed by the 90% isodose surface. The number of voxels is plotted against the difference in relative dose between the two analyzed volumes. Note the different scale of the ordinates.

measurement (figure 5(a)) and the MC simulations (figure 5(b)). This congruency between the gel and MC simulation suggests that this is the region where the TPS may have had difficulties.

These dose deviations between the TPS and the MC simulations agree with recently published data (Gagne *et al* 2008), involving MC evaluation of a RapidArc^{TM} dose calculation,

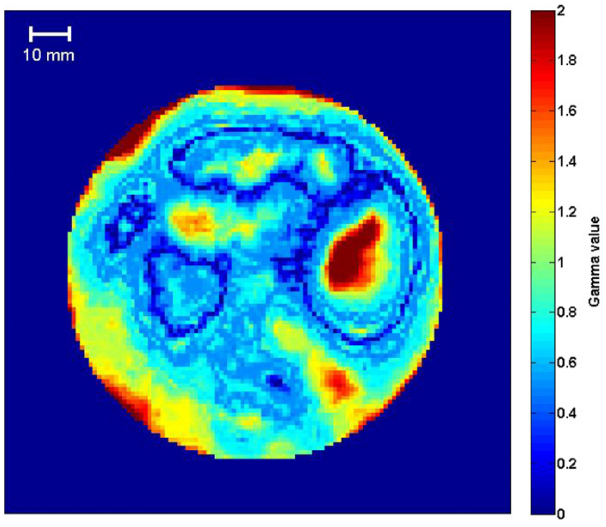

(a) TPS vs. Gel

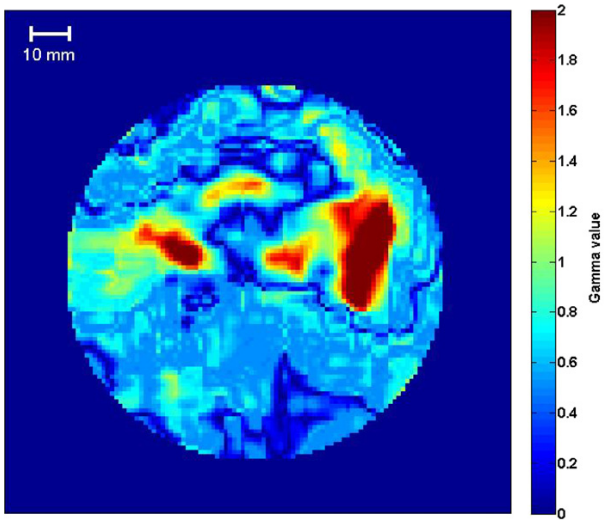

(b) TPS vs. MC

Figure 5. 3D-gamma map resulting from the $1\%/2$ mm evaluation. The cluster of gamma failures was found 15–20 mm from the isocenter within the volume enclosed by the 90% isosurface. In the TPS versus gel evaluation (a), additional gamma failures along the gel container surface are observed. These deviations could probably be attributed to the setting of the gel.

showing a slight over-prediction of the mean target dose calculated by the AAA. The dosimetric errors in the AAA were attributed to the modeling of the leaf end and the modeling of the leaf penumbra. The authors also carried out film dosimetry, which showed better agreement with the MC than with the AAA. However, the composite effect of these errors in a RapidArc^{TM}

calculation produced only a small deviation, which is probably not clinically relevant (Gagne *et al* 2008).

In the TPS versus gel evaluation, additional gamma failures were observed along the gel container surface and up to 10 mm into the phantom, corresponding to an over-dosage of up to 7% in the gel measurement compared to TPS calculations. These deviations could probably be attributed to inhomogeneity in the gel related to the influence of the cooling rate (Deene *et al* 2007), which is more rapid close to the container wall immediately after pouring the gel solution. This could be avoided by using proper margins to the edge when evaluating the data.

According to the gamma evaluation above, using the criteria 1%/2 mm in $VOI_{container}$, a cluster of gamma failures appears in the volume corresponding to the treated volume in both the evaluations between the TPS and gel measurement and between the TPS and MC simulation. However, when using more clinically relevant criteria, i.e. 3%/3 mm, high pass rates were observed when comparing the calculated and measured data in both VOI_{50} and VOI_{90}. Moreover, when evaluating the dose differences only, mean differences were within 1% and standard deviations were smaller than 2.5% (1SD) within VOI_{90}.

4. Conclusions

Gel dosimetry and MC simulation were used for a 3D verification of a RapidArc™ treatment plan and delivery. Inter-comparisons between all datasets—TPS calculations, gel measurement and MC simulation—showed very good agreement. This verification study successfully demonstrated that the RapidArc™ plan was both accurately calculated and delivered as planned. Furthermore, the repeated gel measurements showed excellent consistency, indicating reproducible delivery.

Acknowledgments

This study was financially supported by the Swedish Cancer Society and the Cancer Foundation at Skåne University Hospital in Malmö. Additionally, the study was partly supported by the Lundbeck Foundation Center for Interventional Research in Radiation Oncology (CIRRO). Finally, the authors wish to thank Varian Medical Systems for their support.

References

Alexander A S, Wells D, Berrang T, Parsons C, Mydin A, Shaffer R, Wong F, Sayers D and Otto K 2008 Volumetric arc therapy (VMAT) reduces treatment time compared to conventional IMRT (cIMRT) while maintaining similar plan quality in whole pelvic gynecologic radiotherapy *Int. J. Radiat. Oncol. Biol. Phys.* **72** S366

Baldock C, Deene Y D, Doran S, Ibbott G, Jirasek A, Lepage M, Mcauley K B, Oldham M and Schreiner L J 2010 Topical review polymer gel dosimetry *Phys. Med. Biol.* **55** R1–63

Bjoreland A, Lindvall P, Karlsson A, Gustavsson H, Back S A, Karlsson M and Bergenheim T A 2008 Liquid ionization chamber calibrated gel dosimetry in conformal stereotactic radiotherapy of brain lesions *Acta Oncol.* **47** 1099–109

Bush K, Townson R and Zavgorodni S 2008 Monte Carlo simulation of RapidArc radiotherapy delivery *Phys. Med. Biol.* **53** N359–70

Ceberg S, Karlsson A, Gustavsson H, Wittgren L and Bäck S Å J 2008 Verification of dynamic radiotherapy: the potential for 3D dosimetry under respiratory-like motion using polymer gel *Phys. Med. Biol.* **53** N387–96

Cranmer-Sargison G, Beckham W A and Popescu I A 2004 Modelling an extreme water–lung interface using a single pencil beam algorithm and the Monte Carlo method *Phys. Med. Biol.* **49** 1557–67

Deene Y D, Pittomvils G and Visalatchi S 2007 The influence of cooling rate on the accuracy of normoxic polymer gel dosimeters *Phys. Med. Biol.* **52** 2719–28

Doran S J 2009 The history and principles of chemical dosimetry for 3-D radiation fields: gels, polymers and plastics *Appl. Radiat. Isot.* **67** 393–8

Dumas E, Leclerc G and Lepage M 2006 Effect of container size on the accuracy of polymer gel dosimetry *J. Phys.: Conf. Ser.* **56** 239–41

Feygelman V, Forster K, Opp D and Nilsson G 2009 Evaluation of a biplanar diode array dosimeter for quality assurance of step-and-shoot IMRT *J. Appl. Clin. Med. Phys.* **10** 3080

Gagne I M, Ansbacher W, Zavgorodni S, Popescu C and Beckham W A 2008 A Monte Carlo evaluation of RapidArc dose calculations for oropharynx radiotherapy *Phys. Med. Biol.* **53** 7167–85

Gagne I M and Zavgorodni S 2007 Evaluation of the analytical anisotropic algorithm in an extreme water–lung interface phantom using Monte Carlo dose calculations *J. Appl. Clin. Med. Phys.* **8** 33–46

Gustavsson H, Karlsson A, Back S A, Olsson L E, Haraldsson P, Engstrom P and Nystrom H 2003 MAGIC-type polymer gel for three-dimensional dosimetry: intensity-modulated radiation therapy verification *Med. Phys.* **30** 1264–71

ICRU 1999 Prescribing, recording and reporting photon beam therapy *ICRU Report No 62 (*Supplement to *ICRU Report No 50)* (Bethesda, MD: ICRU)

Karlsson A 2007 Characterization and clinical application of normoxic polymer gel in radiation therapy dosimetry *PhD Thesis* Lund University

Karlsson A, Gustavsson H, Olsson L E and Bäck S Å J 2003 Image processing software for 3D dose evaluation in gel dosimetry *IFMBE Proc. World Congress on Medical Physics and Biomedical Engineering* (CDROM)

Kawrakow I and Fippel M 2000 VMC++, a fast MC algorithm for radiation treatment planning *Proc. 13th Int. Conf. the Use of Computers in Radiotherapy (Heidelberg)* ed W Hamacher and T Bortfeld (Heidelberg: Springer) pp 126–8

Keall P J and Baldock C 1999 A theoretical study of the radiological properties and water equivalence of three types of gels used for radiation dosimetry *Australas. Phys. Eng. Sci. Med.* **22** 85–91

Keall P J, Siebers J V, Arnfield M, Kim J O and Mohan R 2001 Monte Carlo dose calculations for dynamic IMRT treatments *Phys. Med. Biol.* **46** 929–41

Kjær-Kristoffersen F, Ohlhues L and Medin J 2009 RapidArc volumetric modulated therapy planning for prostate cancer patients *Acta Oncol.* **48** 227–33

Korreman S, Medin J and Kjær-Kristoffersen F 2009 Dosimetric verification of RapidArc treatment delivery *Acta Oncol.* **48** 185–92

Li X A, Ma L, Naqvi S, Shih R and Yu C 2001 Monte Carlo dose verification for intensity-modulated arc therapy *Phys. Med. Biol.* **46** 2269–82

Low D A, Harms W B, Mutic S and Purdy J A 1998 A technique for the quantitative evaluation of dose distributions *Med. Phys.* **25** 656–61

Nicolini G, Clivio A, Fogliata A, Vanetti E and Cozzi L 2009 Simultaneous integrated boost radiotherapy for bilateral breast: a treatment planning and dosimetric comparison for volumetric modulated arc and fixed field intensity modulated therapy *Radiat. Oncol.* **4** 27

Olsson L E, Bäck S Å J, Magnusson P and Haraldsson P 1998 3D dosimetry using gels and MRI *Imaging in Radiation Therapy* (*AAPM Monograph No 24*) ed J D Hazle and A L Boyer (Madison, WI: Medical Physics Publishing) pp 475–504

Otto K 2008 Volumetric modulated arc therapy: IMRT in a single gantry arc *Med. Phys.* **35** 310–8

Palma D, Vollans E, James K, Nakano S, Moiseenko V, Shaffer R, Mckenzie M, Morris J and Otto K 2008a Volumetric modulated arc therapy (VMAT) for delivery of prostate radiotherapy: reduction in treatment time and monitor unit requirements compared to intensity modulated radiotherapy *Int. J. Radiat. Oncol. Biol. Phys.* **72** S312

Palma D, Vollans E, James K, Nakano S, Moiseenko V, Shaffer R, Mckenzie M, Morris J and Otto K 2008b Volumetric modulated arc therapy for delivery of prostate radiotherapy: comparison with intensity-modulated radiotherapy and three-dimensional conformal radiotherapy *Int. J. Radiat. Oncol. Biol. Phys.* **72** 996–1001

Popescu C, Olivotto I A, Beckham W A, Ansbacher W, Zavgorodni S, Shaffer R, Wai E S and Otto K 2010 Volumetric modulated arc therapy improves dosimetry and reduces treatment time compared to conventional intensity-modulated radiotherapy for locoregional radiotherapy of left-sided breast cancer and internal mammary nodes *Int. J. Radiat. Oncol. Biol. Phys.* **76** 287–95

Popescu I A, Shaw C P, Zavgorodni S F and Beckham W A 2005 Absolute dose calculations for Monte Carlo simulations of radiotherapy beams *Phys. Med. Biol.* **50** 3375–92

Rogers D W, Faddegon B A, Ding G X, MA C M, We J and Mackie T R 1995 BEAM: a Monte Carlo code to simulate radiotherapy treatment units *Med. Phys.* **22** 503–24

Shaffer R, Morris W J, Moiseenko V, Welsh M, Crumley C, Nakano S, Schmuland M, Pickles T and Otto K 2009 Volumetric modulated arc therapy and conventional intensity-modulated radiotherapy for simultaneous maximal intraprostatic boost: a planning comparison study *Clin. Oncol.* **21** 401–7

Siebers J V, Keall P J, Kim J O and Mohan R 2002 A method for photon beam Monte Carlo multileaf collimator particle transport *Phys. Med. Biol.* **47** 3225–49

Siebers J V, Keall P J, Nahum A E and Mohan R 2000 Converting absorbed dose to medium to absorbed dose to water for Monte Carlo based photon beam dose calculations *Phys. Med. Biol.* **45** 983–95

Stapleton S, Zavgorodni S, Popescu I A and Beckham W A 2005 Implementation of random set-up errors in Monte Carlo calculated dynamic IMRT treatment plans *Phys. Med. Biol.* **50** 429–39

Teke T, Bergman A M, Kwa W, Gill B, Duzenli C and Popescu I A 2010 Monte Carlo based, patient-specific RapidArc QA using Linac log files *Med. Phys.* **37** 116–23

Walters B R, Kawrakow I and Rogers D W 2009 DOSXYZnrc users manual *National Research Council of Canada Report PIRS-794 rev B*

Yu C X 1995 Intensity-modulated arc therapy with dynamic multileaf collimation: an alternative to tomotherapy *Phys. Med. Biol.* **40** 1435–49

Paper V

Real-time dynamic MLC-tracking of moving target during modulated arc radiotherapy: dosimetric verification using 3D polymer gel and a bi-planar diode array

Sofie Ceberg[1], Marianne Falk[2], Per Munck af Rosenschöld[2], Helen Gustafsson[1,3], Stine S Korreman[2,4] and Sven ÅJ Bäck[1]

[1]Department of Medical Radiation Physics, Lund University, Skåne University Hospital, Malmö, Sweden
[2]Department of Radiation Oncology, Rigshospitalet, Copenhagen, Denmark
[3]Department of Medical Physics, ACT Health, Canberra, Australia
[4]Niels Bohr Institute, Copenhagen University, Denmark

sofie.ceberg@med.lu.se

Abstract

The aim of this study was to verify the improved conformity of modulated arc-delivery with the use of real-time dynamic multileaf collimator (DMLC)-based tracking of a moving target with a motion, both parallel and orthogonal to the leaf trajectory .

This type of treatment delivery represents a new level of complexity, and a thorough dosimetric verification is therefore necessary. Large respiratory motion is generally accounted for by increased margins, which implies an increased risk of treatment related toxicity. The advantage of tumour-tracking radiation delivery is the ability to allow a tighter margin around the target by continuously following and adapting the dose delivery to tumour movement. However, there are geometric and dosimetric uncertainties associated with beam-delivery system constraints and output variations, and investigations have to be accomplished before clinical implementation of this tracking technique.

The delivery investigated in this study was a RapidArc® 6 MV lung plan, with a 358-degree arc rotation and a target dose of 4 Gy. The target motion, a 20 mm peak-to-peak motion extent and a period of 4 s, was simulated mechanically. Information about the real-time target location was obtained using the ExacTrac system (BrainLab, Germany). The delivery was verified using 3D polymer gel dosimetry (nPAG) and a bi-planar diode array (Delta$^{4®}$, ScandiDos, Inc.). Post irradiation gel T2 images were acquired using a 1.5 T Siemens MR scanner.

Both detector systems verified that the DMLC-based tumour-tracking delivery system successfully accounts for respiratory target motion during a RapidArc™ delivery. A 3D gamma evaluation of the gel measurement on a moving phantom irradiated during tracking, as compared to a measurement on a static delivery, resulted in a minimum of 96% pass rate within the volume enclosed by the 20% iso-dose surface using a gamma criteria of 2%/2mm. Corresponding Delta4® measurements resulted in a pass rate above 94%.

Good agreement was observed between gel and Delta$^{4®}$ measurements, resulting in a mean value and standard deviation of (0.23 ± 2.5)% when evaluating relative absorbed dose profiles from both detector systems during tracked delivery under motion. Furthermore, no significant dose deviations, due to different collimator settings with or without tracking enabled, were observed.

1. Introduction

The advantage presented by novel radiotherapy techniques introduced in recent years is the increased possibility to deliver high absorbed dose to the target volume while minimizing the dose to normal tissues. However, intra-fractional tumour motion, mostly due to respiration, can be a major challenge to the delivery of the desired dose distributions. Several different strategies have been developed to account for and to reduce motion related uncertainties.

The most widely used approach to account for organ motion today is to collect a large data set of measured respiratory motion, calculate the statistical distribution, and incorporating the results into the treatment planning procedure as an additional margin to the PTV (Giraud et al. 2006). However, this approach does not describe the uncertainties in the absorbed dose to the surrounding normal tissue. Another method is to directly introduce respiratory uncertainties into the dose calculation, by convolving the static dose distribution with a motion function (McCarter et al. 2000).

The most obvious approach to reduce uncertainty related to movements induced by breathing is to ask the patient not to breathe during beam-on. Another approach is to turn the beam on only when the target is in a favourable position during the patient's respiratory cycle, *i.e.* the so called respiratory gating technique (Ohara et al. 1989).

Another method to compensate for respiratory motion during treatment is tumour tracking. A novel promising strategy uses the dynamic multileaf collimator (DMLC) to continuously align and reshape the treatment machine aperture to follow the target motion in real time (Sawant et al. 2008). The advantage of this technique is the ability to allow for a tighter margin around the target by continuously following, and adapting the dose delivery to its motion. Thus the possibility to deliver a high absorbed dose to the target volume while minimizing the dose to normal tissues is increased. Compared to the breath-hold and respiratory gating methods, the tumour tracking technique potentially offers additional benefits such as higher delivery efficiency and less residual target motion. However, real-time beam adaptation is not feasible without precise real-time localization of the tumour position in 3D, which includes parallel and perpendicular motion to the MLC leaf travel direction, in- and out-of-plane rotation as well as translation along the beam direction. Recently, a 4D treatment planning method that accounts for 3D tumour motion was proposed (Suh et al. 2009). The method uses 4D CT and is integrated with the DMLC tumour-tracking delivery. This method opens up for a clinical implementation of the DMLC tumour-tracking system. However, only few dosimetric measurements have been carried out that demonstrates the feasibility of MLC tracking (Zimmer et al. 2009, Falk et al. 2010). Dosimetric uncertainties associated with a DMLC tracking system arise from the estimation of the actual target position, possible delay between target motion detection and beam repositioning and output variations due to dissimilar collimator settings with or without tracking enabled.

The modulated arc-therapy technique RapidArc® was introduced in 2008 by Varian Medical Systems. The treatment is delivered during one or a few rotations of the linear accelerator gantry. The dose distribution is modulated by simultaneously varying the MLC positions, dose rate and gantry rotation speed (Otto et al. 2008). RapidArc™ plans are delivered dynamically with leaf and gantry motion up to approximately 1 cm and 2 degrees per second, respectively, and the technique has recently been verified in 3D using the Delta$^{4®}$ detector system (Korreman et al. 2009) and polymer gel dosimetry (Ceberg et al. 2010).

The combination of volumetric modulated arc therapy with a breathing adapted treatment delivery represents a new level of complexity. Detailed evaluation of the dosimetric

uncertainties associated with target motion, gantry motion, small fields and steep dose gradients are parts of an on-going research area. The uncertainties have to be evaluated in detail, and this requires adequate 3D dose verification tools.
Recently, it was reported that it is feasible to perform DMLC-tracking during a RapidArc™ delivery (Zimmerman et al. 2009). A pre-clinical 3D DMLC-tracking application was dosimetrically evaluated using a 2D ion chamber array (Seven29, PTW) and Delta$^{4®}$. An additional study, also using Delta$^{4®}$, verified that the dosimetric accuracy was independent of the magnitude of the peak-to-peak displacement (5-25 mm) of the target and not significantly affected by the angle between the leaf trajectory and the target movements (Falk et al. 2010). However, further studies using an independent high resolution 3D detector would be of great interest.
Using gel dosimetry (Baldock et al. 2010), the absorbed dose can be obtained in the entire irradiated volume. No correction factors have to be applied since the response is independent of the energy (Novotny et al. 2001, De Deene et al. 2006), the direction of the incident radiation (Olsson et al. 1998) and can be considered as soft tissue equivalent (Keall and Baldock 1999). Further, the gel can be poured into anthropomorphically shaped phantoms. Recently, it was showed that polymer gel is a feasible detector for 3D dose verification of dynamic radiotherapy (Ceberg et al. 2008a) as well as for DMLC-tracking delivery (Ceberg et al. 2008b).
The aim of this study was to verify the improved conformity with the use of real-time DMLC-tracking of a target with a motion, both parallel and orthogonal to the leaf trajectory, during an intensity modulated RapidArc™ delivery. In addition, due to dissimilar collimator positions when the tracking system is connected compared to disconnected, the difference in absorbed dose due to different transmission leakage was investigated as well.

2. Material and methods

RapidArc™ treatment planning, DMLC-tumour tracking delivery and Delta$^{4®}$ data analysis were carried out at Rigshospitalet in Copenhagen. The pre-clinical DMLC-tracking controller that was connected to the linear accelerator was developed at Stanford University. Gel preparation, gel read-out and data analysis were carried out at Lund University, Skåne University Hospital in Malmö.

2.1. Bi-planar diode array Delta$^{4®}$

The bi-planar diode array Delta$^{4®}$ (ScandiDos, Inc., Sweden) is a cylindrical PMMA phantom with two orthogonal detector boards. A 3D dose matrix is obtained by interpolation of the measured data in the two planes. One plane, the so called “main board” has a measurement area of 20 × 20 cm^2 and the other plane consists of two “wings” covering 20 × 10 cm^2 each. The planes are aligned +50° (main board) and -40º (wings). Due to the orthogonally arranged detector arrays it is ensured that the dose modulation information is not lost regardless of the beam incidence angle. Each plane has 1069 p-type cylindrical silicon diodes covering the measurement area. The diode size is 1 mm in diameter and 0.05 mm thick and the centre-to-centre distance is 5 mm in the central 6 x 6 cm^2 region of the detector and 10 mm in the rest of measurement area.
Correction factors for direction-, depth- and field-size dependency are embedded in the software and applied on a segment-by-segment basis to individual diodes (Feygelman et al.

2009). The semi-empirical volumetric dose calculation is based on the incidence rays that are traced from the source through the phantom. Any ray will intercept at least one, and usually both detector planes yielding one or two dose points along the ray. The system renormalizes the TPS calculated depth dose along the ray to fit the measurement points, and uses that data to reconstruct the dose (Feygelman et al. 2009). When summing up all rays a dose distribution in 3D is obtained. For rotational treatments on conventional linacs, additional gantry angle information is obtained from an independent inclinometer mounted on the gantry.

2.2. 3D polymer gel

The polymer gel dosimeter used in this study was a normoxic polyacrylamide gel (nPAG). The main constituents of a polymer gel are water, a radiation sensitive chemical and a matrix substance. When the dosimeter is exposed to irradiation, polymerization occurs as a function of absorbed dose. The matrix holds the polymer structure in place, thus preserving spatial information of the absorbed dose, which consequently enables the dose distribution to be recorded in 3D. The nPAG used in this study contained 89% w/w ultra-pure deionised water (resistivity > 18.2 MΩ cm), 3% w/w acrylamide (electrophoresis grade 99%, powder, Sigma Aldrich), 3% w/w N,N_-methylenebisacrylamide (electrophoresis grade 98%, powder, Sigma Aldrich), 5% w/w gelatine (swine skin, 300 bloom, Sigma Aldrich) and 10 mM tetrakis(hydroxymethyl)–phosphonium chloride (techn. ~80% in water, Sigma Aldrich).
The gelatine, which was used as the matrix substance, was mixed with water in room temperature. The mixture was heated to 45 ◦C to completely dissolve the gelatine. The monomers were added at this temperature before cooling down. The gel was prepared under normal levels of oxygen, and the solution was stirred continuously through the entire mixing procedure. Ten minutes before the gel was poured into bottles and vials the oxygen scavenger was added. Another identical un-irradiated gel phantom was used to acquire a background value and gel vials irradiated to known doses were used to assure the linearity of the gel dose response. The phantoms were left to set in the dark at room temperature for about 24 h before irradiation. Approxiamtely 24 hours post irradiation magnetic resonance imaging (MRI) of the gel was performed. The images were acquired using a 1.5 T MRI unit (Siemens Symphony, Siemens Medical Systems) and a 32echo multi spin echo sequence with an inter-echo spacing of 25 ms. In-house developed software was used for T2 calculations (Karlsson et al. 2003), and MATLAB 7.4.0 was used for image processing and 3D rendering. The R2 data of the irradiated gel phantoms was converted to relative absorbed dose using background subtraction and normalization in a region of homogenous dose. An in-house developed 3D gamma evaluation program was used to compare all the gel measurement. The raw data was smoothed using a 3 x 3 x 3 box-filter and re-sampled from 1 x 1 x 3 mm^3 to 1 x 1 x 1 mm^3 voxel size to enable 3D gamma evaluation.

2.3. The DMLC tumour-tracking system

The 3D MLC-tracking algorithm uses the real-time target motion information to dynamically re-calculate the position of each MLC leaf so as to best account for the target motion, i.e. to optimally adapt to the real-time location of the target (Sawant et al. 2008). The algorithm used in this study accounted for rigid target translation including motion parallel and perpendicular to the MLC leaf motion. Since there is a latency associated with the process involving target detection, recalculation of new MLC positions and MLC response time, the tracking

algorithm uses a prediction filter to estimate future target position (Srivastava et al. 2007). The latency without the prediction filter was measured to 260 ms at the time for this study. To enable DMLC tracking, the jaws are withdrawn to allow any leaf pairs to be opened if the target starts to move. On both sides of the MLC shaped opening there are always a constant number of adjacent central leaf pairs, ready to open if the target is start to move in that direction (Falk et al. 2010). To minimize the transmission between the closed leaf tips of remaining leaf pairs outside the adjacent central leaf pairs, the tracking system moves the closed leaves to the side underneath one of the x-jaws.
The MLC will be positioned so as to optimally fit the instantaneous target location and minimize the leakage through MLC leaves by moving non-tracking pairs under nearest jaw. The DMLC-tracking controller methodology also includes conservation of the integral fluence at the target plane and d) enabling of beam-off when anomalous situations occur, such as sudden change in respiratory pattern or coughing (Sawant et al. 2008). The DMLC real-time motion-tracking system was used together with the optical part of the ExacTrac system (BrainLab, Germany). The infrared (IR) tracking component of the ExacTrac includes two IR cameras and passive IR reflecting spheres that were placed on a surface of the respectively detector (Jin et al. 2008). The IR cameras emit a low IR signal that is reflected and analyzed for positioning information. The signal is corrected for any distortions in the IR system and provides the location of the linear accelerator isocenter. It has been shown that the position of each IR reflecting sphere can be determined to within 0.3 mm (Wang *et al.* 2001). Since the IR system samples the marker positions at a frequency of 20 Hz it can not only be used for a precise set-up verification of a patient or detector but also to monitor patient respiratory motion (Hugo et al. 2002, Jin et al. 2005). The ExacTrac system is widely used in radiotherapy clinics while the DMLC tumour-tracking system (Keall et al. 2001) is a non-clinical research tool under development.

2.4. The RapidArc™ tumour-tracking plan and delivery

To simulate lung tumour movement caused by respiratory motion, the gel phantoms and the Delta$^{4®}$ were positioned on a programmable motion platform (Standard Imaging, Inc), which was set to carry out sinusoidal motion in the superior–inferior (SI) direction with a peak-to-peak distance of 20 mm during a period of 4 s. The combined motion extent and cycle time are within the reported span of lung tumour motion (Seppenwoolde et al. 2002). Further, since the collimator rotation was set to 45 degrees as customary for a RapidArc™ plan (Otto et al. 2008) the target motion had a non-parallel component compared to the leaf trajectory.
A RapidArc™ 6 MV lung plan created in Eclipse version 8.6 treatment planning system (TPS) using inverse optimisation and calculated with Anisotropic analytical algorithm (AAA) with a 0.1 cm3 grid size. The RapidArc™ plan, used a 358-degree arc rotation and was delivered to both detector systems using a Novalis TX™ linear accelerator with a high definition MLC. The small target had a 4.86 cm^3 volume (2.3 cm (SI) x 1.8 cm (AP) x 1.7 cm (LR)), and was irradiated with a planned target dose of 4 Gy using 790 MU. To enable the plans for DMLC tracking, the jaws opening was set to 6 x 6 cm^2, in order to avoid covering the moving target.
The delivery was carried out in the following set-up modes: *i*) detector in motion and the tracking system disconnected, *ii*) detector at rest and the tracking system disconnected, *iii*) detector at rest and the tracking system connected and *iv*) detector in motion and the tracking

system connected. All irradiations were delivered to four identical 500 ml circular gel phantoms and to the Delta$^{4®}$ detector.
The measurement in mode *iii*) was used as reference when evaluating mode *iv*) due to the potential difference in inter leaf leakage during a connected or disconnected tracking system.
By evaluating the difference between the measurement during motion and the static measurement, for each detector system, any possible discrepancy compared to the TPS was excluded, isolating the DMLC tracking performance. For a dosimetric verification of the RapidArc™ plan, however, the deliveries to the static detector system with the tracking system disconnected (mode *ii*) were compared to the TPS data.
During tracking the non-participating closed leaf pairs are moved to the side underneath one of the x-jaws, to minimize the transmission. This is however not the case during a delivery with the tracking system disconnected. To investigate if this difference in radiation leakage may contribute to difference in absorbed dose, two static measurements, with and without the tracking system connected, were compared (i.e. mode *ii vs*. mode *iii*).
The vials used for a linearity verification of the polymer gel R2-signal vs. absorbed dose were placed at 3 cm depth in a 30 × 30 × 30 cm^3 cubic water phantom and irradiated using a 20 × 20 cm^2 6 MV photon beam, with the linear accelerator set to deliver 600 MU/min.

2.5. *Data analysis*
Three dimensional gamma evaluation of the gel measurements was carried out using an in-house developed program implemented into the MATLAB software environment (The MathWorks Inc.). For corresponding analysis of Delta$^{4®}$ data the detector vendor's software was used. However, both the in-house and the Delta$^{4®}$ softaware are based on the theory by Low *et al* (1998), enabling direct comparisons of the obtained data.
The treatment plan and the measured relative absorbed dose volumes were aligned by matching the inner surface of the gel containers at the isocenter plane. No correction for any potential rotation was needed due to a gel phantom fixation.
The RapidArc™ lung plan was calculated using a 0.1x0.1x0.1 cm^3 voxel size and the gel data were acquired with a 0.1x0.1x0.3 cm^3 voxel size. The gel data was linearly interpolated and re-sampled to 0.1x0.1x0.1 cm^3 to enable the 3D gamma analysis. All gel dose arrays were normalized to 100% using the mean value in a 0.3x0.3x0.3 cm^3 volume (27 voxels) close to the isocenter in a region of homogeneous absorbed dose.
Previous to the evaluation of the DMLC-tracking performance, by comparing static and tracked measurements carried out for respective detector system, the 6MV RapidArc™ lung-plan was verified. The treatment planning system (TPS) dose calculations was compared to the gel and Delta$^{4®}$ measurement, respectively. The clinical gamma criteria of 3%/3mm was used in the 3D gamma evaluation.
Evaluations were carried out for comparisons of the dosimetric measurements for each detector system. Both dose deviation histograms and 3D gamma evaluations were carried out. The volumes of interest investigated were the volumes enclosed by the 5% and 20% isodose surface for the Delta$^{4®}$ system and 20%, 50% and 90% isodose surface for the gel measurements (VOI_5, VOI_{20}, VOI_{50} and VOI_{90}). The gamma criteria were 2%/1mm (% dose difference and mm distance to agreement). In addition, when investigating whether a potential dose contribution due to transmission leakage is detectable, a comparison of the static measurements was carried out.

By using 3D gel measurements the volume of interest investigated was able to be located only in the low dose volume. That is, a volume enclosed by the 20% iso-dose surface, with a central hole enclosed by the 50% iso-dose surface, i.e. VOI_{20-50}.
To perform a direct comparison between the gel- and Delta$^{4®}$ results, measurement points were plotted along three orthogonal profiles, i.e. along the two detector boards, x´and z´, and along the central longitudinal axis, y (Figure 1). All measurements, both for the gel and the Delta$^{4®}$, were normalized to 100 % at isocenter.

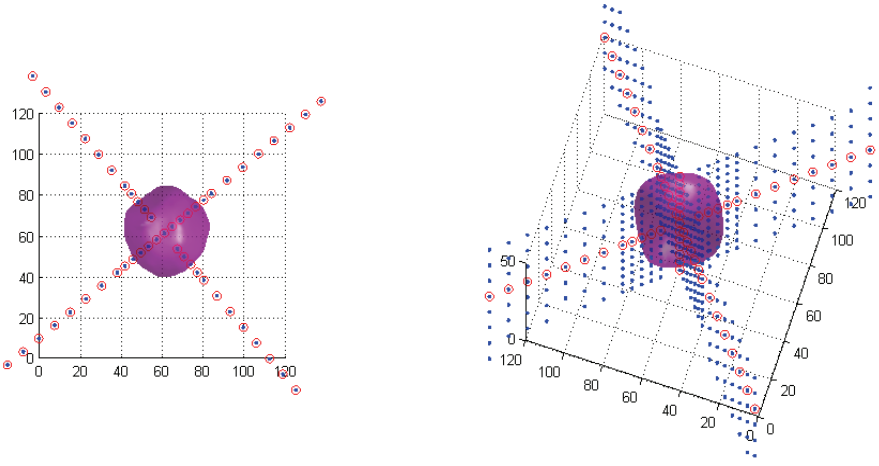

a) **b)**

Figure 1. The purple volume corresponds to the gel measurement (VOI_{50}) and the blue dots denotes the location of the diodes within the Delta$^{4®}$. The red circles point out the diodes whose measurements are compared with the gel measurement. In the view a) are the diode boards within the Delta$^{4®}$ easy to recognise. In b) a tilt of the a) is presented. The gel measurement cover the part of Delta4® with the highest resolution (5 mm)

3. Results and discussion

Good agreement was found when comparing the treatment planning system (TPS) dose calculations for the 6MV RapidArc™ lung-plan and the static measurements for both detector systems. Using the clinical 3%/3mm gamma criteria within VOI_5 when comparing TPS with the Delta$^{4®}$ measurement resulted in a 100% pass rate. Due to the limited extent of the gel phantom in the axial plane (phantom radius) the gamma evaluation was carried out within the volume enclosed by the 20% isodose surface (VOI_{20}), which resulted in a 99.5% pass rate using the same gamma criteria.
A fair evaluation of the DMLC-tracking performance, avoiding any possible contributions from discrepancy between measurements and TPS was achieved by just comparing measurements carried out for respective detector system, i.e. mode *iii*) *vs*. mode *iv*) as described in section 2.4. To illustrate the good agreement between the static and tracked gel measurement, and thus a good result of the tracking performance, an overlay of the measured 90% iso-dose surfaces are presented (figure 2a).

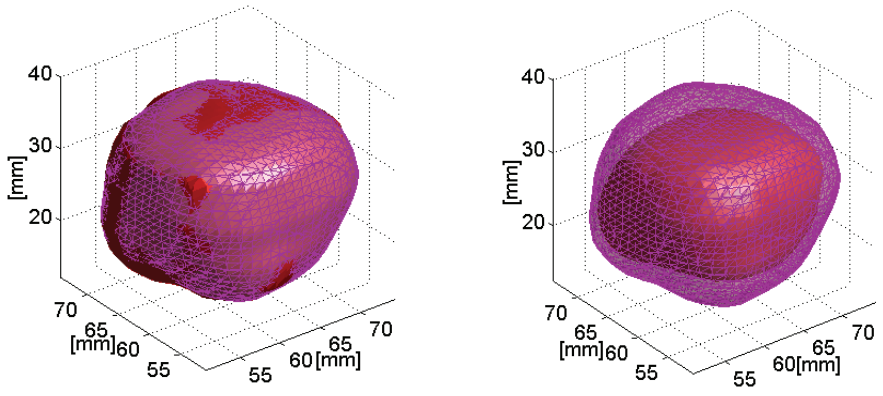

Figure 2. The 90% isodose surface overlay of the gel measurements. The wire framed pink volumes represent the static gel measurements and the red volumes represent the gel measurements obtained during motion. The good agreement between the static and tracked measurements are presented in a). The red non-tracked volume in b) visualizes the reduction of the 90% isodose volume.

The relative absorbed dose differences were calculated voxel-by-voxel within VOI_{90} for measured static gel *vs.* the gel in motion. The dose difference calculation was carried out for the two set of measurements, one with the tracking system connected during both measurements, *i.e.* mode *iii*) *vs*. *iv*) and one with a disconnected tracking system during both measurements, *i.e.* mode *ii*) *vs. i*), were A *vs.* B corresponds to $A_{voxel(i)}$–$B_{voxel(i)}$.

Investigating the tracking performance, the dose volume comparison showed a very good agreement with 97.1% of the voxels having less than 2% dose difference. The mean value and standard deviation of the distributed deviations were (0.078±0.80)% (figure 3a). The results showed that the DMLC-tracking system has the capability to account for target motion during intensity modulated arc therapy.

If not taking the 20mm target motion into account, an obvious target under dosage will occur (figure 2b). The mean value and standard deviation of the differences obtained from the measurements were (3.70±2.56)% with only 26.6% of the voxels within 2% dose difference (figure 3b). The smeared distribution of the deviations was expected, and due to that the gel in motion obtained a decreased absorbed dose was there a positive shift in mean value within VOI_{90}.

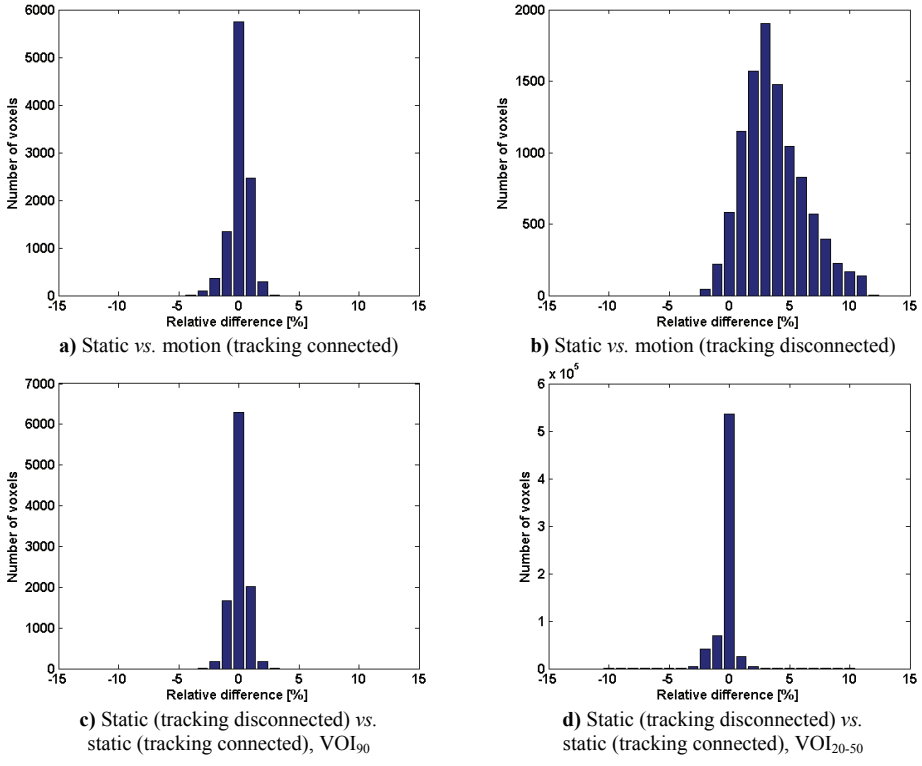

a) Static *vs.* motion (tracking connected)

b) Static *vs.* motion (tracking disconnected)

c) Static (tracking disconnected) *vs.* static (tracking connected), VOI_{90}

d) Static (tracking disconnected) *vs.* static (tracking connected), $VOI_{20\text{-}50}$

Figure 3. The distribution of voxel-by-voxel deviations between the different gel measurement sets within the volumes enclosed by the 90% isodose surface, a) - c), and the volumes enclosed by the isodose surface interval 20-50%, d). The number of voxels is plotted against the difference in relative dose between the two analyzed volumes. Note the different scale of the ordinates.

The deviations between the two static gel measurements with the tracking system disconnected and connected, *i.e. ii*) *vs*. *iii*) were investigated in the same way. As expected, no significant dose difference due to leakage was found in VOI_{90}. The mean value and standard deviation were (0.029±0.65)% and with 99.2% of the voxels within 2% dose difference (figure 3c). The comparisons of the same static measurements within the low dose volumes, i.e. $VOI_{20\text{-}50}$ resulted in a mean value and a standard deviation of (-0.21± 0.82)%, with 96.5% of the voxels within 2% dose difference (figure 3d). Still, no significant dose contribution due to leakage was detected.

In addition, 3D gamma evaluations of the gel measurements were carried out. The smearing effect was investigated by evaluating mode *ii*) *vs. i*), and was compared to the investigated tracking performance by evaluating mode *iii*) *vs. iv*). Using the criteria 2%/1mm resulted in an increased pass rate from 22.1% to 81.7% within VOI_{50} and 31.4% to 98.6% within VOI_{90}. These results thus verified the greatly improved conformity with the use of real-time DMLC-based tracking of a target with 20mm motion, during an intensity modulated arc-delivery.

The Delta[4®] measurements, obtained for three delivery modes (*i, iii* and *iv*) are presented as absorbed dose profiles through the isocentre (figure 4). Even though the spatial resolution is quite poor a good agreement between the static and tracked measurement is indicated. If the target motion is not taken into account, a significant dose smearing effect is obtained, which result in under dosage in the target and over dosage outside the field.

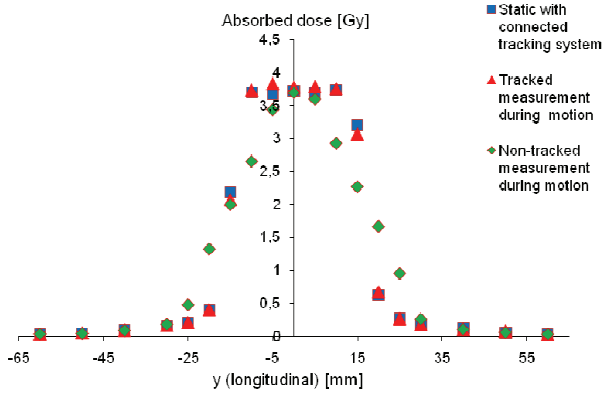

Figure 4. Absorbed dose profiles through the isocenter of the Delta[4®] detector. Data from three measurements are presented: non-tracked delivery during motion (green dots), tracked delivery during motion (red dots) and static delivery with the tracking system connected (blue dots).

The gel measurement were compared with the Delta[4®]-results, and very good agreement was showed. Three orthogonal dose profiles along the gel and Delta[4®] for the DMLC-tracked RapidArc™ delivery during 20 mm motion, are presented (Figure 5). Each gel measurement point was selected from the 3D gel array at the position corresponding to the diode location in the Delta[4®]. The relative dose differences between the measurement points acquired for both the detector systems were small; 22 out of 34 points were within 2% difference and only 4 points, located in the low dose volume, showed a difference larger than 5%. The mean value and standard deviation of the differences were (0.23 ± 2.5)%. In addition, comparing the complete gel dose profile to the measurement points obtained with the Delta[4®] the distance to agreement was within 1 mm except from two points in the low dose region obtained in the axial plane.

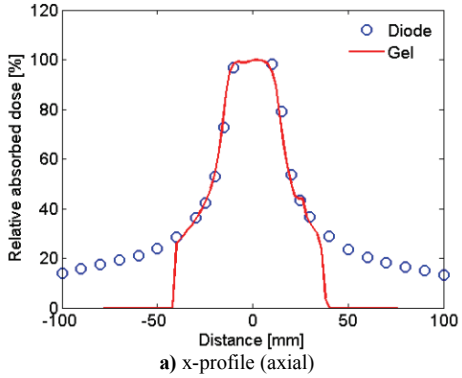

a) x-profile (axial)

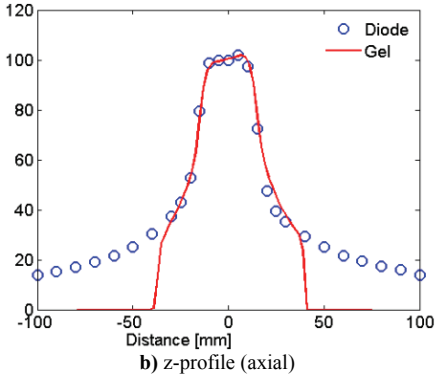

b) z-profile (axial)

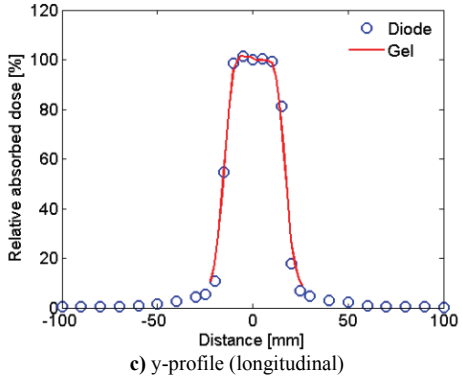

c) y-profile (longitudinal)

Figure 5. Orthogonal relative absorbed dose profiles of the gel and the bi-planar diode array measurements, which were obtained during a volumetric arc delivery using DLMC-tracking of a 20 mm target motion. The gel measurements are limited by the container wall in the axial plane (a and b) and to the evaluation interval in the longitudinal plane (c).

The Delta$^{4®}$ system also has an built-in 3D gamma evaluation software. Using the same gamma criteria as for the gel measurement evaluation, i.e. 2%/1mm, the smearing effect (mode *ii vs. i*) and the tracking performance (*iii vs. iv*) were investigated within VOI_5.

By accounting for the target motion using DMLC-tracking the pass rate was increased from 29.7% to 96.9%, which agrees with the outcome of the gel measurement 3D gamma evaluation. Due to the very small target volume, and thus few measurement points, 3D gamma evaluation of the Delta$^{4®}$ measurements was carried out using the VOI_5. On the other hand, regarding the gel measurements, the VOI_5 reached outside the gel phantom. A 3D gamma evaluation, within VOI_{20} was carried out for respective detector system with associated 3D gamma evaluation method. In consistency with recently published results involving DMLC-tracking and RapidArc™ (Falk et al. 2010 and Zimmerman et al. 2009) the criteria 2%/2mm was used. The tracking performance (*iii vs. iv*) was investigated and resulted in a 94.4% pass rate for the Delta$^{4®}$ measurements and 96.4% for the gel measurements.

Further, the two static Delta$^{4®}$-measurements, with the tracking system disconnected and connected, were investigated. The 3D gamma evaluation resulted in a 100% pass rate using the 2%/1mm criteria within VOI_5, and thus no absorbed dose difference due to different collimator settings during tracking mode, was detected by the Delta$^{4®}$. This result also agrees with the outcome of the gel measurement when investigating the potential leakage by dose deviation histogram analysis.

4. Conclusion

This study verified that an intensity modulated RapidArc™ treatment of a moving target was delivered with greatly improved conformity when real-time DMLC-tracking was incorporated. For the first time, the MLC tracking technique was verified using a completely independent 3D QA tool, i.e. polymer gel dosimetry. The delivery was verified both using gel and a bi-planar diode array, showing that that the DMLC-based tumour-tracking delivery system successfully accounted for respiratory-like target motion. If the breathing motion was not taken into account, smeared dose distributions were obtained. Very good agreement was observed between the tracked measurement points obtained for the gel and Delta$^{4®}$, which add extra confidence to the tracking performance technology used in this work. Furthermore, no increase in absorbed dose caused by different collimator setting was detected neither by gel nor Delta$^{4®}$ measurement, using the evaluation methods within this study.

Acknowledgments

The authors thank Paul Keall, Byung Chul Cho, Amit Sawant and Dan Ruan at Stanford University and Varian Medical Systems for the access to the dynamic-MLC tracking code.
We also acknowledge Crister Ceberg (Lund University) for his valuable advice in Matlab programming.
This study was financially supported by the Swedish Cancer Society, the Cancer Foundation at Skåne University Hospital in Malmö and by a research grant from Varian Medical Systems, Inc (Palo Alto, California).

References

T. R. Mackie et al., Tomotherapy: a new concept for the delivery of dynamic conformal radiotherapy. Med Phys 20 (1993) 1709.
K. Otto. Volumetric modulated arc therapy: IMRT in a single gantry arc. Med Phys 35 (2008) 310.
C. X. Yu. Intensity-modulated arc therapy with dynamic multileaf collimation: an alternative to tomotherapy. Phys Med Biol 40 (1995) 1435.
M. Falk et al. Real-time dynamic MLC tracking for inversely optimized arc radiotherapy. Radiother Oncol 94 (2010) 218.
R. McMahon et al. A real-time dynamic-MLC control algorithm for delivering IMRT to targets undergoing 2D rigid motion in the beam's eye view. Med Phys 35 (2008) 3875.
J. Zimmerman et al. DMLC motion tracking of moving targets for intensity modulated arc therapy treatment: a feasibility study. Acta Oncol 48 (2009) 245.
C. Baldock et al. TOPICAL REVIEW Polymer gel dosimetry. Phys Med Biol 55 (2010) R1.
S. Ceberg et al. Verification of dynamic radiotherapy: the potential for 3D dosimetry under respiratory-like motion using polymer gel. Phys Med Biol 53 (2008) N387.
S. Ceberg et al. RapidArc treatment verification using polymer gel dosimetry 2010
A. Karlsson et al. Image Processing Software for 3D Dose Evaluation in Gel Dosimetry. World Congress on Medical Physics and Biomedical Engineering, 2003.
D. A. Low et al. A technique for the quantitative evaluation of dose distributions. Med Phys 25 (1998) 656.
P. Giraud, E. Yorke, S. Jiang, L. Simon, K. Rosenzweig, and G. Mageras, Cancer Radiother 10 (2006) 269
J. Jin et al. 2008, Medical Dosimetry, Vol. 33, No. 2, pp. 124-134, 2008
Wang, L.T.; Solberg, T.D.; Medin, P.M.; et al. Infrared patient positioning for stereotactic radiosurgery of extracranial tumours. Comp. Biol. Med. **31:**101–11; 2001.
Hugo, G.D.; Agazaryan, N.; Solberg, T.D. An evaluation of gating window size, delivery method, and composite field dosimetry of respiratory-gated IMRT. Med. Phys. **29:**2517–25; 2002.
Jin, J.Y.; Yin, F.F. Time delay measurement for linac based treatment delivery in synchronized respiratory gating radiotherapy. Med. Phys. **32:**1293–6; 2005.